Prediction of Tower Loading of Floating Offshore Wind Turbine Systems in the Extreme Wind and Wave Conditions

（浮体式洋上風車のタワーに作用する暴風波浪時の荷重の評価）

A Dissertation Submitted to the University of Tokyo
in Partial Fulfillment of the Requirements
for the Degree of Doctor of Philosophy

By

Xu Nan
（許　楠）

Department of Civil Engineering
The University of Tokyo
Tokyo, Japan

September, 2012

ABSTRACT

The urgent concern about global warming from the emission of greenhouse gases has provided a strong impetus for engineers and scientists worldwide to research alternative renewable and clean energy. Wind power is one of the fastest growing renewable energy technologies. Onshore wind farms are, however, unsightly and they swallow up valuable land for agriculture and urban development. Already some countries, are considering constructing huge wind farms offshore to take advantage of the generally steadier and stronger winds found in the sea. Moreover, the wind turbines can be larger than those on land because they can be transported to the site by sea. In Japan, the offshore consist of a vast wind resource in deep water where use of conventional bottom-mounted wind turbines is not possible, and floating wind turbines are the most attractive. Thus, it is necessary to consider the effect of floater motion on the tower loading to check the serviceability of the wind turbines which are designed for the bottom-mounted systems.

In this study, the theoretical formulae to predict the tower loading of floating offshore wind turbine systems in the extreme wind and wave conditions are proposed. Since the floating offshore wind turbine is affected significantly by floater motion, the conventional fixed-foundation model which is applicable to the onshore wind turbine can not be used theoretically to predict the tower loading of floating offshore wind turbine systems. In this study, SR (Sway-Rocking) model is proposed to consider the floater surge and pitch motions which have large influence on the tower loading of floating wind turbine, so that the tower loading can be estimated by the equivalent static method. In addition, the fluctuating wave load and fluctuating wind load become non-Gaussian processes with multiple peaks corresponding to different frequencies in their spectra, hence, a non-Gaussian peak factor model is proposed in order to predict wave-induced load and wind-induced load on the floating offshore wind turbine tower analytically. Furthermore, in the combination of wave-induced load and wind-induced load, the load reduction factor is proposed since the correlation between their maximum values can be neglected. The essentials of each chapter are as following:

Chapter 1 is a review of current situation of offshore wind energy around the world and in Japan. It explains why it is essential to use floating wind turbine systems in Japan. The outline of this dissertation is also presented.

In Chapter 2, a literature survey of research and development on floating wind turbines is presented. An overview of the research work that has been undertaken pertaining to floating wind turbine technology thus far is carried out, and based on its conclusions and limitations, objectives of this research are presented.

In Chapter 3, two kinds of mooring systems: tension leg mooring and catenary mooring are considered. The methods of describing the behavior of the wind turbines installed with these two kinds of mooring systems are presented. Since surge and pitch are two main wave-induced motions, the equivalent stiffness and damping for these two modes are

identified. Thus SR model is proposed, which can be used to calculate the tower loading of floating offshore wind turbine systems. Meanwhile, the problems of using conventional fixed-foundation model have been clarified.

In Chapter 4, the tower loading due to surge motion as well as pitch motion is investigated separately by locking the other mode. Then their combination is performed to get the wave-induced load on the floating offshore wind turbine tower. Under irregular wave, the fluctuating wave load on wind turbine tower is a non-Gaussian process with two main peaks in its spectrum corresponding to wave peak frequency and wind turbine tower natural frequency respectively, therefore, a non-Gaussian peak factor model is proposed, so that the maximum wave-induced load under irregular wave can be predicted by the equivalent static method.

Chapter 5 gives the details of the prediction of wind-induced load. Equivalent static method is adopted to estimate the maximum wind load on floating offshore wind turbine towers. The analytical formulae are proposed to predict the mean wind load, standard deviation and peak factor of fluctuating wind load. The critical parameters in the standard deviation such as mode correction factor, aerodynamic damping ratio and size reduction factor are investigated to identify their dominant influence factors and their characteristics. A consistent non-Gaussian peak factor model which can be reduced to the standard Gaussian form for a Gaussian process is proposed to estimate the maximum wind load by equivalent static method. Finally, considering the wind response correlation between along-wind direction and across-wind direction, a combination formula for wind load on towers is proposed.

Chapter 6 presents the combination of wave-induced load and wind-induced load. The reason why the assumption of perfect correlation between them causes overestimation has been clarified. It is shown that the combination without considering any correlation can predict the tower loading accurately. In addition, considering the correlation between wind and wave conditions, the load reduction factor of wave-induced load is proposed, which is found to be almost constant to the mean wind speed at hub height. For tension leg system, the load reduction factor is lower than that given in IEC 61400-3 used for bottom-mounted system, while for catenary system it is a little higher than that of IEC.

Chapter 7 summarizes the conclusions of this study. An equivalent SR model which can consider the floater motion is proposed, so that the wave-induced load and wind-induced load on the floating offshore wind turbine tower can be predicted analytically. In addition, the peak factor model considering the non-Gaussian characteristics of fluctuating wave load and fluctuating wind load is proposed in order to predict the maximum wave-induced load and maximum wind-induced load on the floating offshore wind turbine tower analytically. Furthermore, the load reduction factor is proposed in the combination of wave-induced load and wind-induced load by clarifying their characteristics, considering the correlation between wind and wave conditions.

ACKNOWLEDGEMENT

The author would like to express her highest gratitude for her esteemed and erudite supervisor Prof. Takeshi Ishihara for his guidance and advice on every step of this research. This thesis cannot be completed successfully without his instruction and supports. The author is indebted to Prof. Yozo Fujino for his advice and comments in this study. The author is greatly thankful to the rest of her advisory committee: Prof. Hiroshi Katsuchi, Assoc. Prof. Riki Honda, Assoc. Prof. Yoshimitsu Tajima and Dr. Tomonori Nagayama for their constructive comments and suggestions to make improvements for this research. The author is also grateful to Dr. Yamaguchi and Dr. Sarwar for their guidance and help which contribute a lot to this thesis. A special thank is given to Dr. Waris for his teaching to use the FEM simulation and his valuable suggestions in this research. Gratitude is due to all the members of Bridge and Structures Laboratory for their encouragement and friendship. The author is grateful to the Chinese government for the grant of CSC scholarship, enabling this study to be carried out. The support of Foreign Students Office (Ms. Hayashi and Ms. Sembokuya) is also gratefully acknowledged.

Finally, the author would like to praise and acknowledge the supports of her parents, relatives and boyfriend. Their sacrificial support, supplications and encouragement helped the author through desperate times, and empowered her with courage to complete this study. While this study was performing, many other teachers and friends have supported. The author would like to extend sincere appreciation to all the people who have helped for completing this thesis.

Xu Nan

September, 2012

TABLE OF CONTENTS

List of Figures

LIST OF TABLES

Chapter 1. INTRODUCTION

1.1. Background

The urgent concern about global warming from the emission of greenhouse gases has provided a strong impetus for engineers and scientists worldwide to research alternative renewable and clean energy. Mankind could be weaned from the 'dirty' burning of oil, gas and coal for the ever increasing energy demands to power development and modern living by switching to renewable and clean energy [1]. Wind power is one of the fastest growing renewable energy technologies.

The total amount of available power from the wind is considerably more than present human power use from all sources. At the end of 2011, worldwide nameplate capacity of wind-powered generators was 238 gigawatts (GW), growing by 41 GW over the preceding year. 2010 data from the World Wind Energy Association, an industry organization states that wind power now has the capacity to generate 430 TWh annually, which is about 2.5% of worldwide electricity usage [2]. Over the past five years (2010 data) the average annual growth in new installations has been 27.6 percent. Wind power market penetration is expected to reach 3.35 percent by 2013 and 8 percent by 2018. Several countries have already achieved relatively high levels of wind power penetration, such as 28% of stationary (grid) electricity production in Denmark (2011), 19% in Portugal (2011), 16% in Spain (2011) [3], 14% in Ireland (2010) and 8% in Germany (2011). As of 2011, 83 countries around the world are using wind power on a commercial basis [4]. The top 10 countries by wind power electricity production are tabulated in Table 1.1.

Table 1.1 Top 10 countries by wind power electricity production (2010 totals) [4]

Country	Wind power production (TWh)	% world total
United States	95.2	27.6
China	55.5	15.9
Spain	43.7	12.7
Germany	36.5	10.6
India	20.6	6.0
United Kingdom	10.2	3.0
France	9.7	2.8
Portugal	9.1	2.6
Italy	8.4	2.5
Canada	8.0	2.3
(rest of world)	(48.5)	(14.1)
World total	344.8 TWh	100%

Figure 1.1 shows the figures from Global Wind Energy Council (GWEC). It indicates that 2007 recorded an increase of installed capacity of 20 GW, taking the total installed wind energy capacity to 94 GW, up from 74 GW in 2006. Despite constraints facing supply chains for wind turbines, the annual market for wind continued to increase at an estimated rate of 37%, following 32% growth in 2006. Over the past five years the average growth in new installations has been 27.6 percent each year. In the forecast to 2013 the expected average annual growth rate is 15.7 percent. More than 200 GW of new wind power capacity could come on line before the end of 2013. Wind power market penetration is expected to reach 3.35 percent by 2013 and 8 percent by 2018 [5], [6].

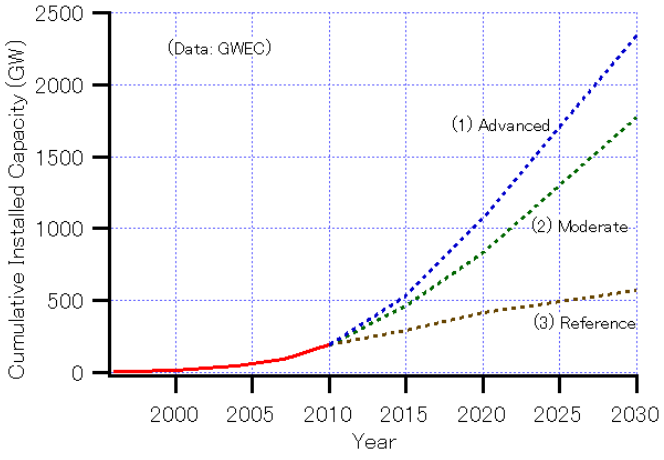

Figure 1.1 Worldwide installed wind power capacity forecast [5]

Onshore wind farms are, however, unsightly and they swallow up valuable land for agriculture and urban development. Already some countries, are considering constructing huge wind farms offshore to take advantage of the generally steadier and stronger winds found in the sea. Moreover, the wind turbines can be larger than those on land because they can be transported to the site by sea, so offshore wind power's contribution in terms of electricity supplied is higher.

1.2. Offshore Wind Power

Offshore wind power can help to reduce energy imports, reduce air pollution and greenhouse gases (by displacing fossil-fuel power generation), meet renewable electricity standards, and create jobs and local business opportunities. Figure 1.2 shows the Lillgrund Wind Farm in Sweden.

Figure 1.2 Aerial view of Lillgrund Wind Farm, Sweden

As of October 2010, 3.16 GW of offshore wind power capacity was operational, mainly in Northern Europe. According to BTM Consult, more than 16 GW of additional capacity will be installed before the end of 2014 and the UK and Germany will become the two leading markets. Offshore wind power capacity is expected to reach a total of 75 GW worldwide by 2020, with significant contributions from China and the US [7].

At the end of 2011, there were 53 European offshore wind farms in waters off Belgium, Denmark, Finland, Germany, Ireland, the Netherlands, Norway, Sweden and the United Kingdom, with an operating capacity of 3,813 MW [8], while 5,603 MW is under construction [9]. More than 100 GW (or 100, 000 MW) of offshore projects are proposed or under development in Europe. The European Wind Energy Association has set a target of 40 GW installed by 2020 and 150 GW by 2030 [10].

Table 1.2 shows the world's largest offshore wind farms. As of February 2012, Walney Wind Farm in the United Kingdom is the largest offshore wind farm in the world at 367 MW, followed by Thanet (300 MW), also in the United Kingdom.

Table 1.2 World's largest offshore wind farms

Wind farm	Capacity (MW)	Country	Commissioned
Walney	367	United Kingdom	2012
Thanet	300	United Kingdom	2010
Rødsand II	207	Denmark	2010
Lynn and Inner Dowsing	194	United Kingdom	2008
Horns Rev II	209	Denmark	2009

1.3. Floating Offshore Wind Turbines

As of 2003, existing offshore fixed-bottom wind turbine technology deployments had been limited to water depths of 30 m. Worldwide deep-water wind resources are extremely abundant in subsea areas with depths up to 600 m, which are thought to best facilitate transmission of the generated electric power to shore communities [11].

As of October 2010, new feasibility studies are supporting that floating turbines are becoming both technically and economically viable in the UK and global energy markets. "The higher up-front costs associated with developing floating wind turbines would be offset by the fact that they would be able to access areas of deep water off the coastline of the UK where winds are stronger and reliable" [12]. The recent Offshore Valuation study conducted in the UK has confirmed that using just one third of the UK's wind, wave and tidal resource could generate energy equivalent to 1 billion barrels of oil per year; the same as North Sea oil and gas production.

Ishihara and Yamaguchi [13] showed that the annual wind speed offshore is over 7m/s in the Kanto area of Japan. As shown in Figure 1.1 considering economic and social criteria the available potential is estimated to be 94TWh per year, which is nearly 32% of the annual demand of Tokyo Electric Power Company. Of this amount, only 0.4TWh per year can be exploited in areas where water depth is less than 20m employing bottom-mounted foundation. Almost, 60% of the total available potential is located in areas where water depth is between 20 and 200m. At such depths, the commonly used bottom mounted technology is not economically feasible. Figure 1.4 shows the progression of the offshore technology as the water depth increase. It is therefore essential in Japan to employ floating wind turbine technology to efficiently harvest the available offshore wind energy.

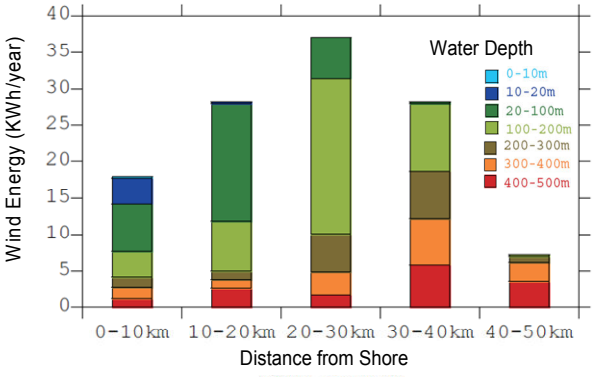

Figure 1.3 Offshore Wind Resource in Japan [13]

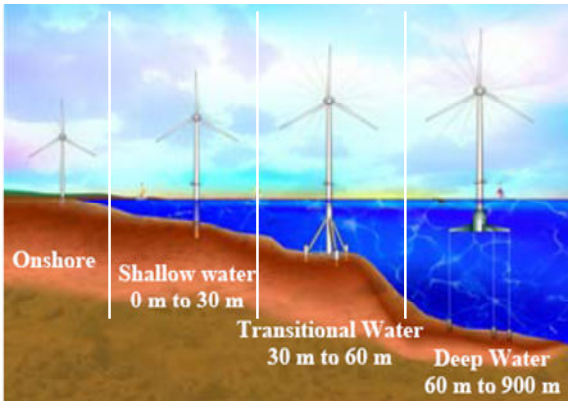

Figure 1.4 Progression of offshore wind technology [14]

All the existing floating wind turbines in the world are deployed in Europe. Blue H deployed the first 80 kW floating wind turbine 113 kilometers off the coast of Italy in December, 2007 (Figure 1.5 (a)). It was then decommissioned at the end of 2008 after completing a planned test year of gathering operational data. The wind turbine was neither grid connected nor operational during the trials. The first large-capacity, 2.3 megawatt floating wind turbine is Hywind (Figure 1.5 (b)), which became operational in the North Sea off of Norway in September 2009, and is still operational as of October 2010. In October 2011, Principle Power's Wind Float Prototype was installed 4km offshore of Agucadoura, Portugal in approximately 45m of water. The Wind Float was fitted with a Vestas V80 2.0MW offshore wind turbine and grid connected. The installation was the first offshore wind turbine to be deployed without the use of any offshore heavy lift vessels as the turbine was fully commissioned onshore prior to the unit being towed offshore. Additionally this is the first offshore wind turbine installed in open Atlantic waters and make use of a semi-submersible type floating foundation. SeaTwirl deployed their first floating grid connected wind turbine off the coast of Sweden in August, 2011. It was tested and de-commissioned. This design intends to store energy in a flywheel. Thus, energy could be produced even after the wind has stopped blowing [15].

The tower loading of floating wind turbine shall be much affected by significant floater motion due to wave, since wind turbines have large tower height and heavy nacelle and blades at tower top. Therefore, it is necessary to check whether the wind turbines designed for fixed foundation are suitable or not. This research will focus on two kinds of floating systems: tension-legged (TLP) mooring and catenary (CAT) mooring as shown in Figure 1.6. For TLP system, the surge motion is dominant, while the pitch motion is also critical and can't be neglected for CAT system. The influence of each motion on tower loading will be clarified theoretically using sway-rocking model.

(a) Blue H Prototype

(b) The world's first full-scale floating wind turbine, Hywind

Figure 1.5 Existing floating wind turbines

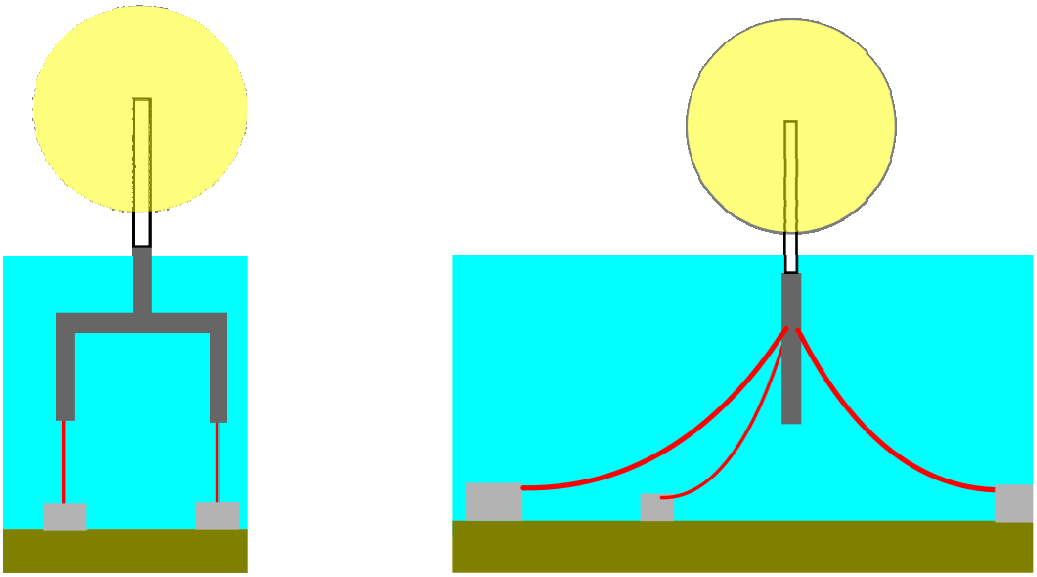

(a) TLP

(b) CAT

Figure 1.6 Types of Floating systems analyzed in this study

1.4. Thesis Outline

A layout of the thesis is shown in Figure 1.7.

Chapter 1 has given a general introduction to the current situation of development of wind energy and offshore wind power. It explains the necessity of using floating offshore wind turbines in Japan.

Chapter 2 reviews the research that has been undertaken pertaining to floating wind turbine technology thus far and gives the objectives of this research.

Chapter 3 proposes an equivalent sway-rocking model to consider the influences of floater motions on the tower loading of floating wind turbine systems, and the reason why the conventional fixed-foundation model can not be used is presented.

Chapter 4 proposes the theoretical formulae for wave-induced load with SR model and modal analysis. The influence of each floater motion is investigated separately and then their combination is performed. A non-Gaussian peak factor model is proposed to calculate the maximum wave-induced load under irregular wave.

Chapter 5 proposes the theoretical formulae for wind-induced load. The critical parameters in the equivalent static method are investigated to identify the dominant influence factors and their characteristics. SR model should be employed due to its reasonable frequency and damping ratio.

Chapter 6 presents the combination of wave-induced load and wind-induced load. By clarifying their characteristics, the load reduction factors are proposed for floating wind turbine systems.

Chapter 7 summarizes the current work, conclusions that can be deduced and suggestions for future study.

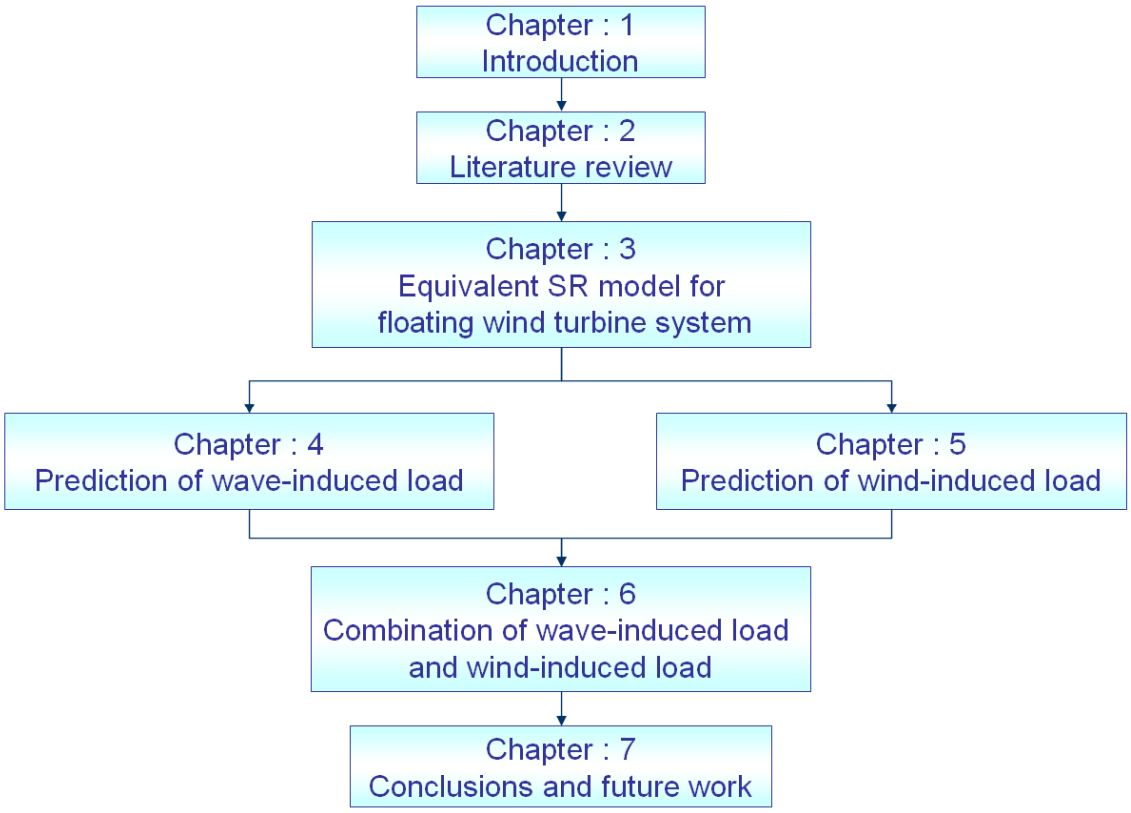

Figure 1.7 Layout of thesis

References

1. Wang C.M., Utsunomiya T., Wee S.C., Choo Y.S., “Research on floating wind turbines: a literature survey”. The IES Journal Part A: Civil & Structural Engineering, Vol. 3, No. 4, November 2010, 267–277.
2. World Wind Energy Report 2010. World Wind Energy Association. February 2011 [Retrieved 8-August-2011].
3. The Spanish electricity system: preliminary report 2011. Jan 2012. p. 13.
4. Renewables 2011: Global Status Report. p. 11.
5. GWEC, Global Wind Report Annual Market Update". Gwec.net. [Retrieved 14 May 2011].
6. Continuing boom in wind energy – 20 GW of new capacity in 2007. Gwec.net. [Retrieved 29 August 2010].
7. Madsen & Krogsgaard. Offshore Wind Power 2010 BTM Consult, 22 November 2010 [Retrieved: 22 November 2010].
8. Justin Wilkes et al. The European offshore wind industry key 2011 trends and statistics European Wind Energy Association, January 2012. [Accessed: 26 March 2012].
9. 17 EU countries planning massive offshore wind power ROV world, 30 November 2011. [Accessed: 10 December 2011].
10. Offshore Wind Energy. Environmental and Energy Study Institute, October 2010.
11. Musial W., Butterfield S., Boone A., “Feasibility of Floating Platform Systems for Wind Turbines”, [Retrieved 2009-09-10].
12. Floating turbines promise to deliver reliable wind, says report, guardian.co.uk, 2010-10-11. [Accessed 2010-11-02].
13. Ishihara T, Yamaguchi A. (2005), “Offshore Potential in Japan – Offshore Resource Assessment Using a Mesoscale Model and GIS”, Windtech International, 18-21.
14. Jonkman J.M. (2007), “Dynamic modeling and load analysis of an offshore floating wind turbine”, Department of Aerospace Engineering Sciences, University of Colorado, Ph.D dissertation.
15. Justin Wilkes et al. The European offshore wind industry key 2011 trends and statistics, p5. European Wind Energy Association, January 2012. [Accessed: 26 March 2012].

Chapter 2. LITERATURE REVIEW OF RESEARCH ON FLOATING WIND TURBINES

2.1. Introduction

In this chapter, a literature survey of research and development on floating wind turbines is presented. An overview of the research work that has been undertaken pertaining to floating wind turbine technology thus far is carried out, and based on its conclusions and limitations, objectives of this research are presented.

2.1.1. Components of a Floating Wind Turbine System

A floating support structure is recognized by the fact that the support comes from the water and not from the ground. Generally, the contact to the seabed is through anchor lines, also called mooring cables. All the different types of floating structures have their origin in the oil and gas industry, but modifications and hybrids are beginning to emerge in their use for wind turbines.

As shown in Figure 2.1, floating offshore wind turbine system can be divided into two major components: wind turbine and sub-structure. The wind turbine can be further divided into tower, rotor-nacelle assembly (RNA), with generator and gearbox equipment housed within the nacelle. The sub-structure is divided into floater system and mooring system. The mooring system consists of chain/ tether connecting floater to the anchor fixed to the seabed.

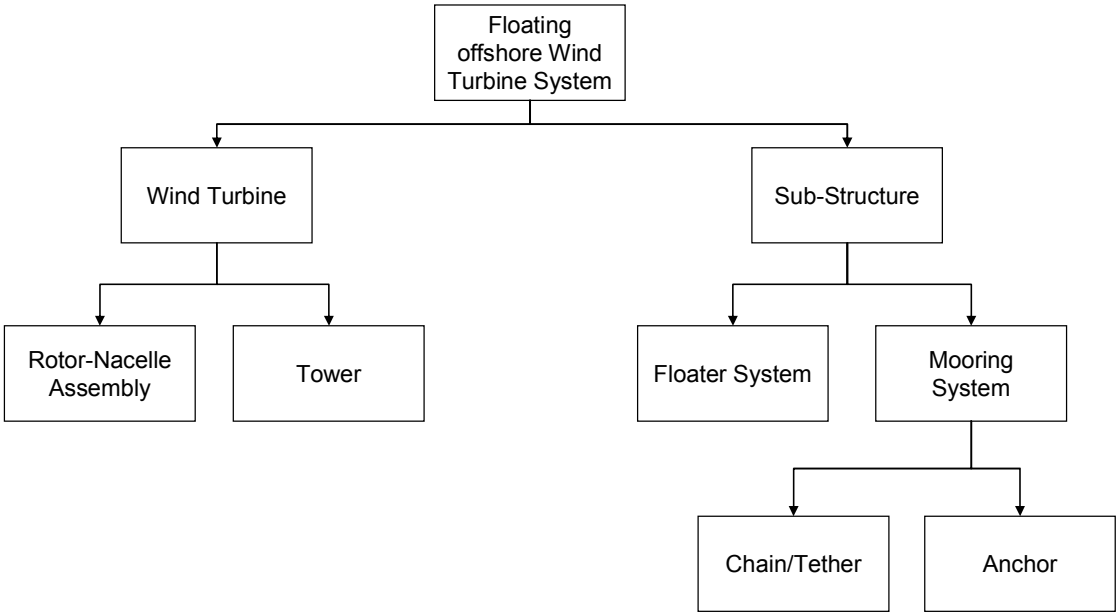

Figure 2.1 Components of floating offshore wind turbine [1]

2.1.2. Types of Floating Wind Turbines

Drawing from the design classifications of floating offshore platforms for the offshore oil and gas industry, floating wind turbines can also be categorized into four main types. They are:

- Spar-buoy type
- Tension-leg platform (TLP) type
- Semi-submersible type
- Pontoon-type.

Spar-buoy Type

As shown in Figure 2.2, the basic structure of the spar floater is cylindrical. It is a large tube that floats due to large amounts of air in the top of the structure, and stays upright due to a large amount of ballast at the bottom. The spar floater is secured to the seabed with mooring lines. It tilts slightly as the water and wind affects the structure. This is the main disadvantage for all floating concepts, as wind turbines are designed for a stable base and an angle no more than 0.5 degrees out of vertical. The solution for this in the case of the spar floater is weight. The larger the ballast, the calmer the movements. The advantage of the spar floater in comparison with other floaters is the small cross-section at the surface. This way, the spar floater is not as sensitive to wave motions.

Figure 2.2 Spar-buoy type floating wind turbine (Hywind) [2]

Tension Leg Platform Type (TLP)

Also in actual use is the tension leg platform or TLP for short. The TLP type comprises a floating platform structure to carry the wind turbine as shown in Figure 2.3.The Dutch company Blue H has so far been the only one to produce a tension leg platform. At full scale it will be suited for waters with depth over 60 meters. The principle of the tension leg platform is to create an underwater platform with buoyancy instead of the large amount of ballast to keep the structure stable. The buoyancy exceeds the weight of the platform and hence causes a pretension in the vertical cables which keep the platform on location. The legs can either be secured to a template (i.e. a large concrete ring) at the seabed, by individual piles or by suction anchors. The platform is kept underwater to create a small cross-section at the waterline. This limits the amount of hydrodynamic loads from waves.

Figure 2.3 TLP type floating wind turbine [3]

Semi-submersible Type

The semi-submersible type comprises a few large column tubes connected to each other by tubular members. A wind turbine may sit on one of the column tubes or there could be wind turbines sitting in all the columns. Alternatively, the wind turbine may be positioned at the geometric centre of the column tubes and supported by lateral bracing members. The column tubes provide the ballast and they are partially filled with water. This design is good in providing stability to the wind turbine and its relatively shallow draft allows for site flexibility. The semi-submersible floating wind turbine is kept in position by mooring lines. This type of floating wind turbine may be constructed onshore. Until now, there is no semi-submersible floating wind turbine in operation. Principle Power Inc. is promoting the semi-submersible type which consists of three column tubes with patented horizontal water entrapment heave plates at the bases as shown in Figure 2.4 (a). Figure 2.4 (b) shows another concept design of semi-submersible type as proposed by Ishihara et al. [4], [5]. It has three wind turbines seated on three tubular columns.

(a) Principle Power, Inc

(b) Ishihara et al [4], [5]

Figure 2.4 Semi-submersible type floating wind turbine

Pontoon Type

The pontoon-type has a very large pontoon structure to carry a group of wind turbines. The large pontoon structure achieves stability via distributed buoyancy and by taking advantage of the weighted water plane area for righting moment. The pontoon-type may be moored by conventional catenary anchor chains. The main advantage of this design would be the installation. It allows for complete installation in port, without any up-ending, lowering or other maneuvers that are needed for the other floating designs. However, the setback of the pontoon-type wind turbine is that the large surface makes it very receptive to hydrodynamic loads, and it is susceptible to the roll and pitch motions in waves experienced by ocean-going shipshaped vessels and may only be sited in calm seas, like

in a harbour, sheltered cove or lagoon. The National Maritime Research Institute (NMRI) in Tokyo has made some studies on such pontoon-type floating wind turbines, as shown in Figure 2.5.

Figure 2.5 Pontoon type floating wind turbine (NMRI) [http://www.nmri.go.jp/4]

2.1.3. Environmental Conditions

Offshore wind turbines are subject to some environmental conditions [20], such as:

- wind loads
- hydrodynamic loads induced by waves and current, including drag forces and inertia forces
- earthquake loads
- current-induced loads
- tidal effects
- marine growth
- snow and ice loads.

Among these environmental conditions, wind and wave are the essential ones which have the significant effect on the tower loading. Hence, wind and wave shall be considered in this study.

2.2. Previous Research

2.2.1. Dynamic Response Analysis with FEM

In order to properly explain the response characteristics of floating offshore wind turbine systems it is essential to understand their coupling behavior. Figure 2.6 shows the schematic representation this coupled behavior. The wind turbine is acted upon by inflowing wind producing aerodynamic loads that effect the Rotor, Nacelle and Tower while wave and currents results in hydrodynamic loads on floater and mooring system. In

addition mooring may also be affected by seabed contact. As shown, the dynamic behavior of each component of the system is codependent on one or more components. This indicates that the response of the system is mutually inter-dependent and linearization or simplification of a particular component, if done without considering the real situation might result is an inaccurate response prediction.

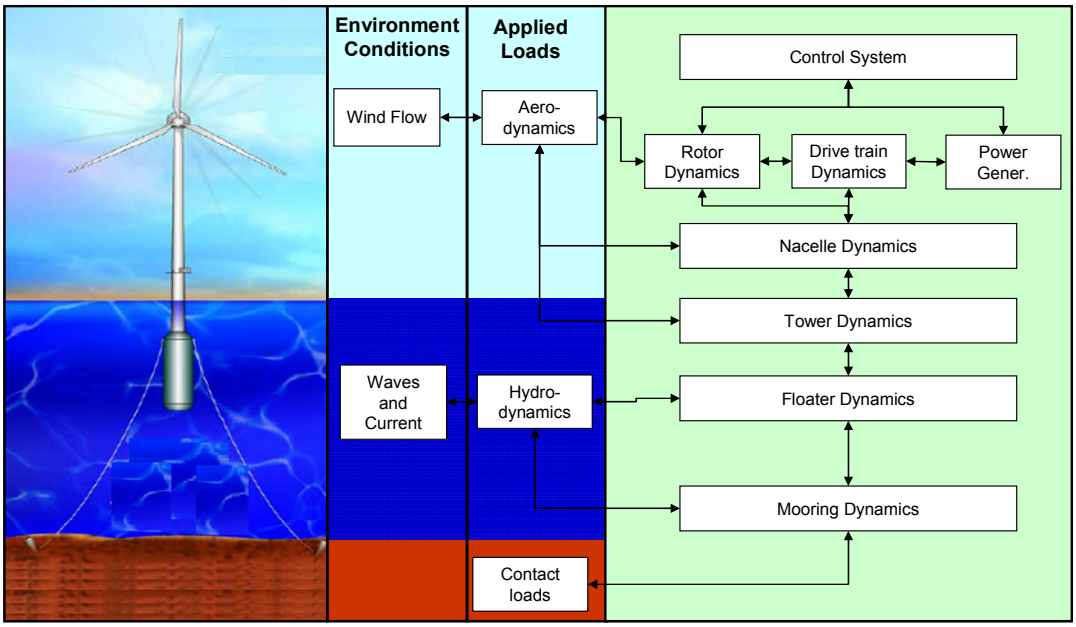

Figure 2.6 Schematic representation fully coupled floating wind turbine system [7]

A lot of research has been done on the design of the floater. Sophisticated simulation tools capable of fully coupled, integrated dynamic response analysis in combined wind and wave loading have been developed. The dynamic response characteristics of floating offshore wind turbine systems depend upon its several structural attributes. The most significant are:

- Aerodynamic effects from the rotor.
- Effect of control system of wind turbines.
- Hydrodynamic effects.
- Restoring effects.
- Resonance effect due to elastic deformations.
- Mooring system effect.

To have accurate and realistic prediction of dynamic response of floating wind turbine systems, all these attributes should be considered. Henderson [14] is one of the first to work on floating wind turbine systems. He investigated the contribution of floater motion to wind turbine tower and blade loads. He applied Morison's equation to large floating systems ignoring hydrodynamic damping and elastic effects. Ishihara and Phuc ([15], [16]) investigated a multi-turbine floater with slender elements to discuss resonance effects due

to elastic deformation. They also investigated contributions of hydrodynamic and aerodynamic damping discussing importance of these factors through comparison with water tank experiment. These studies ([14], [15], [16]), however, used linear model for mooring system and employed linear model for restoring force that can have significant effect on small semi-submersible floater having large response. Jonkman [7] recently discussed dynamic response for a single turbine barge floater system using an analytical model for Catenary mooring system, but accuracy of the model is not validated through experiment. In view of these studies, it is observed that use of nonlinear models for estimation of all applied forces in a coupled simulation is still required. Waris [1], developed a fully nonlinear finite element model to investigate dynamic response of floating offshore wind turbine systems considering coupling between wind turbine, floater and mooring system, thus can give more accurate and realistic prediction of floater motion and tower loading due to wind and wave. This model can use beam, truss and spring type elements. The time domain analysis enables the model to efficiently capture nonlinear effects. Morison equation with Srinivasan's Model is used for estimation of hydrodynamic force on the system, restoring force is investigated using a proposed non-hydrostatic model and mooring force is estimated using nonlinear model considering mooring contact with seabed for Catenary mooring and pre-tension for Tension Leg mooring [1]. This model has been verified by a water tank experiment. This study will employ Waris's model to simulate the floater motion and verify the analytical solution of tower loading.

Figure 2.7 shows the comparison of land-based wind turbine under the same wind conditions as considered for the offshore wind turbines. The loads for the two offshore cases is normalized w.r.t land based loads to represent the contribution of surge motion in case of tension legged mooring and surge and pitch motion for the Catenary mooring. It is obvious that floater motion increases the tower base moment. Waris [1] also discussed the contribution of the environmental loads. The wind turbine loads for Catenary mooring and Tension leg mooring are considered together. The two critical points for design of wind turbine is the tower base moment for support structure and the tower top moment for the yaw system. Figure 2.8 shows these two loads for the two types of mooring systems. The results show that both the wind and wave loads are critical for tower base, while wind loads govern the tower top for both types of mooring system. The pitch motion of floater increases the tower base and top moment, especially tower base moment.

The problem is that all the previous research is based on numerical simulation, and the wave-induced load and wind-induced load are coupled together and the effects from different degrees of freedom of floater motion are also coupled, as a result the contribution of each motion is unclear yet. In most of the real designs of floating offshore wind turbine, the work of wind engineers and ocean engineers is separated. The ocean engineers can provide the floater response without considering the effect from the superstructure (wind turbine part), and the wind engineers usually only concern the wind load acting on wind turbine. Hence, the most important significance of this study is providing the connection work for wind engineers to calculate the wave-induced load using the floater motion

provided by the ocean engineers. Therefore, it would make sense for the wave-induced load and wind-induced load to be investigated independently, and then their combination can be performed to get the final design value. For each kind of load, the analytical formulae should be proposed to make the application more convenient and identify their dominant influence factors as well, which would be very useful for the optimization of floating wind turbine system.

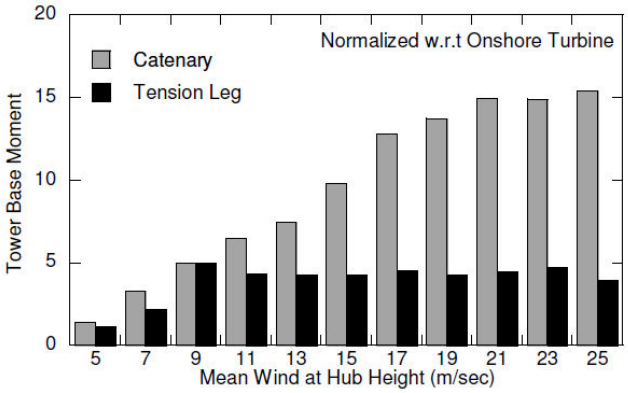

(a) Tower Base Moment

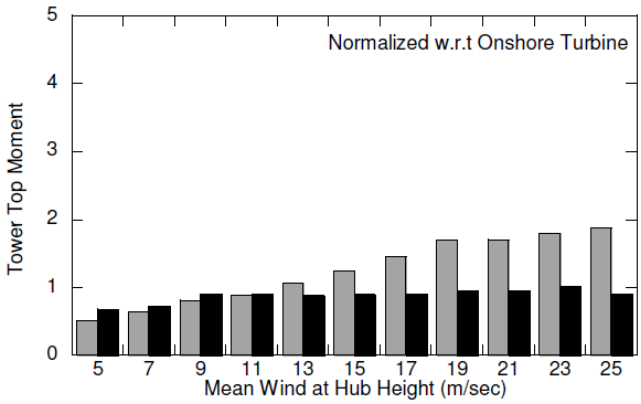

(b) Tower Top Moment

Figure 2.7 Comparison of tower load from Catenary and Tension Legged Mooring [1]

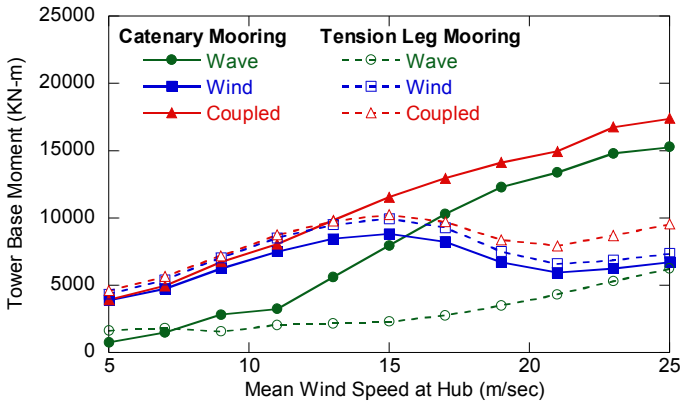

(a) Tower Base Moment

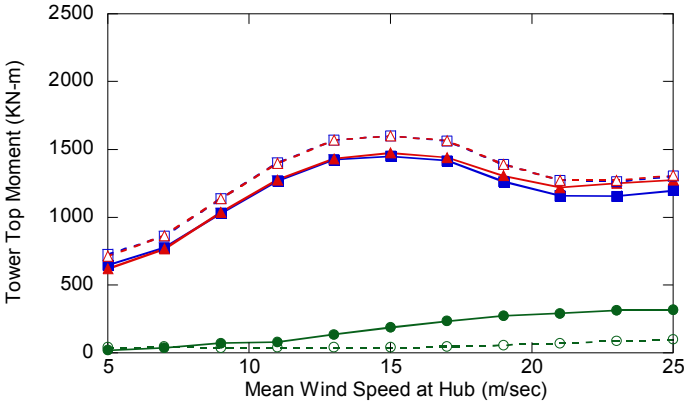

(b) Tower Top Moment

Figure 2.8 Standard Deviation of Wind turbine Loads of Tension Leg mooring [1]

2.2.2. Calculating Model

The floater system has six degrees of freedom, three translational (Surge, Sway and Heave) and three rotational (Roll, Pitch and Yaw) as shown in Figure 2.9. The tension legged mooring and catenary mooring shown in Figure 2.10, will be used in this research to investigate the influence of floater motion on tower loading, respectively.

Tension-Legged Mooring

For the tension-legged mooring the floater is buoyant by 15–25%. Vertical tethers anchored to the seabed are used to support the buoyant floater. The buoyancy results in very high pre-tension in the tethers. The restoring force for wave-induced floater motions is provided by these pre-tensioned tethers. In such mooring system, the heave motion is almost completely restrained, and depending on configuration, sway, pitch, roll and yaw may also be restraint [1]. Hence, the floater with tension-legged mooring is statically stable, and only the surge motion will have significant effect on the tower loading.

Catenary Mooring

Catenary moorings are defined by standard Catenary equation, which relate submerged weight of suspended lines, horizontal mooring load, line tension and line slope at fairlead. The restoring force for wave-induced floater motions is ensured by geometrical change in catenary shape and partially through axial elasticity of lines. Large geometrical changes make catenary mooring systems subject to significant dynamic effects due to transverse drag load. The chain length is usually so adjusted that the anchor does not experience any uplift force, which leads to a large portion of the line always lying on the seabed. This leads to a very large foot area for the mooring system but it is economical and easy to design [1]. Unlike the tension-legged mooring, the pitch motion will also affect the tower loading as well as the surge motion.

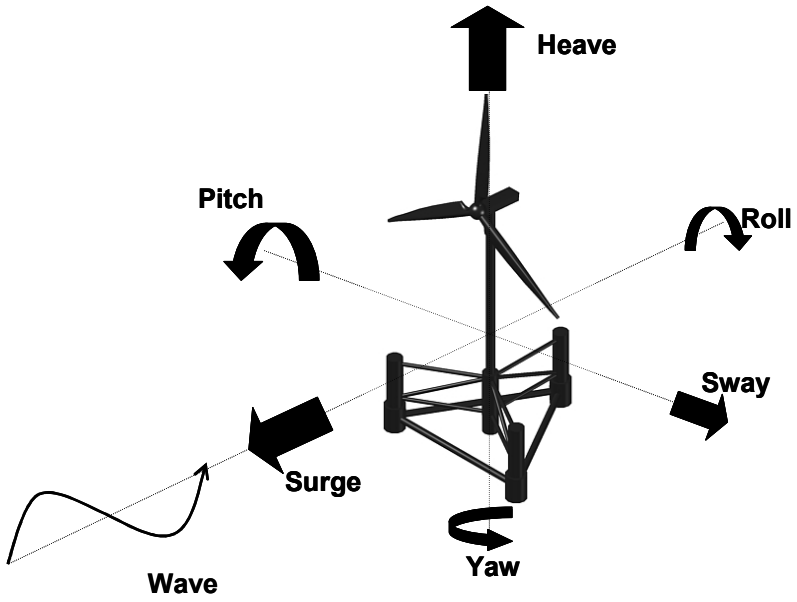

Figure 2.9 Degrees of freedom of a floating wind turbine system [1]

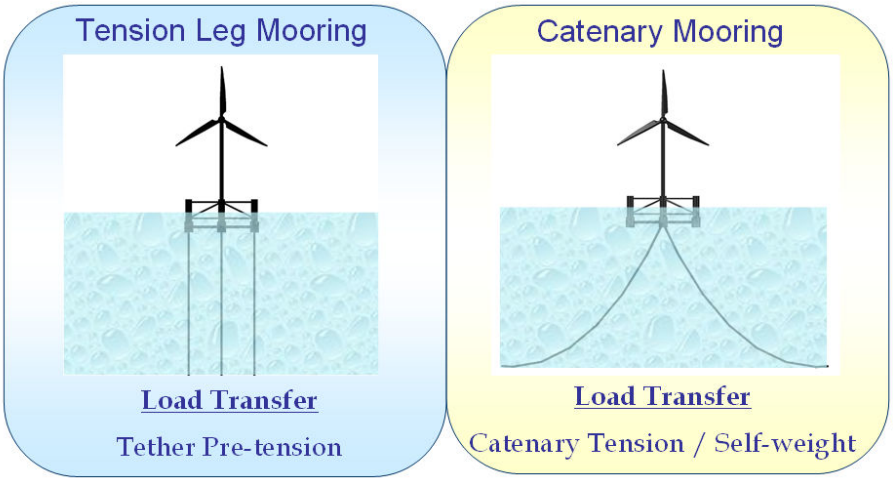

Figure 2.10 Types of Floating systems analyzed in this study

Wind engineers always consider the wind turbine as fixed-foundation. Takahashi [17] used the fixed-foundation model with acceleration acting on tower base to consider the influence of floater motion on the fatigue load, as shown in Figure 2.11. However, this fixed-foundation model is not verified, and in most cases it can't be used. Hence, in this study it is necessary to propose an equivalent sway-rocking model to consider the floater surge and pitch motions which have large influence on the tower loading of floating wind turbine, so that the tower loading can be estimated by the equivalent static method. Meanwhile, the problems of using conventional fixed-foundation model will be clarified. All these issues will be discussed in Chapter 3.

In the sway-rocking model shown in Figure 2.12, sway (surge motion) can be represented with the lateral spring and rocking (pitch motion) with rotational spring. The

effects of floater motion will be considered by acting a wave force on the floater in the sway-rocking model. Different from earthquake engineering, the stiffness, damping and wave force will be determined by known tower base response.

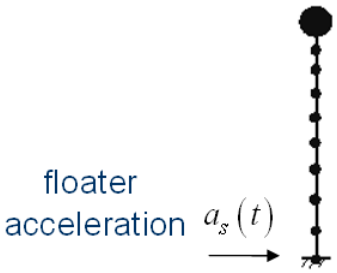

Figure 2.11 Fixed-foundation model

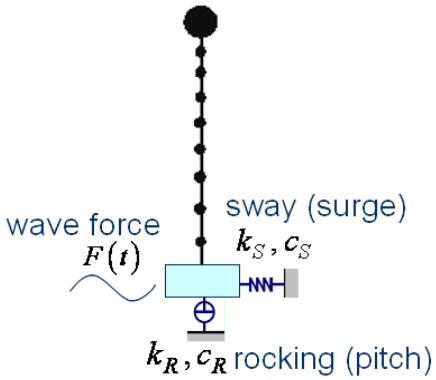

Figure 2.12 Sway-rocking model

2.2.3. Wave-induced Load

With SR model, the effect of sway motion as well as rocking motion can be determined separately by locking the other mode. Since the maximum response of sway and rocking can't occur simultaneously, the combination of them becomes important. Referring to the seismic loads specified in AIJ [18], square root of sum of squares (SRSS) and complete quadratic combination (CQC) are used for the combination. In Chapter 4, it will be determined which kind of combination can give good result for floating wind turbine system.

In addition, the superstructure is not considered in the floater motion. Hence, in the connection work, the coupling between wind turbine and floater should be considered, which will cause the tower vibration. The resonance of tower vibration results in the non-Gaussian feature and increases the tower loading. Therefore, a non-Gaussian peak factor model will be proposed, so that the maximum wave-induced load under irregular wave can be predicted by the equivalent static method.

2.2.4. Wind-induced Load

Unlike high-rise buildings and chimneys, wind turbines are designed based on the IEC classes, which requires the assessment of structural integrity by load calculations with reference to site specific conditions [9]. The wind load on wind turbine can be evaluated by FEM, but it requires the detailed information of wind turbine which is not usually available from the manufacture, and moreover, FEM is time-consuming and costly. Therefore, the formulae for wind load estimation are in need instead of FEM simulation. Wind Energy Handbook [10] adopts equivalent static method to estimate the design wind load of wind turbine, which is taken as a Gaussian process and the non-linear part of wind pressure is neglected. Therefore, for wind turbines exposed to high wind turbulence in mountain areas, the design wind load may be underestimated, since contribution of the non-linear part of wind pressure is large and the response is non-Gaussian. Binh et al. [11] considers the non-linear part of wind pressure in the mean wind load and proposed a non-Gaussian peak factor. This model gives a good performance for the prediction of design wind load compared with that in Wind Energy Handbook.

Binh's model is conducted for along-wind load which is maximum for stall-regulated wind turbine. IEC 61400-1 [9] specifies the abnormal case (loss of electrical network connection) in which the yaw control may fail at any wind direction. In some wind directions, the lift force on rotor may become significant, which is different from the conventional high-rise buildings and chimneys, and neglecting this across-wind load would underestimate the design load and cause the collapse of wind turbine [12], [13]. Therefore, the across-wind load should be considered and the combination with along-wind load is necessary as a matter of course. Waris [1] compared the wind loads between tension leg system and catenary system, which were found to be different, but no clear explanation was given yet. It also means that the fixed-foundation model can't be used to calculate the wind load, too. However, SR model can solve these problems. All these issues will be discussed in Chapter 5.

2.2.5. Combination of Wave-induced Load and Wind-induced Load

IEC 61400-3 [19] has given the combination of wave-induced load and wind-induced load for bottom-mounted wind turbine, using reduced extreme wind speed or reduced wave height. There is no stipulation about the combination for floating wind turbine system in IEC yet. Hence, first the correlation between wave-induced load and wind-induced load needs to be clarified. Furthermore, it needs to be confirmed whether the constant value of load reduction factor given in IEC for bottom-mounted system can be used for the floating wind turbine system or not. These will be the targets of Chapter 6.

2.3. Objectives of this Study

In view of the earlier discussions, the current research sets the following objectives:

- Propose an equivalent SR model to consider the influences of floater motions on the tower loading of floating wind turbine systems.
- Propose the evaluation formulae for wave-induced load with SR model, considering the non-Gaussian characteristics mainly due to the resonance of tower vibration.
- Propose the evaluation formulae for wind-induced load, identifying the characteristics of critical parameters, and explain why SR model should be used.
- Propose the load reduction factor for floating wind turbine systems in the combination of wave-induced load and wind-induced load, clarifying their correlation.

Reference

1. Syed Muhammad Bilal Waris Ali, Fully Nonlinear Finite Element Model for Dynamic Response Analysis of Floating Offshore Wind Turbine System, Ph. D dissertation, Department of Civil Engineering, The University of Tokyo, Japan, 2010.9.
2. Musial W., Butterfield S. and Boone A. (2003), “Feasibility of Floating Platform Systems for Wind Turbines”, NREL/CP-500-34874.
3. "Hywind floating wind turbine". Statoil. 2009-09-08. [Retrieved 2009-09-29].
4. Ishihara, T., Phuc, P.V., and Sukegawa, H., 2007a. Numerical study on the dynamic response of a floating offshore wind turbine system due to resonance and nonlinear wave. Proceedings of 2nd EOW, Berlin, Germany, December 4-6, 2007.
5. Ishihara, T., et al., 2007b. A study on the dynamic response of a semi-submersible floating offshore wind turbine system Part 1: a water tank test. Proceedings of the 12th International Conference on Wind Engineering, Cairns, Australia.
6. Henderson, A. R. (2000). "Analysis Tools for Large Floating Offshore Wind Farms," PhD Thesis, Unversity College London.
7. Jonkman J.M. (2007), “Dynamic modeling and load analysis of an offshore floating wind turbine”, Department of Aerospace Engineering Sciences, University of Colorado, Ph.D dissertation.
8. Phuc, P.V., (2008), “Dynamic response analysis of floating offshore wind turbine systems in the parked condition”, Ph.D. dissertation, Department of Civil Engineering, The University of Tokyo.
9. International Electrotechnical Commission, 2005. International Standard: Wind turbines – Part 1: Design requirements, IEC 61400-1, Edition 3.0, Geneva.
10. Burton, T., Sharpe, D., Jenkins, N., Bossanyi, E., 2001. Wind energy handbook. WILEY, England.
11. Binh, L.V., Ishihara, T., Phuc, P.V., Fujino, Y., 2008. A peak factor for non-Gaussian response analysis of wind turbine tower. Journal of Wind Engineering and Industrial Aerodynamics 96, 2217-2227.
12. Ishihara, T., Yamaguchi, A., Takahara, K., Mekaru, T., Matsuura, S., 2005a. An analysis of damaged wind turbines by Typhoon Maemi in 2003. Proceedings of 6th Asia-Pacific Conference on Wind Engineering, 1413-1428.
13. Ishihara, T., Phuc, P.V., Fujino, Y., Takahara, K., Mekaru, T., 2005b. A field test and full dynamic simulation on a stall regulated wind turbine. Proceedings of 6th Asia-Pacific Conference on Wind Engineering, 599-612.
14. A. Henderson, M. Patel, Rigid-Body Motion of a floating offshore wind farm, Int. Journal of Ambient Energy, Vol.19, No.3, 1998, pp: 167-180.

15. T. Ishihara, P.V. Phuc, H. Sukegawa, K. Shimada, T. Ohyama, A study on the dynamic response of a semisubmersible floating offshore wind turbine system Part 1: water tank test with considering the effect of wind load, ICWE12, Australia 2007.

16. P.V. Phuc, T. Ishihara, A study on the dynamic response of a semi-submersible floating offshore wind turbinesystem Part 2: Numerical simulation, ICWE12, Australia 2007.

17. Takahashi K., “Study on fatigue strength of wind turbine affected by floater motion and wind turbulence”, Master thesis, Department of Civil Engineering, The University of Tokyo, Japan, 2006.

18. Architectural Institute of Japan (AIJ), 2004. Recommendations for loads on buildings.

19. IEC-61400-3 (2008), Edition-1: Wind turbines – Part 3: Design requirements for offshore wind turbines.

20. Offshore Standard DNV-OS-J101, Design of offshore wind turbine structures, 2011.

Chapter 3. EQUIVALENT SR MODEL FOR FLOATING WIND TURBINE SYSTEM

3.1. Introduction

In this chapter, two kinds of mooring systems: tension leg mooring and catenary mooring are considered. The methods of describing the behavior of the wind turbines installed with these two kinds of mooring systems are presented. Takahashi [1] used the fixed-foundation model with acceleration acting on tower base to consider the influence of floater motion on the fatigue load. However, this fixed-foundation model is not verified, and in most cases it can't be used. Since surge and pitch are two main wave-induced motions, SR model is used as the equivalent calculating model to consider the influences of floater motions on the tower loading of floating wind turbine systems. The equivalent stiffness, damping and wave force (moment) for sway (surge) and rocking (pitch) modes are identified. The effect of each motion is investigated separately by locking the other mode. Meanwhile, a theoretical comparison between SR model and fixed-foundation model is performed with modal analysis and thus the problems of using the latter model have been clarified.

3.2. Full Model of Floating Wind Turbine System

This study will use a semi-submersible type floater installed with NREL 5-MW baseline wind turbine with catenary mooring and tension legged mooring to investigate the influence of floater motion to tower loading, respectively.

3.2.1. Properties of Floating Wind Turbine System

NREL 5-MW Baseline Wind Turbine

The National Renewable Energy Laboratory's (NREL) offshore 5-MW baseline wind turbine is used here. For detail regards the wind turbine reference made by Jonkman [2].

As the developed CAsT program is not able to consider pitch control, wind turbine is considered as stall regulated. The basic properties of this wind turbine are summarized in Table 3.1.

Table 3.1 Properties of NREL 5MW wind turbine [2]

Rated Power	5 MW
Rotor Orientation, Configuration	Upwind, 3-blades
Drivetrain	High Speed, Multi-stage gearbox
Rotor, Hub diameter	126, 3 m
Hub Height	90 m
Cut-In, Rated, Cut-Out wind speed	5.0, 11.4, 25 m/sec
Cut-In, Rated Rotor Speed	6.9 rpm, 12.1 rpm
OverHang, Tilt	5.0 m, 5.0°
Rotor Mass	110,000 Kg
Tower Mass	240,000 Kg

Semi-submersible Type Floater

The details of floater are available in Waris's doctoral dissertation [3]. The salient features of the floater are listed in Table 3.2.

Table 3.2 Details of semi-submersible floater [3]

Description	Detail	Dimension
Span		60.0 m
Submerged Depth		20.0 m
Overall Height		30.0 m
Total Weight		5,638,760 Kg
Peripheral Bracing		ϕ 2.5 m
Inner Bracing	Top Inclined Bottom	ϕ 1.8 m ϕ 1.8 m ϕ 1.8 m
Corner Column	Top Bottom	ϕ 9.0 m ϕ 10.0 m
Central Column		ϕ 9.0 m

Mooring System

The catenary mooring system is considered to consist on three mooring lines, each having span of 400 m. The mooring lines are separated at 120°, with front two lines having an angle of 60° with the incident wave and the third aligned in the wave direction. All the three lines have a common fairlead at the base of the central column of the floater that supports the wind turbine on top. The mooring arrangement is shown in Figure 3.1, where the circles denote nodes in the finite element model [3].

The tension legged mooring arrangement is shown in Figure 3.2. Three tethers are considered, that are connected to each of the corner columns. The mooring arrangement is so considered to eliminate pitching motion of the floater [3].

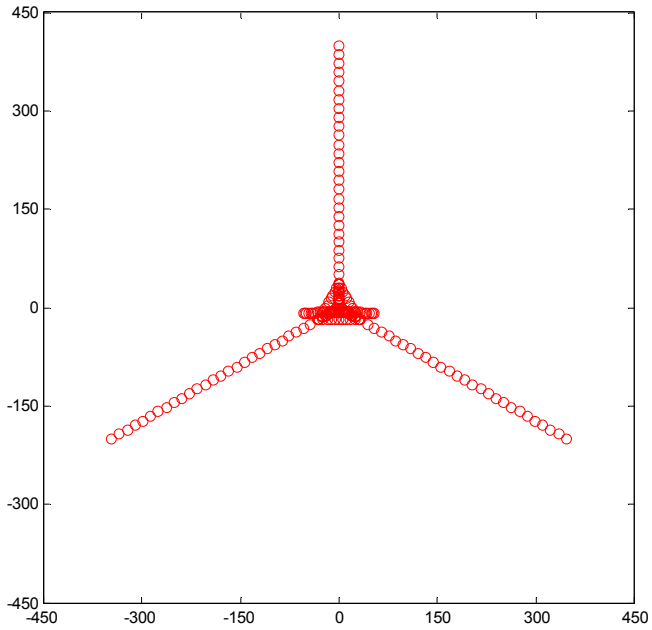

(a) Plan

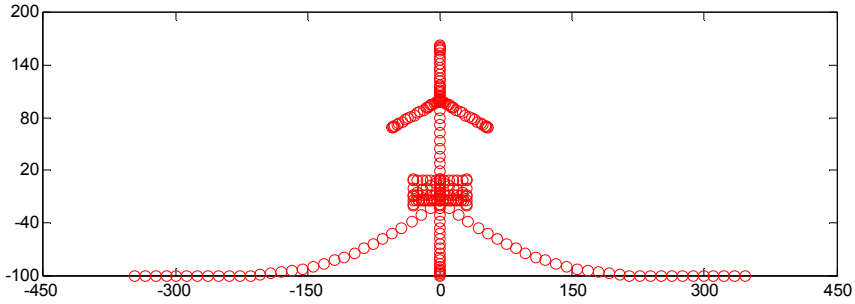

(b) Front Elevation

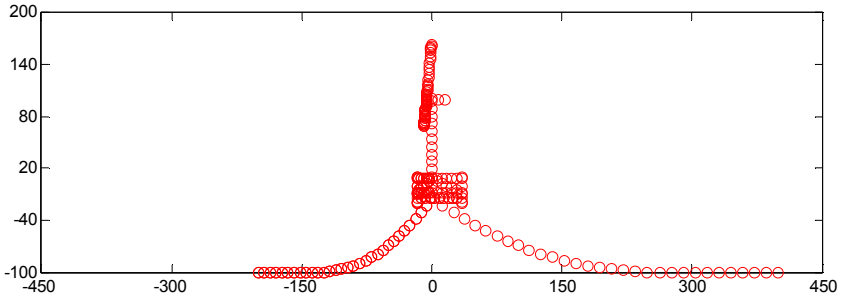

(c) Side Elevation

Figure 3.1 Catenary Mooring Arrangement [3]

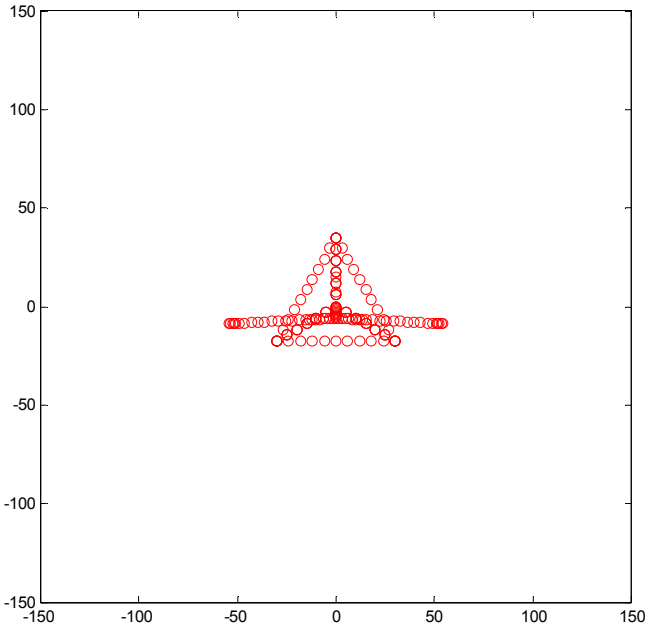

(a) Plan

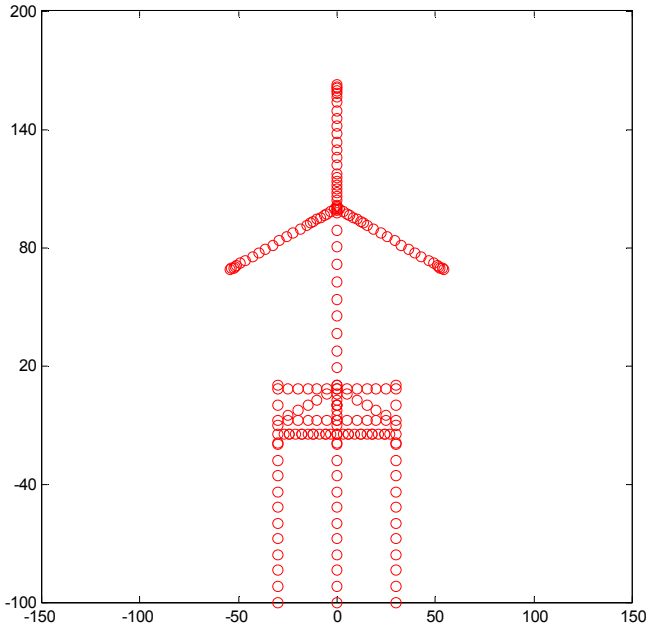

(b) Front Elevation

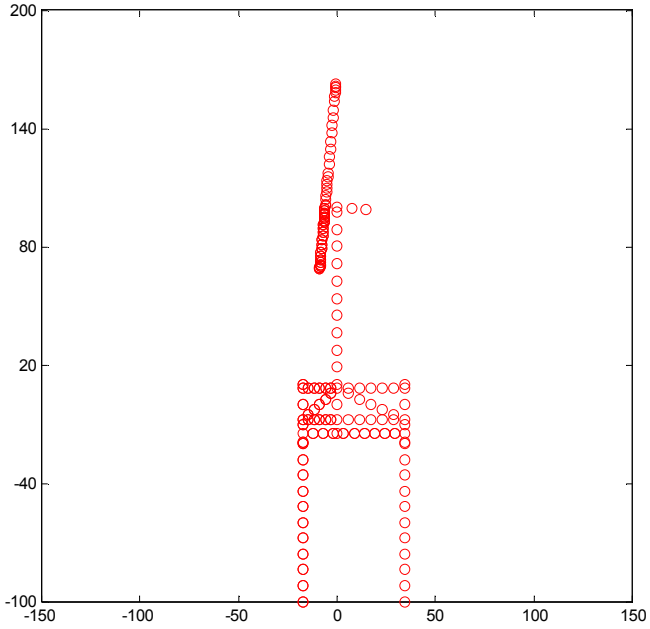

(c) Side Elevation

Figure 3.2 Tension Leg Mooring Arrangement [3]

3.2.2. Finite Element Model

A finite element model that can use beam, truss and spring type elements and can consider full coupled interaction between wind turbine, floater and mooring system has been developed by Waris [3]. The time domain analysis enables the model to efficiently capture nonlinear effects. Morison equation with Srinivasan's Model is used for estimation

of hydrodynamic force on the system, restoring force is investigated using a proposed non-hydrostatic model and mooring force is estimated using nonlinear model considering mooring contact with seabed for catenary mooring and pre-tension for tension leg mooring. For details of this finite element model refers to Waris's doctoral thesis [3], and here a summary of the numerical scheme and description of the FE-model are presented in Table 3.3 and Table 3.4.

Table 3.3 Description of the finite element numerical scheme

Dynamic Analysis	Direct Implicit Integration (Newmark- β)
Formulation	Total Lagrangian formulation
Convergence	Newton-Raphson Method
Damping Estimation	Caughey Series
Element Type	Ordinary Beam (12-DOF), Pre-stressed Beam (12-DOF), Truss (8-DOF),
Aerodynamic force	Quasi-static aerodynamic theory
Hydrodynamic Force	Morison Equation + Srinivasan Model
Restoring Force	Non-Hydrostatic Model
Mooring Force	Nonlinear
Seabed contact	Penalty Method

Table 3.4 Description of FE-model used in the study

Component	Description	No. of Element	Type
Wind Turbine	Tower	10	Beam
	Nacelle	4	Beam
	Blades	24/ blade	Beam
Floater	-	109	Beam
Mooring System	Catenary	30 / line	Truss
	Tension leg	10 / tether	Pre-stressed Beam

3.3. Sway-Rocking Model

In order to propose the analytical formulae for wave-induced tower loading, an equivalent calculating model of floating wind turbine system is in need. In this study, sway-rocking model shown in Figure 3.3 is borrowed from earthquake engineering [4] to clarify the contribution of each motion to the tower loading. The complex mooring system of

floating wind turbine system is modeled as two kinds of springs and dampers. Sway (surge motion) can be represented with the lateral spring and rocking (pitch motion) with rotational spring. The effects of floater motion will be considered by acting a wave force on the floater. Different from earthquake engineering, the stiffness, damping and wave force should be determined by known tower base response.

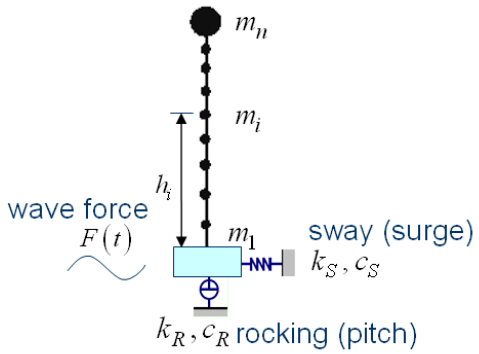

Figure 3.3 Sway-rocking model

Table 3.5 Lumped mass of wind turbine

	Node number i	Height from tower base h_i (m)	Lumped mass m_i (kg)
floater, added mass	1	0	4134403.52
tower	2	8.76	45861.86
	3	17.52	42825.06
	4	26.28	39891.40
	5	35.04	37060.89
	6	43.80	34333.51
	7	52.56	31709.23
	8	61.32	29188.10
	9	70.08	26770.12
	10	78.84	24455.25
three blades, hub, nacelle	11	87.60	361661.80

In order to give a clear explanation about the tower loading, the wind turbine (three blades, hub, nacelle, and tower) and floater can be modeled as 11 lumped masses (Table 3.5), since the aerodynamic force is not considered here. The mass of floater including the

added inertial mass is the base mass m_1. The added inertial mass is function of volume of half sphere under the floater base and will cause added inertia force [3]. The tower is divided into nine masses $m_2 \sim m_{10}$. The three blades are regarded as rigid approximately and can be modeled as a large mass m_{11} above the tower top with hub and nacelle together.

3.3.1. Stiffness and Damping

With the full model of floating wind turbine system, taking the superstructure (wind turbine and floater) as rigid body, the sway frequency ω_S and rocking frequency ω_R can be obtained by eigenvalue analysis or free vibration simulation using FEM. Thus, the stiffness of the two springs can be calculated as follows:

$$k_S = \left(\sum_{i=1}^{n} m_i \right) {\omega_S}^2 \qquad 3.1$$

$$k_R = \left(\sum_{i=1}^{n} m_i h_i^2 \right) {\omega_R}^2 \qquad 3.2$$

From the displacement time series of free vibration simulation, the sway damping ratio ξ_S and rocking damping ratio ξ_R can be recognized. Thus, the damping of the two dampers can be calculated as follows:

$$c_S = 2\left(\sum_{i=1}^{n} m_i \right) \omega_S \xi_S \qquad 3.3$$

$$c_R = 2\left(\sum_{i=1}^{n} m_i h_i^2 \right) \omega_R \xi_R \qquad 3.4$$

3.3.2. Equivalent Wave Force

Since the tower base response can be known from the ocean engineer in the real project, which means the displacement $[x_1]$, velocity $[v_1]$ and acceleration $[a_1]$ at the tower base are given. In this study, the tower base response can be obtained from simulation. With modal analysis, the equivalent wave force can be calculated.

Sway Direction

By locking the rocking motion as shown in Figure 3.4, the modal equation of motion of *j* th mode in sway direction is:

$$M_j^S \ddot{f}_j^S(t) + C_j^S \dot{f}_j^S(t) + M_j^S \omega_j^{S2} f_j^S(t) = \begin{bmatrix} \phi_{nj}^S \\ \vdots \\ \phi_{1j}^S \end{bmatrix}^T \begin{bmatrix} 0 \\ \vdots \\ F_{wave}(t) \end{bmatrix} = \phi_{1j}^S F_{wave}(t) \quad (j = 1, \cdots, n) \qquad 3.5$$

where $M_j^S = \sum_{k=1}^{n} m_k \phi_{kj}^{S2}$,

$$C_j^S = \sum_{k=1}^{n} c_k \phi_{kj}^{S2} \quad (c_1 = c_S)$$

M_j^S is the generalized mass, C_j^S is the generalized damping and ω_j^S is the modal natural frequency in radians per second, f_j^S is the modal displacement, $\phi_{kj}^S (k = 1, \cdots, n)$ is the normalized mode shape of the *j* th mode, and $F_{wave}(t)$ is the equivalent wave force in sway direction.

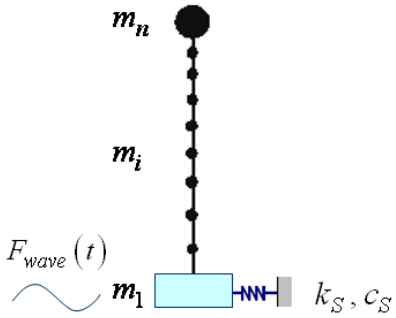

Figure 3.4 Sway model

In modal analysis the excitations of the various different natural modes of vibration are computed separately and the results superposed. Thus the displacement x_{kj}^S of the *j* th mode at node *k* is given by:

$$x_{kj}^S(t) = f_j^S(t) \cdot \phi_{kj}^S \qquad 3.6$$

If the regular wave is used, the modal displacement $f_j^S(t)$ can be shown as:

$$f_j^S(t) = \phi_{1j}^S F_{wave}(t) \left| H_j^S(\omega) \right| \qquad 3.7$$

$$\left| H_j^S(\omega) \right| = \frac{1}{M_j^S \omega_j^{S2} \sqrt{\left(1 - \beta_j^{S2}\right)^2 + 4\xi_j^{S2} \beta_j^{S2}}} \qquad 3.8$$

where $\beta_j^S = \frac{\omega}{\omega_j^S}$,

$$\xi_j^S = \frac{C_j^S}{2M_j^S \omega_j^S}$$

β_j^S is the ratio between external wave frequency ω and structural natural frequency, and ξ_j^S is the damping ratio, which can be identified by free vibration simulation or Eq. (5.44) in Chapter 5 for the first mode and the same way is used for ξ_j^R in rocking direction.

From Eqs. (3.6) and (3.7), the tower base displacement can be calculated as:

$$x_1^S(t) = \sum_{j=1}^{n} f_j^S(t)\phi_{1j}^S = F_{wave}(t)\sum_{j=1}^{n}\left|H_j^S(\omega)\right|\phi_{1j}^{S2} \qquad 3.9$$

Hence, the equivalent wave force in sway direction can be calculated as:

$$F_{wave}(t) = \frac{x_1^S(t)}{\sum_{j=1}^{n}\left|H_j^S(\omega)\right|\phi_{1j}^{S2}} \qquad 3.10$$

Rocking Direction

By locking the sway motion as shown in Figure 3.5, the modal equation of motion in rocking direction is:

$$M_j^R \ddot{f}_j^R(t) + C_j^R \dot{f}_j^R(t) + M_j^R \omega_j^{R2} f_j^R(t) = \begin{bmatrix} \phi_{nj}^R \\ \vdots \\ \phi_{1j}^R \end{bmatrix}^T \begin{bmatrix} 0 \\ \vdots \\ M_{wave}(t) \end{bmatrix} = \phi_{1j}^R M_{wave}(t) \qquad 3.11$$

where $M_j^R = \sum_{k=1}^{n} m_k h_k^2 \phi_{kj}^{R2}$,

$$C_j^R = \sum_{k=1}^{n} c_k \phi_{kj}^{R2} \quad (c_1 = c_R)$$

M_j^R is the generalized mass, C_j^R is the generalized damping and ω_j^R is the modal natural frequency in radians per second, f_j^R is the modal displacement, $\phi_{kj}^R(k = 1, \cdots, n)$ is the normalized mode shape of the *j* th mode, and $M_{wave}(t)$ is the equivalent wave moment in rocking direction.

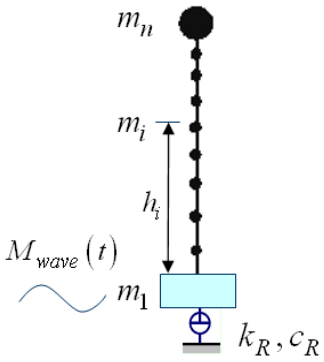

Figure 3.5 Rocking model

Thus the angular displacement θ_{kj}^R of the *j* th mode at node *k* is given by:

$$\theta_{kj}^R(t) = f_j^R(t) \cdot \phi_{kj}^R \tag{3.12}$$

The modal displacement $f_j^R(t)$ can be shown as:

$$f_j^R(t) = \phi_{1j}^R M_{wave}(t) \left| H_j^R(\omega) \right| \tag{3.13}$$

$$\left| H_j^R(\omega) \right| = \frac{1}{M_j^R \omega_j^{R2} \sqrt{\left(1-\beta_j^{R2}\right)^2 + 4\xi_j^{R2}\beta_j^{R2}}} \tag{3.14}$$

where $\beta_j^R = \dfrac{\omega}{\omega_j^R}$,

$$\xi_j^R = \frac{C_j^R}{2M_j^R \omega_j^R}$$

From Eqs. (3.12) and (3.13), the tower base angular displacement can be calculated as:

$$\theta_1^R(t) = \sum_{j=1}^{n} f_j^R(t) \phi_{1j}^R = M_{wave}(t) \sum_{j=1}^{n} \left| H_j^R(\omega) \right| \phi_{1j}^{R2} \tag{3.15}$$

Hence, the equivalent wave moment can be calculated as:

$$M_{wave}(t) = \frac{\theta_1^R(t)}{\sum_{j=1}^{n} \left| H_j^R(\omega) \right| \phi_{1j}^{R2}} \tag{3.16}$$

From Eqs. (3.10) and (3.16), the equivalent wave force or moment can be calculated with the tower base displacement, damping ratio, the ratio between external wave frequency and structural natural frequency, and the mode shape of tower base.

3.4. Verification of Sway-Rocking Model

The natural periods of the two kinds of floating wind turbine system are tabulated in Table 3.6. The first mode shape is shown in Figure 3.6. It is noticed that the sway-rocking model is able to give very close natural periods and mode shape to the full model.

Figure 3.7 shows the comparison of the shear force on wind turbine tower. It is obvious that sway-rocking model shows good agreement with full model. Therefore, sway-rocking model is verified as the equivalent model to calculate the wave-induced tower loading for floating wind turbine system.

Table 3.6 The first natural periods

	Tension leg Full model / SR model	Catenary Full model / SR model
Sway	31.3 s / 31.9s	26.8s / 26.2s
Rocking	-	14.3s / 15.0s

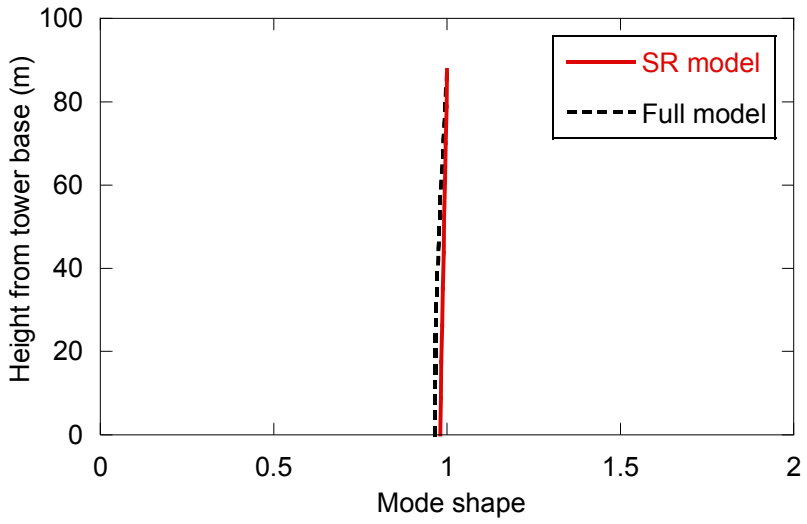

(a) Sway of tension leg system

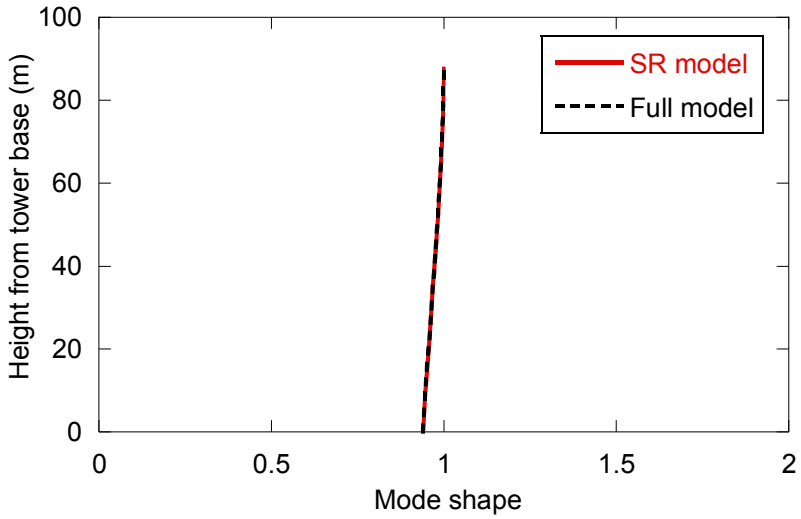

(b) Rocking of catenary system

Figure 3.6 The first mode shape of wind turbine tower

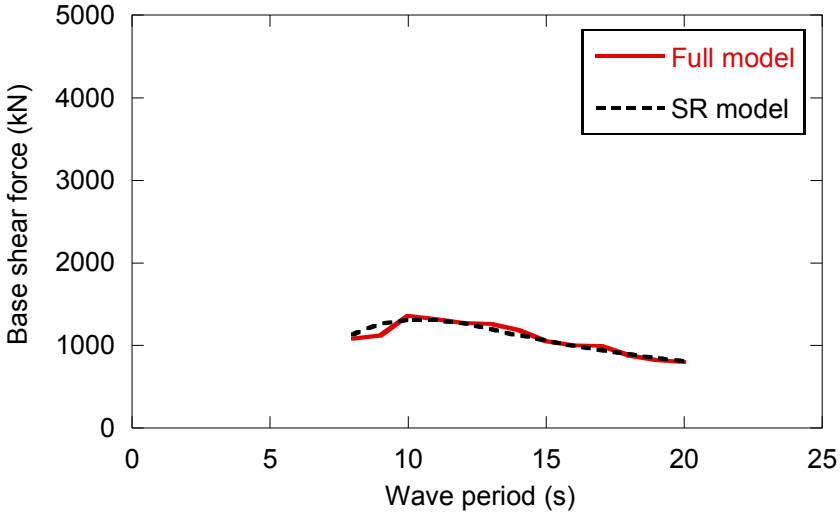

(a) Base shear force

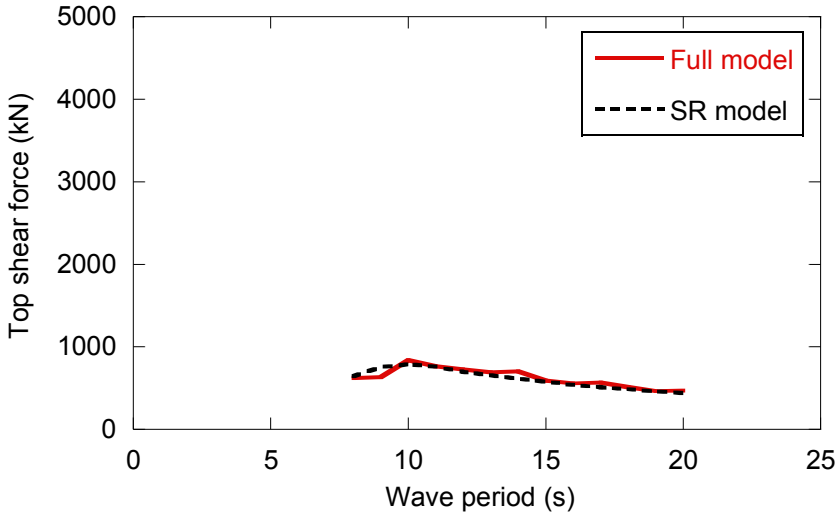

(b) Top shear force

Figure 3.7 The shear force on wind turbine tower of tension leg system

3.5. Comparison between SR Model and Fixed-foundation Model

A theoretical comparison between sway-rocking model and fixed-foundation model is performed to make their difference clear. The shear force at different tower height is derived with modal analysis for the sway-rocking model and fixed-foundation model. For the two models, since the first mode is dominant, the shear force from the first mode is compared.

3.5.1. Shear Force of Sway-Rocking Model

Sway Direction

From Eq. (3.6), the displacement at node *k* can be calculated as:

$$x_k^S = \sum_{j=1}^{n} f_j^S(t)\phi_{kj}^S \tag{3.17}$$

Then substituting (3.7), the acceleration at node *k* can be calculated as:

$$\ddot{x}_k^S = \sum_{j=1}^{n} \ddot{f}_j^S(t)\phi_{kj}^S = -\omega^2 \sum_{j=1}^{n} f_j^S(t)\phi_{kj}^S = -\omega^2 F_{wave}(t) \sum_{j=1}^{n} \left| H_j^S(\omega) \right| \phi_{1j}^S \phi_{kj}^S \tag{3.18}$$

Then the shear force at node *i* can be calculated as:

$$Q_i^S(t) = \sum_{k=i}^{n} m_k \ddot{x}_k^S = -\omega^2 F_{wave}(t) \sum_{k=i}^{n} m_k \sum_{j=1}^{n} \left| H_j^S(\omega) \right| \phi_{1j}^S \phi_{kj}^S \quad 3.19$$

Since the equivalent wave force $F_{wave}(t)$ is calculated from the tower base response, the shear force due to sway motion can be obtained from the tower base response as well:

$$Q_i^S(t) = \sum_{k=i}^{n} m_k \frac{\ddot{x}_k^S}{\ddot{x}_1^S} a_S(t) = \sum_{k=i}^{n} m_k a_S(t) \frac{\sum_{j=1}^{n} \left| H_j^S(\omega) \right| \phi_{1j}^S \phi_{kj}^S}{\sum_{j=1}^{n} \left| H_j^S(\omega) \right| \phi_{1j}^{S\,2}} \quad 3.20$$

where $a_S(t)$ is the known sway acceleration at tower base. If only the first mode is considered, the shear force becomes

$$Q_i^S(t) = \sum_{k=i}^{n} m_k a_S(t) \frac{\phi_{k1}^S}{\phi_{11}^S} = \sum_{k=i}^{n} m_k a_S(t) \left(1 + \frac{\Delta\phi_{k1}^S}{\phi_{11}^S} \right) \quad 3.21$$

where $\Delta\phi_{k1}^S = \phi_{k1}^S - \phi_{11}^S$. $\Delta\phi_{k1}^S / \phi_{11}^S$ is defined as the elastic/solid ratio of mode shape at node *k*.

Rocking Direction

From Eq. (3.12), the angular displacement at node *k* can be calculated as:

$$\theta_k^R = \sum_{j=1}^{n} f_j^R(t) \phi_{kj}^R \quad 3.22$$

Then substituting (3.13), the angular acceleration at node *k* can be expressed as:

$$\ddot{\theta}_k^R = \sum_{j=1}^{n} \ddot{f}_j^R(t) \phi_{kj}^R = -\omega^2 \sum_{j=1}^{n} f_j^R(t) \phi_{kj}^R = -\omega^2 M_{wave}(t) \sum_{j=1}^{n} \left| H_j^R(\omega) \right| \phi_{1j}^R \phi_{kj}^R \quad 3.23$$

The linear displacement at node *k* can be expressed as:

$$x_k^R = \sum_{r=1}^{k-1} \theta_r^R (h_{r+1} - h_r) \quad 3.24$$

Then substituting (3.23), the linear acceleration at node *k* can be calculated as:

$$\begin{aligned}\ddot{x}_k^R &= \sum_{r=1}^{k-1} \ddot{\theta}_r^R \left(h_{r+1} - h_r\right) \\ &= -\omega^2 M_{wave}(t) \sum_{r=1}^{k-1} \left(h_{r+1} - h_r\right) \sum_{j=1}^{n} \left|H_j^R(\omega)\right| \phi_{1j}^R \phi_{rj}^R\end{aligned} \tag{3.25}$$

Then the shear force at node *i* can be calculated as:

$$\begin{aligned}Q_i^R(t) &= \sum_{k=i}^{n} m_k \ddot{x}_k^R \\ &= -\omega^2 M_{wave}(t) \sum_{k=i}^{n} m_k \sum_{r=1}^{k-1} \left(h_{r+1} - h_r\right) \sum_{j=1}^{n} \left|H_j^R(\omega)\right| \phi_{1j}^R \phi_{rj}^R\end{aligned} \tag{3.26}$$

Like sway direction, since the equivalent wave moment $M_{wave}(t)$ is calculated from the tower base response, the shear force due to rocking motion can be obtained from the tower base response as well:

$$\begin{aligned}Q_i^R(t) &= \sum_{k=i}^{n} m_k \sum_{r=1}^{k-1} \frac{\ddot{\theta}_r^R}{\ddot{\theta}_1^R} a_R(t) \left(h_{r+1} - h_r\right) \\ &= \sum_{k=i}^{n} m_k a_R(t) \sum_{r=1}^{k-1} \frac{\sum_{j=1}^{n} \left|H_j^R(\omega)\right| \phi_{1j}^R \phi_{rj}^R}{\sum_{j=1}^{n} \left|H_j^R(\omega)\right| \phi_{1j}^{R2}} \left(h_{r+1} - h_r\right)\end{aligned} \tag{3.27}$$

where $a_R(t)$ is the known rocking acceleration at tower base. If only the first mode is considered, the shear force becomes

$$Q_i^R(t) = \sum_{k=i}^{n} m_k a_R(t) \sum_{r=1}^{k-1} \frac{\phi_{r1}^R}{\phi_{11}^R} \left(h_{r+1} - h_r\right) = \sum_{k=i}^{n} m_k a_R(t) \left(h_k + \sum_{r=1}^{k-1} \frac{\Delta\phi_{r1}^R}{\phi_{11}^R} \left(h_{r+1} - h_r\right) \right) \tag{3.28}$$

where $\Delta\phi_{r1}^R = \phi_{r1}^R - \phi_{11}^R$. $\Delta\phi_{r1}^R / \phi_{11}^R$ is defined as the elastic/solid ratio of mode shape at node *r*.

3.5.2. Shear Force of Fixed-foundation Model

The sway and rocking acceleration at tower base from the FEM simulation of floating wind turbine system will be used to a fixed-foundation wind turbine in each corresponding direction.

Sway Direction

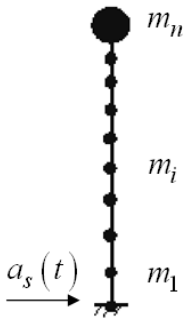

Figure 3.8 Fixed-foundation model with sway acceleration

Figure 3.8 shows the fixed-foundation model with sway acceleration. The modal equation of motion is expressed as:

$$M_j \ddot{f}_j^s(t) + C_j \dot{f}_j^s(t) + M_j \omega_j^2 f_j^s(t) = -a_S(t) \sum_{k=1}^{n} m_k \phi_{kj} \qquad 3.29$$

where $M_j = \sum_{k=1}^{n} m_k \phi_{kj}^2$,

$$C_j = \sum_{k=1}^{n} c_k \phi_{kj}^2$$

M_j is the generalized mass, C_j is the generalized damping and ω_j is the modal natural frequency in radians per second, f_j^s is the modal displacement, ϕ_{kj} is the normalized mode shape of the *j* th mode.

Thus the displacement x_{kj}^s of the *j* th mode at node *k* is given by:

$$x_{kj}^s(t) = f_j^s(t) \cdot \phi_{kj} \qquad 3.30$$

The modal displacement $f_j^s(t)$ can be shown as:

$$f_j^s(t) = \frac{-a_S(t) \sum_{k=1}^{n} m_k \phi_{kj}}{M_j \omega_j^2} \cdot D_j(\omega) \qquad 3.31$$

$$D_j(\omega) = \frac{1}{\sqrt{\left(1-\beta_j^2\right)^2 + 4\xi_j^2 \beta_j^2}} \qquad 3.32$$

where $\beta_j = \dfrac{\omega}{\omega_j}$,

$$\xi_j = \frac{C_j}{2M_j\omega_j}$$

$D_j(\omega)$ is the dynamic magnification factor, β_j is the ratio between external wave frequency and structural frequency, and ξ_j is the damping ratio.

Then the acceleration is expressed as:

$$\ddot{x}_{kj}^s(t) = \ddot{f}_j^s(t)\cdot\phi_{kj} = \frac{\omega^2 a_S(t)\sum_{k=1}^{n} m_k\phi_{kj}}{M_j\omega_j^2}\cdot D_j(\omega)\cdot\phi_{kj} = \gamma_j^s\cdot\phi_{kj}\cdot A_j(\beta_j,\xi_j)\cdot a_S(t) \tag{3.33}$$

$$\gamma_j^s = \frac{\sum_{k=1}^{n} m_k\phi_{kj}}{\sum_{k=1}^{n} m_k\phi_{kj}^2} \tag{3.34}$$

$$A_j(\beta_j,\xi_j) = \frac{\beta_j^2}{\sqrt{\left(1-\beta_j^2\right)^2 + 4\xi_j^2\beta_j^2}} \tag{3.35}$$

where γ_j^s is the well-known participation factor. Therefore, the shear force at node *i* of tower can be calculated as:

$$Q_{i,s}^F(t) = \sum_{k=i}^{n} m_k\left(\sum_{j=1}^{n}\ddot{x}_{kj}^s(t) + a_S(t)\right) = \sum_{k=i}^{n} m_k\left(\sum_{j=1}^{n}\gamma_j^s\phi_{kj}A_j(\beta_j,\xi_j)a_S(t) + a_S(t)\right) \tag{3.36}$$

If only the first mode is considered, the shear force becomes

$$Q_{i,s}^F(t) = \sum_{k=i}^{n} m_k a_S(t)\left(1+\gamma_1^s\phi_{k1}A_1(\beta_1,\xi_1)\right) \tag{3.37}$$

Rocking Direction

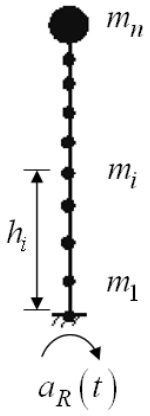

Figure 3.9 Fixed-foundation model with rocking acceleration

Figure 3.9 shows the fixed-foundation model with rocking acceleration. The modal equation of motion is expressed as:

$$M_j \ddot{f}_j^r(t) + C_j \dot{f}_j^r(t) + M_j \omega_j^2 f_j^r(t) = -a_R(t) \sum_{k=1}^{n} m_k \phi_{kj} h_k \qquad 3.38$$

The displacement x_{kj}^r of the *j* th mode at node *k* is given by:

$$x_{kj}^r(t) = f_j^r(t) \cdot \phi_{kj} \qquad 3.39$$

The modal displacement $f_j^r(t)$ can be shown as:

$$f_j^r(t) = \frac{-a_R(t) \sum_{k=1}^{n} m_k \phi_{kj} h_k}{M_j \omega_j^2} \cdot D_j(\omega) \qquad 3.40$$

Then the acceleration is expressed as:

$$\ddot{x}_{kj}^r(t) = \ddot{f}_j^r(t) \cdot \phi_{kj} = \frac{\omega^2 a_R(t) \sum_{k=1}^{n} m_k \phi_{kj} h_k}{M_j \omega_j^2} \cdot D_j(\omega) \cdot \phi_{kj} = \gamma_j^r \cdot \phi_{kj} \cdot A_j(\beta_j, \xi_j) \cdot a_R(t) \qquad 3.41$$

$$\gamma_j^r = \frac{\sum_{k=1}^{n} m_k \phi_{kj} h_k}{\sum_{k=1}^{n} m_k \phi_{kj}^2} \qquad 3.42$$

where γ_j^r is the participation factor for the rocking direction. Therefore, the shear force at node *i* of tower can be calculated as:

$$Q_{i,r}^F(t)=\sum_{k=i}^{n}m_k\left(\sum_{j=1}^{n}\ddot{x}_{kj}^r(t)+a_R(t)h_k\right)=\sum_{k=i}^{n}m_k\sum_{j=1}^{n}\gamma_j^r\phi_{kj}A_j(\beta_j,\xi_j)a_R(t)+\sum_{k=i}^{n}m_k a_R(t)h_k \quad 3.43$$

If only the first mode is considered, the shear force becomes

$$Q_{i,r}^F(t)=\sum_{k=i}^{n}m_k a_R(t)\left(h_k+\gamma_1^r\phi_{k1}A_1(\beta_1,\xi_1)\right) \quad 3.44$$

3.5.3. Comparison of Shear Force

Taking the sway direction as example, from Eqs. (3.21) and (3.37) it is found that both the shear forces of the sway-rocking model and fixed-foundation model consist of solid part and elastic part, as shown in Figure 3.10. The solid parts are totally same, but the elastic parts are different. Therefore, the elastic parts of the shear force on the tower base are compared for the two models in this research.

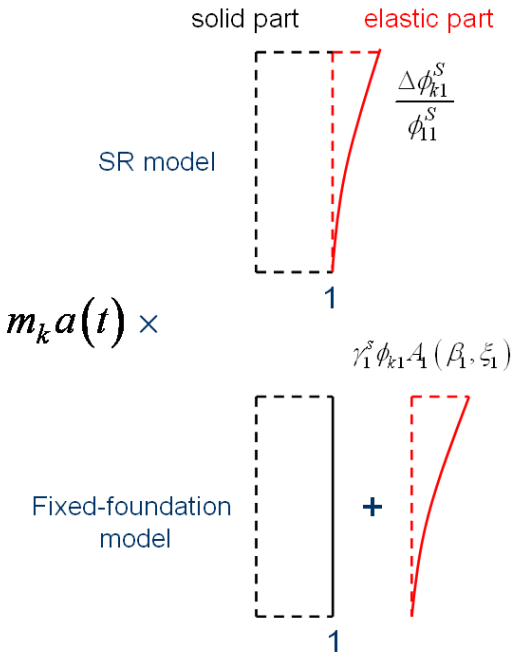

Figure 3.10 Solid part and elastic part of shear force

SR Model

From Figure 3.10, it can be seen that the elastic part of shear force for SR model is the function of elastic/solid ratio of mode shape $\Delta\phi_{k1}^S/\phi_{11}^S$. The mode shape will change with the stiffness k_S of sway spring, as shown in Figure 3.11. Take the elastic/solid ratio of

mode shape at tower top $\Delta\phi_{n1}^S / \phi_{11}^S$ as indicator. It increases when the stiffness k_S increases. Since the solid parts of the two models are the same, the elastic part of shear force is normalized by the solid part, as shown in Figure 3.12. It is noticed that the elastic part increases with $\Delta\phi_{n1}^S / \phi_{11}^S$ linearly, which means it increases when the stiffness k_S increases.

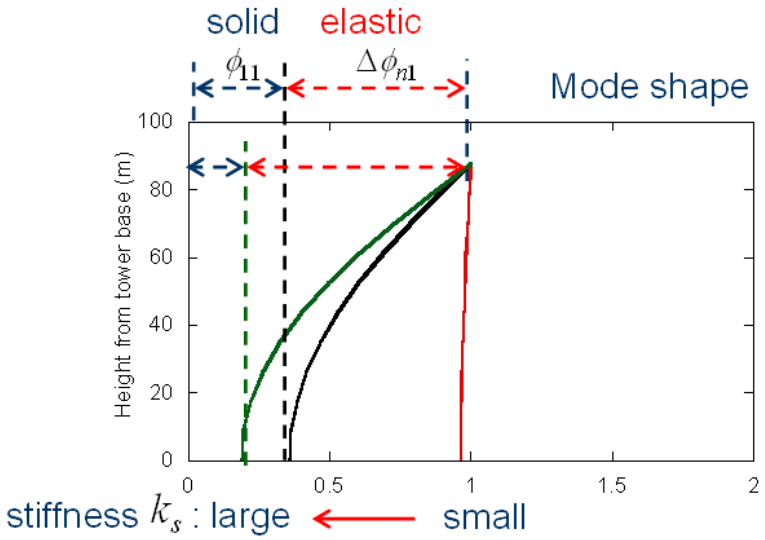

Figure 3.11 Variation of mode shape of SR model with stiffness k_S

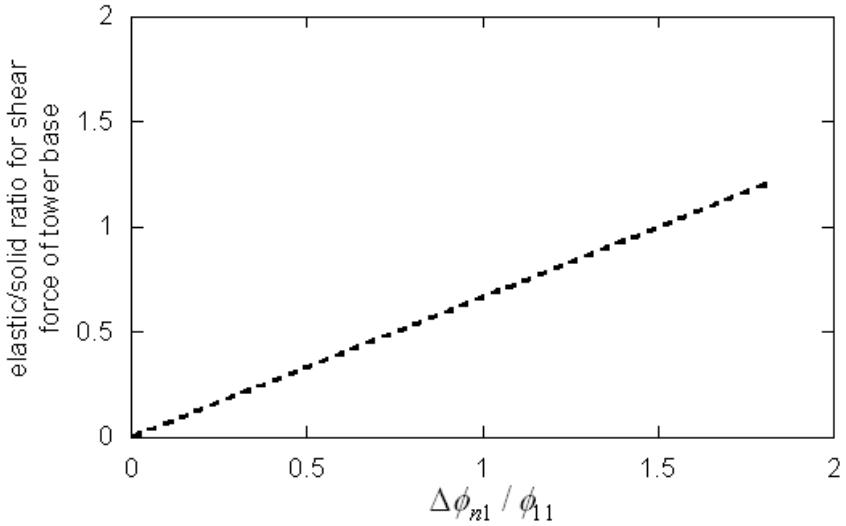

Figure 3.12 Elastic part of shear force normalized by solid part for SR model

Fixed-foundation Model

For fixed-foundation model, from Figure 3.10 it can be seen that the elastic part of shear force is the function of β_1, the ratio between external wave frequency and structural natural frequency. It can be interpreted as that the elastic part of shear force only change

with T/T_1, the ratio between external wave period and tower natural period, as shown in Figure 3.13. If T/T_1 is larger than 1, the elastic part of shear force decreases when T/T_1 increases, which means it decreases with the external wave period.

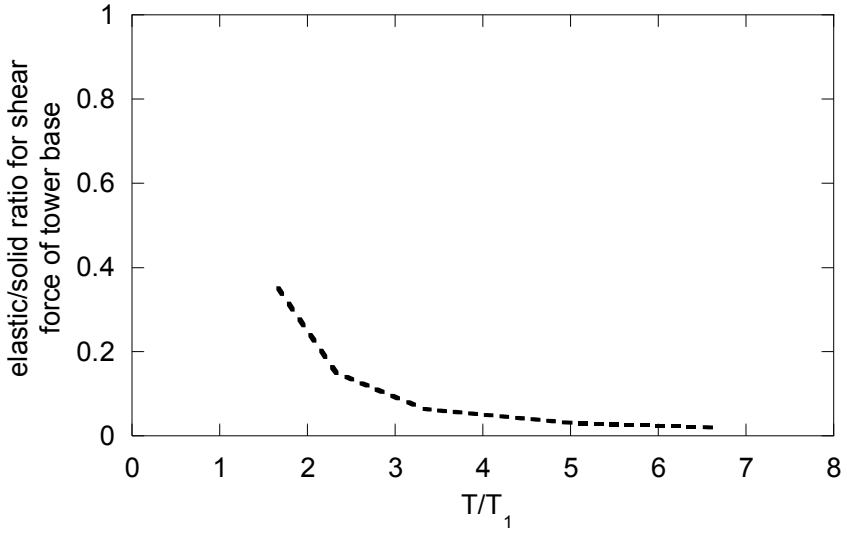

Figure 3.13 Elastic part of shear force normalized by solid part for fixed-foundation model

In the real situation, since $\Delta\phi_{n1}^S / \phi_{11}^S$ of floating wind turbine system is usually less than 15%, the elastic/solid ratio of shear force will be less than 0.08, and doesn't change with wave period.

Figure 3.14 ($\Delta\phi_{n1}^S / \phi_{11}^S = 0.1$ for SR model) compares the elastic parts of shear force from the two models. It is noticed that when T/T_1 > 4, the fixed-foundation model underestimates the shear force, while when T/T_1 < 4, it may give significant overestimation, which can be larger than 15%. Especially when T/T_1 becomes close to 1, the resonance would happen, so in this case this model is not reasonable at all. Therefore, the fixed-foundation model can not be used as the calculating model for floating wind turbine system, but sway-rocking model is the equivalent model, which will be used to predict the wave-induced load in Chapter 4.

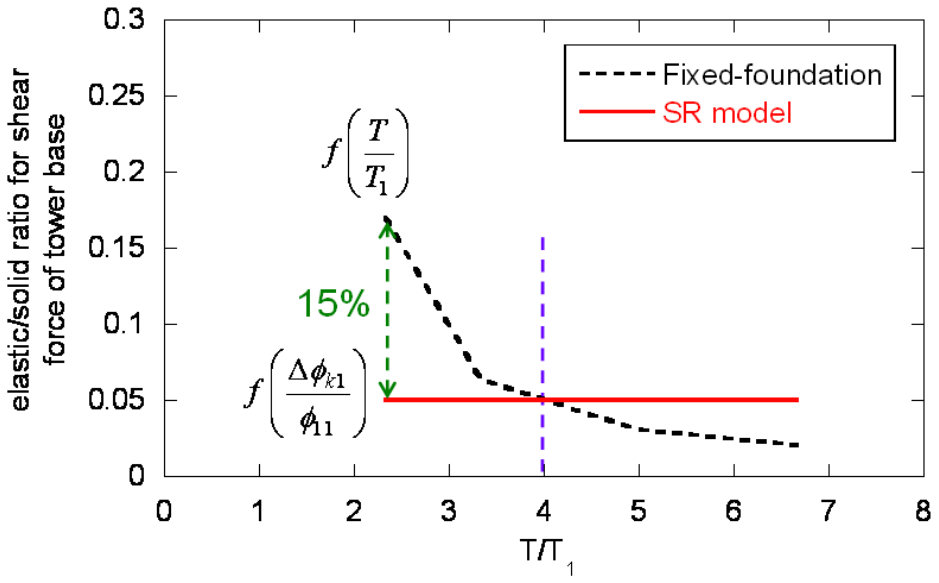

Figure 3.14 Comparison of elastic parts of shear force ($\Delta\phi_{n1}^S / \phi_{11}^S = 0.1$)

3.6. Conclusions

The conclusions and findings of this chapter are summarized as follows:

- An equivalent SR model is proposed to consider the influence of floater surge and pitch motions on the tower loading of floating wind turbine. The stiffness and damping of sway and rocking modes are recognized by eigenvalue analysis or free vibration simulation using FEM; the equivalent wave force and moment are obtained with the tower base displacements.
- The evaluation formulae of tower loading due to sway as well as rocking motion of floater are investigated separately by locking the other mode with modal analysis.
- Through the theoretical comparison between SR model and fixed-foundation model, it is found that in short wave period, the fixed-foundation model may give significant overestimation, which can be larger than 15%; while in long wave period, it underestimates the tower loading.

Reference

1. Takahashi K., “Study on fatigue strength of wind turbine affected by floater motion and wind turbulence”, Master thesis, Department of Civil Engineering, The University of Tokyo, Japan, 2006.
2. Jonkman J.M. (2007), “Dynamic modeling and load analysis of an offshore floating wind turbine”, Department of Aerospace Engineering Sciences, University of Colorado, Ph.D dissertation.
3. Syed Muhammad Bilal Waris Ali, Fully Nonlinear Finite Element Model for Dynamic Response Analysis of Floating Offshore Wind Turbine System, Ph. D dissertation, Department of Civil Engineering, The University of Tokyo, Japan, 2010.9.
4. Architectural Institute of Japan (AIJ), 2004. Recommendations for loads on buildings.

Chapter 4. PREDICTION OF WAVE-INDUCED LOAD

4.1. Introduction

This chapter uses SR model to predict the wave-induced load under regular and irregular wave respectively. The combination of sway motion effect and rocking motion effect is calculated with complete quadratic combination (CQC) rule, and their correlation only depends on the damping and natural frequency of the system. Under irregular wave, the fluctuating wave load on wind turbine tower is a non-Gaussian process with two main peaks in its spectrum corresponding to wave peak frequency and wind turbine tower natural frequency respectively, therefore, a non-Gaussian peak factor model is proposed, so that the maximum wave-induced load under irregular wave can be predicted by the equivalent static method.

4.2. Wave Conditions

4.2.1. Regular Wave

In Chapter 3, the linear Airy wave is used to derive the shear force with modal analysis, since this kind of regular wave has single wave period and is easier to explain the effect of external frequency on the structural response. The extreme wave height $H_{extreme} = 20m$ and wave periods varying from 10s - 20s at intervals of 1s are used in regular wave case.

4.2.2. Irregular Wave

In the absence of information defining the long term joint probability distribution of extreme wind and waves, it shall be assumed that the extreme 10-min mean wind speed with a 50-year recurrence period occurs during the extreme 3-hour sea state with a 50-year recurrence period [1]. The wave climate is represented by the significant wave height H_s and the spectral peak period T_p. In the short term, i.e. over a 3-hour or 6-hour period,

stationary wave conditions with constant H_s and constant T_p are assumed to prevail. In this study the extreme 3-hour sea state with a 50-year recurrence period will be considered.

The extreme wave height (EWH) of 3-hour reference period is taken as $H_{extreme} = 20m$ in this study. Assuming a Rayleigh distribution of wave heights, it may be assumed that:

$$H_{s,3hour} = \frac{H_{extreme}}{1.86} = \frac{20}{1.86} = 10.75m \qquad 4.1$$

The significant wave height for a 1-hour simulation period may be obtained from the value corresponding to a 3-hour reference period by the use of the conversion factor $k_2 = 1.09$ for deep water sites:

$$H_{s,1hour} = 1.09 \times H_{s,3hour} = 11.72m \qquad 4.2$$

There are several models available for the estimation of spectrum for the wave time history. All these models consider a fully developed sea-state for the estimation of the spectrum. Some of the more renowned models are:

- Neumann-Pierson Model
- Pierson-Moskowitz
- SMB (Sverdrup-Munk-Bretschneider) Method
- JONSWAP

The time history of wave elevation is generated using model developed by Chaplin [2] for JONSWAP spectrum.

$$S(\omega) = \alpha^* H_S^2 . \frac{T_P}{2\pi}\left(\frac{\omega T_P}{2\pi}\right)^{-5} \exp\left[-1.25\left(\frac{\omega T_P}{2\pi}\right)^{-4}\right] . \gamma^{\exp\left[-\frac{1}{2\tau^2}\left(\frac{\omega T_P}{2\pi}-1\right)^2\right]} \qquad 4.3$$

$$\alpha^* = \frac{0.0624}{0.230 + 0.0336\gamma - 0.185 \big/ (1.9+\gamma)} \qquad 4.4$$

where ω is the angular frequency of wave, H_S is significant wave height, T_P is peak wave period, γ is peakedness parameter ($\gamma = 3.3$ is used here) and τ is the shape parameter ($\tau = \tau_a$ for $\omega \le 2\pi / T_P$ and $\tau = \tau_b$ for $\omega > 2\pi / T_P$). The values used in this study are $\tau_a = 0.07$, $\tau_b = 0.09$ according to Chakrabarti [3].

In the simulation of this research, significant wave height $H_{s,1hour} = 11.72m$ and peak wave periods T_P varying from 10 - 20 sec at intervals of 1s are used in irregular wave case.

4.3. Tower Loading Under Regular Wave

The tower loading due to sway motion and rocking motion can be calculated from Eqs. (3.21) and (3.28) with the known tower base acceleration accordingly. Defining the tower base acceleration in sway direction as $a_S(t) = a_{S0}\sin(\omega t)$, and that in rocking direction as $a_R(t) = a_{R0}\sin(\omega t)$, where a_{S0} and a_{R0} are the acceleration amplitude, ω is the angular frequency, the same as that of wave. Then the amplitude of shear force on tower can be calculated from the acceleration amplitude.

$$Q_{i0}^S = \sum_{k=i}^{n} m_k a_{S0}\left(1+\frac{\Delta\phi_{k1}^S}{\phi_{11}^S}\right) \tag{4.5}$$

$$Q_{i0}^R = \sum_{k=i}^{n} m_k a_{R0}\left(h_k + \sum_{r=1}^{k-1}\frac{\Delta\phi_{r1}^R}{\phi_{11}^R}(h_{r+1}-h_r)\right) \tag{4.6}$$

where Q_{i0}^S and Q_{i0}^R are the amplitude of shear force due to sway motion and rocking motion, respectively.

4.3.1. Tension Leg System

Figure 4.1 shows the comparison of shear force amplitude on tower base and top with FEM simulation. It is obvious that for tension leg system the rocking motion has no contribution to the shear force, and the sway motion can determine the total load.

$$Q_{i0} = Q_{i0}^S \tag{4.7}$$

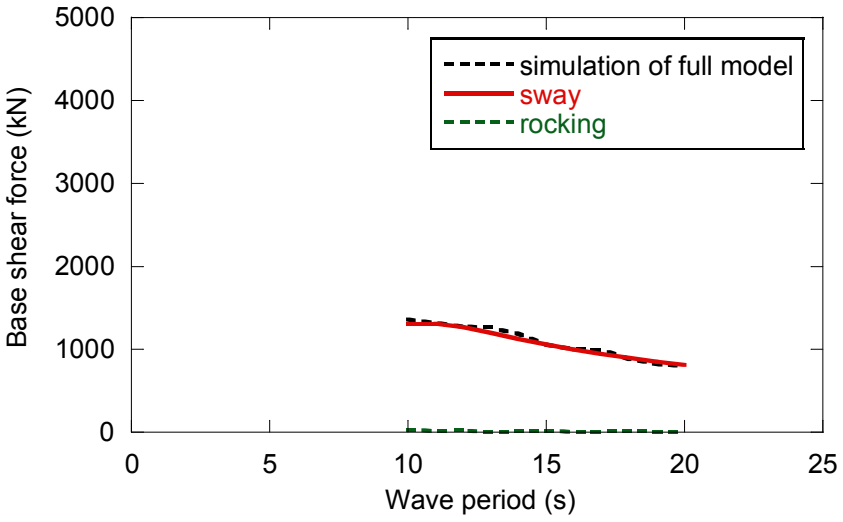

(a) Base shear force

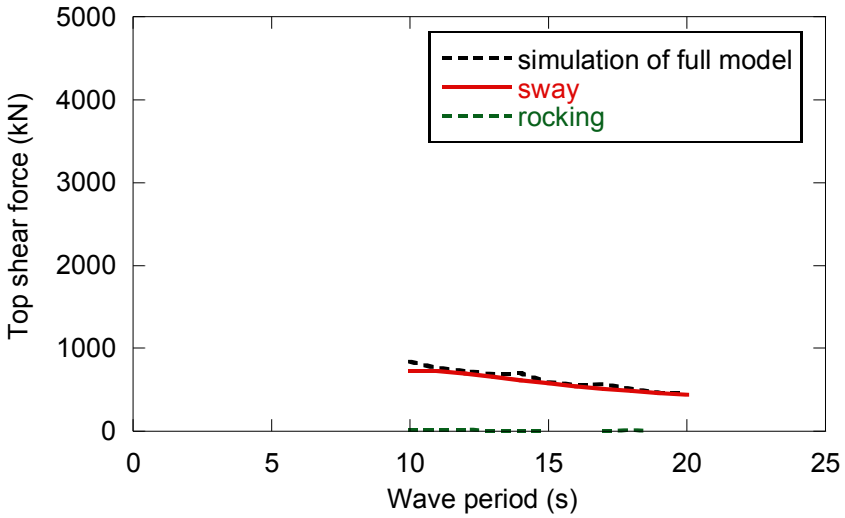

(b) Top shear force

Figure 4.1 Comparison of shear force on wind turbine tower for tension leg system

4.3.2. Catenary System

Figure 4.2 shows the comparison of shear force for catenary system. It indicates that sway motion effect can't reproduce the tower loading of catenary system, and so can't rocking motion, because both the two motions have significant effect on tower loading of catenary system. Hence, the influence of the two motions should be combined together.

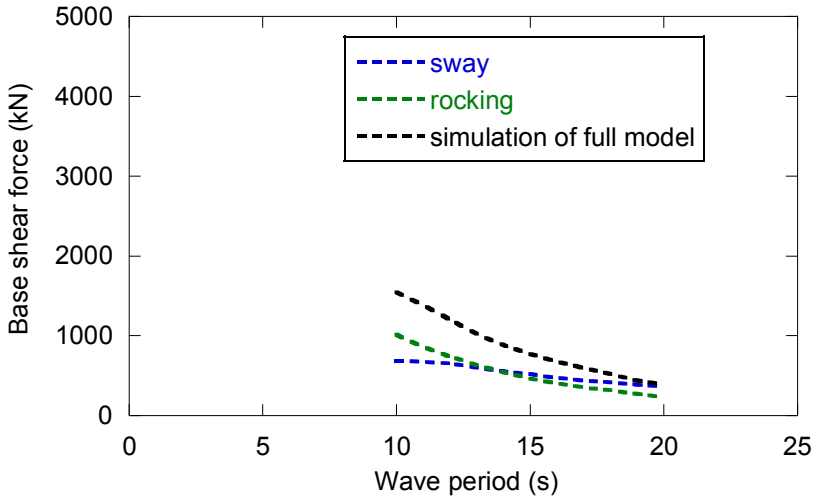

(a) Base shear force

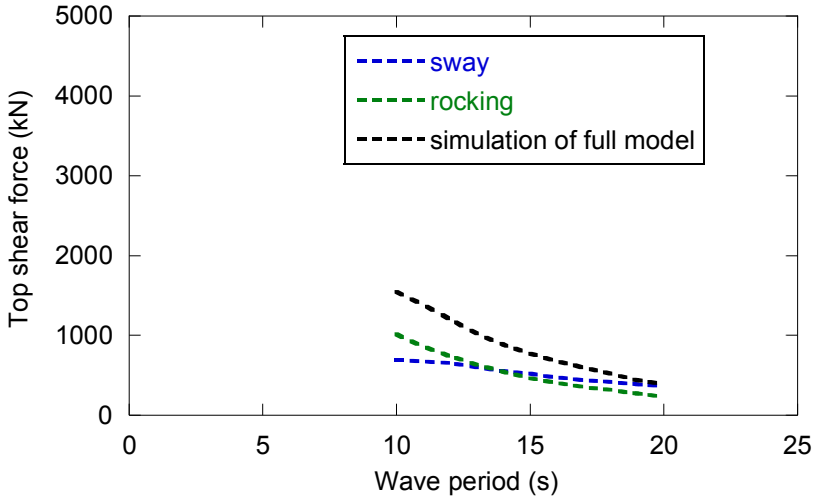

(b) Top shear force

Figure 4.2 Comparison of shear force on wind turbine tower for catenary system

From the FEM simulation, it is recognized that the maximum response of sway and rocking don't occur concurrently, but a certain correlation exists between them. Referring to the seismic loads specified in AIJ [4], complete quadratic combination (CQC) is used here for the combination.

$$Q_{i0}^{CQC} = \sqrt{\left(Q_{i0}^{S}\right)^2 + \rho_{SR} Q_{i0}^{S} Q_{i0}^{R} + \left(Q_{i0}^{R}\right)^2} \tag{4.8}$$

where ρ_{SR} is the correlation factor between sway and rocking modes.

$$\rho_{SR} = \frac{8\sqrt{\xi_S \xi_R}\left(\xi_S + r_{SR}\xi_R\right) r_{SR}^{3/2}}{\left(1-r_{SR}\right)^2 + 4\xi_S\xi_R r_{SR}\left(1+r_{SR}^2\right) + 4\left(\xi_S^2 + \xi_R^2\right) r_{SR}^2} \tag{4.9}$$

where ξ_S, ξ_R are the damping ratios of sway and rocking, respectively. $r_{SR} = \omega_S / \omega_R$ is the ratio between the natural frequency of sway and rocking modes. Therefore, the correlation between sway and rocking modes doesn't change with the external excitation, i.e., wave force, and it only depends on the damping and natural frequency of the system. Here, ξ_S = 0.20, ξ_R = 0.21, ω_S = 0.26, ω_R = 0.37 have been obtained from the free vibration simulation. Thus, ρ_{SR} = 0.79 is calculated.

Referring to AIJ [4], there is another method for sway-rocking combination: square root of sum of squares (SRSS), which is expressed as:

$$Q_{i0}^{SRSS} = \sqrt{\left(Q_{i0}^{S}\right)^2 + \left(Q_{i0}^{R}\right)^2} \tag{4.10}$$

Figure 4.3 indicates that SRSS rule underestimates the shear force. As the sway and rocking modes have closer eigenvalues, CQC rule can give much better results. In addition, the catenary system has the larger shear force than tension leg system, since the rocking (pitch) motion of tension leg system is restrained.

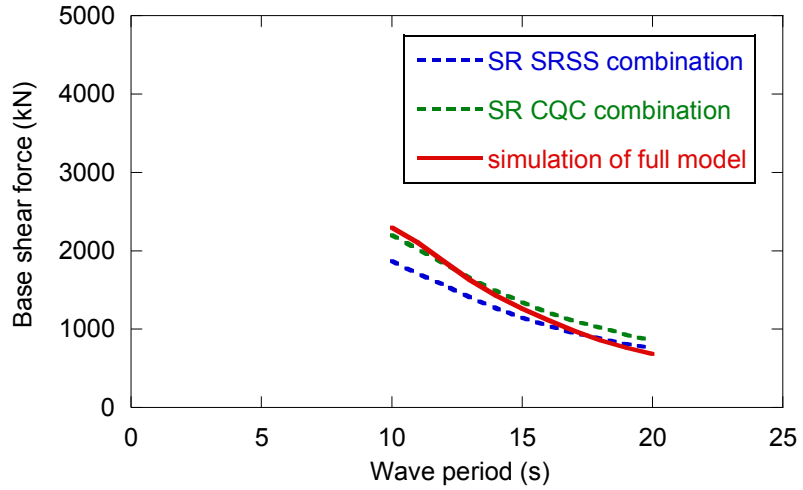

(a) Base shear force

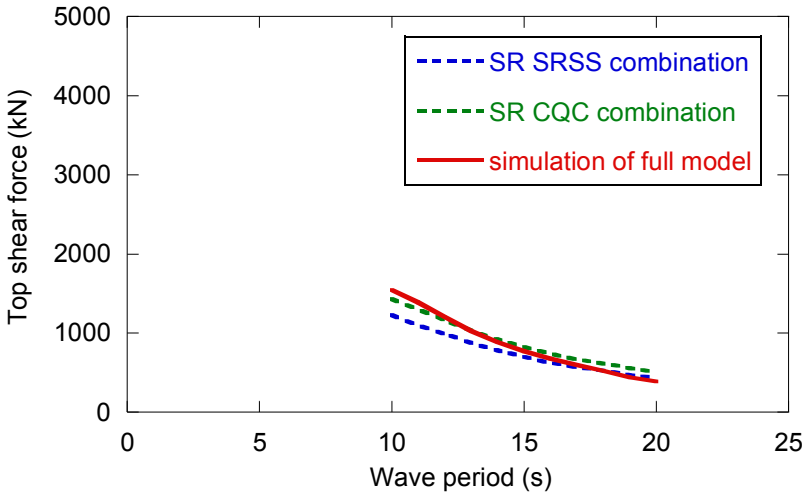

(b) Top shear force

Figure 4.3 Comparison of shear force from CQC and SRSS

4.4. Tower Loading Under Irregular Wave

In real situation, the irregular wave should be used. For irregular wave, the tower loading is a random process. Hence, the standard deviation and peak factor is considered and their product is used to calculate the maximum load.

4.4.1. Standard Deviation

Derived from Eqs. (3.21) and (3.28), Eq. (4.11) and Eq. (4.12) can be employed to calculate the shear force standard deviation due to the sway motion and rocking motion, respectively.

$$\sigma_{i,S} = \sum_{k=i}^{n} m_k \sigma_{aS} \left(1 + \frac{\Delta\phi_{k1}^{S}}{\phi_{11}^{S}} \right) \tag{4.11}$$

$$\sigma_{i,R} = \sum_{k=i}^{n} m_k \sigma_{aR} \left(h_k + \sum_{r=1}^{k-1} \frac{\Delta\phi_{r1}^{R}}{\phi_{11}^{R}} \left(h_{r+1} - h_r \right) \right) \tag{4.12}$$

where σ_{aS} and σ_{aR} are the standard deviation of sway acceleration and rocking acceleration at the tower base, respectively.

Tension Leg System

For tension leg system, the sway motion can determine the total standard deviation:

$$\sigma_i = \sigma_{i,S} \tag{4.13}$$

Figure 4.4 shows that the proposed formula Eq. (4.13) agrees well with the simulation for the standard deviation of shear force at tower base and top. It is found that the standard deviation decreases with the peak period of wave.

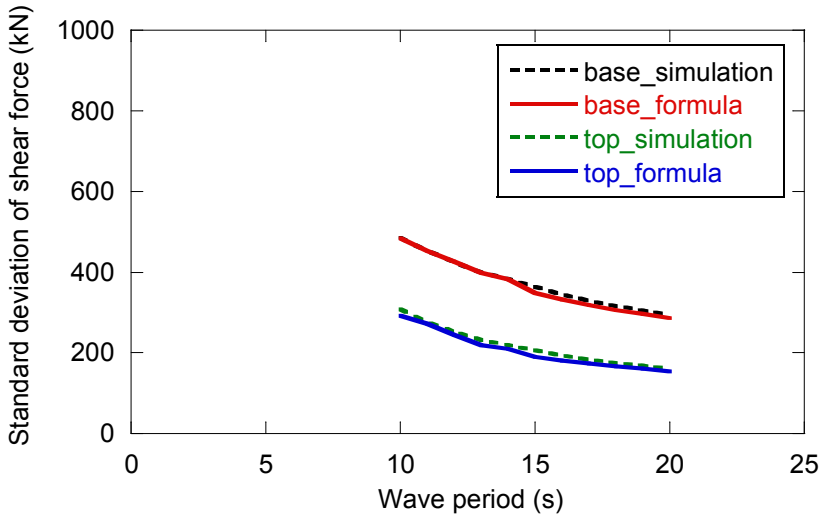

Figure 4.4 Comparison of shear force standard deviation of tension leg system

Catenary System

Based on the same idea for the calculation of shear force amplitude on tower under regular wave, the standard deviation of shear force under irregular wave can also be considered as the combination of sway effect and rocking effect using CQC rule:

$$\sigma_i = \sqrt{\sigma_{i,S}^2 + \rho_{SR}\sigma_{i,S}\sigma_{i,R} + \sigma_{i,R}^2} \qquad 4.14$$

where σ_i is the standard deviation of shear force at the *ith* node, $\sigma_{i,S}$ is the standard deviation due to the sway motion, $\sigma_{i,R}$ is that due to the rocking motion, and ρ_{SR} is the correlation factor between sway and rocking modes, which is the same as that of regular wave as shown in Eq. (4.9).

Figure 4.5 shows that the proposed formula Eq. (4.14) agrees well with the simulation for the standard deviation of shear force at tower base and top. It is found that the standard deviation decreases with the peak period of wave as well.

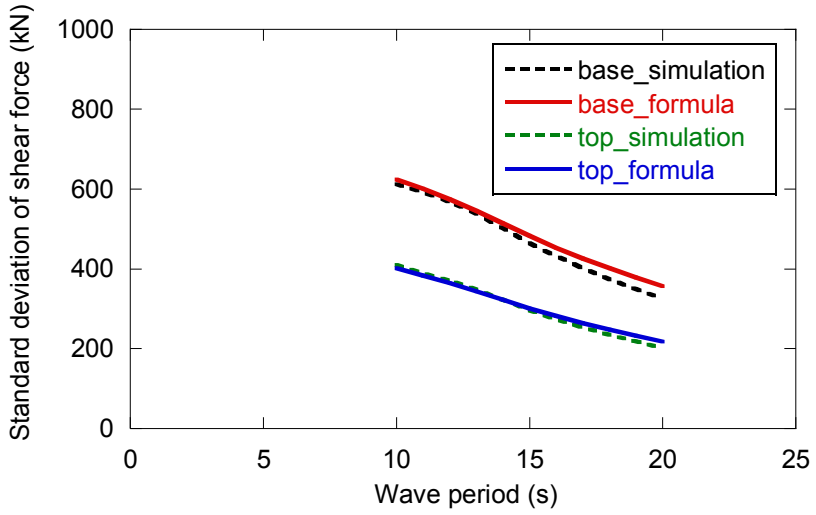

Figure 4.5 Comparison of shear force standard deviation of catenary system

4.4.2. Peak Factor

Tension Leg System

Before proposing the formulae of peak factor, power spectrum density of tower base shear force is investigated. Figure 4.6 shows the comparison of power spectrum density of tower base shear force for the wave periods: 10s, 15s and 20s. It is noted that the dynamic tower loading consists of three parts. Take the 10s case for example, the range around the first peak is the background motion part, which has the same peak frequency as the wave $n_p = 0.1$, corresponding to the wave peak period 10s; The range around the

second peak is due to the peak acceleration of the floater sway motion with the peak frequency $n_s = 0.167$, corresponding to the peak period of sway acceleration 6s (shown in Figure 4.7); The range around the third peak is the resonant part due to the tower vibration with the peak frequency $n_t = 0.289$, corresponding to the natural period of tower 3.5s. The second and third peaks result in the non-Gaussian characteristics of the shear force, especially the third peak. From the comparison with 15s case and 20s case, it is found that when the wave period becomes longer, the two peaks will be reduced since the frequency difference from the wave becomes larger and external exciting effect becomes weaker, which means the non-Gaussianity will decrease when wave period increases. This feature is just the reason why the skewness of tower base shear force in Figure 4.8 is significant for 10s-15s, and can be neglected after 16s. Therefore, the tower loading is considered as a non-Gaussian process, and a non-Gaussian peak factor should be used for tension leg system.

In this study, the skewness is obtained from the simulation results. Actually, the shear force is a bi-normal process with two main narrow normal peaks in the spectrum. It is a non-Gaussian process certainly, but can be decomposed into two Gaussian (normal) processes. The spectrum model of each Gaussian process can be easily proposed based on their standard deviation. With the spectra, the correlation between these two Gaussian processes can be calculated and the time series of shear force can be obtained by program. Then the skewness can be known from the time series. This numerical method can be used to determine the skewness.

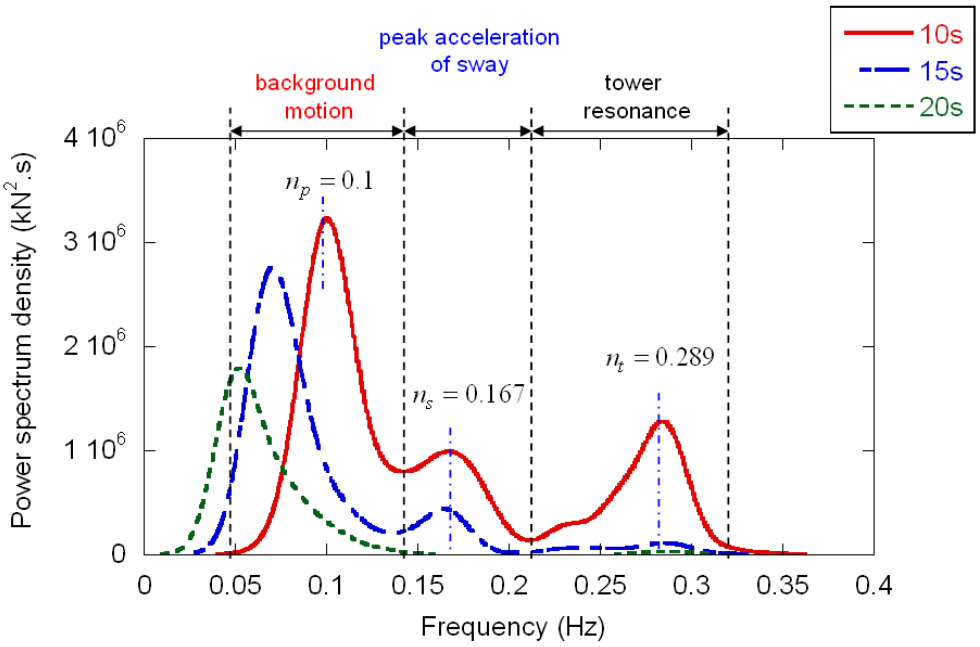

Figure 4.6 Comparison of power spectrum density of tower base shear force for tension leg system

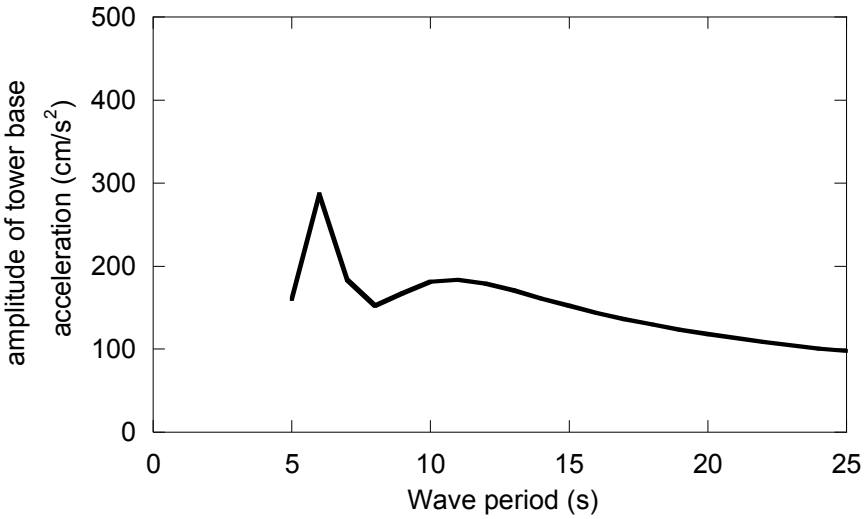

Figure 4.7 Amplitude of sway acceleration at tower base for tension leg system

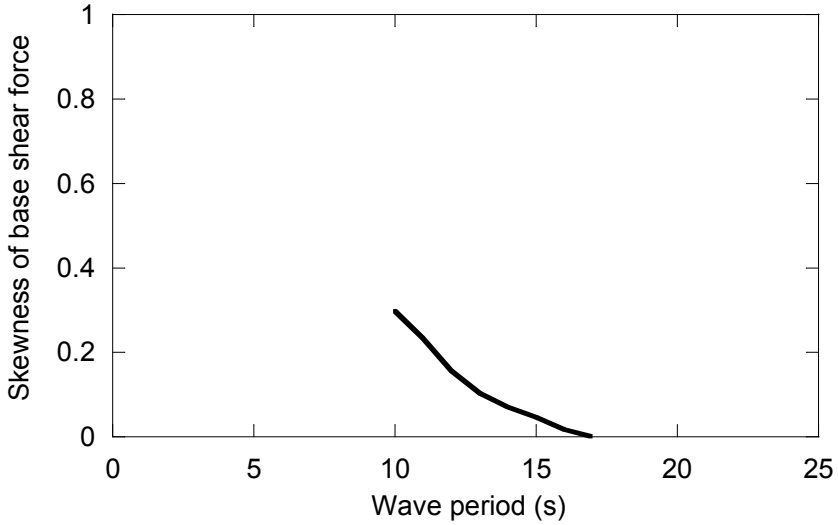

Figure 4.8 Skewness of tower base shear force of tension leg system

Based on the model of Kareem et al. [5], the non-Gaussian peak factor for the tower shear force under irregular wave is proposed as:

$$g_{TLP} = \frac{1}{\sqrt{1+\frac{\alpha_3^2}{18}}}\left\{\left(\sqrt{2\ln\left(\nu_0' T\right)}+\frac{0.5772}{\sqrt{2\ln\left(\nu_0' T\right)}}\right)+\frac{\alpha_3}{6}\left(2\ln\left(\nu_0' T\right)-1\right)\right\} \qquad 4.15$$

$$\nu_0' = \nu_0 / \sqrt{\left(1+\alpha_3^2/18\right)\left(1+\alpha_3^2/9\right)} \qquad 4.16$$

where α_3 is the skewness of tower base shear force, ν_0' and ν_0 are the zero up-crossing frequency of tower base shear force for non-Gaussian process and Gaussian process,

respectively. When $\alpha_3 = 0$, this non-Gaussian peak factor is reduced to Gaussian form. ν_0 can be calculated by:

$$\nu_0 = \sqrt{\frac{m_2}{m_0}} = \sqrt{\frac{\int_0^\infty n^2 S(n)\,dn}{\int_0^\infty S(n)\,dn}} \qquad 4.17$$

where m_2 and m_0 are the second order spectral moment and the variance of the base shear force, respectively, n is the frequency in Hertz, and $S(n)$ is the power spectrum density. Since the three parts of the spectrum in Figure 4.6 are all narrow band, the Eq. (4.17) can be expressed approximately by:

$$\nu_0 = \sqrt{\frac{n_p^2\sigma_b^2 + n_s^2\sigma_s^2 + n_t^2\sigma_t^2}{\sigma_b^2 + \sigma_s^2 + \sigma_t^2}} = n_p\sqrt{\frac{1+\gamma_s R_s + \gamma_t R_t}{1+R_s+R_t}} \qquad 4.18$$

where

$$\gamma_s = \left(\frac{n_s}{n_p}\right)^2, \quad \gamma_t = \left(\frac{n_t}{n_p}\right)^2, \quad R_s = \left(\frac{\sigma_s}{\sigma_b}\right)^2, \quad R_t = \left(\frac{\sigma_t}{\sigma_b}\right)^2$$

σ_b^2 , σ_s^2 and σ_t^2 are the variance of background motion part, peak sway acceleration part and tower resonant part, respectively. Thus the zero up-crossing frequency of tower base shear force can also be written into three parts, then the contribution of each part is able to understood clearly. The proposed formula Eq. (4.18) shows good agreement with the simulation, as shown in Figure 4.9. The non-Gaussian peak factor shown in Figure 4.10 decreases with the wave period, since the skewness and zero up-crossing frequency have the same tendency.

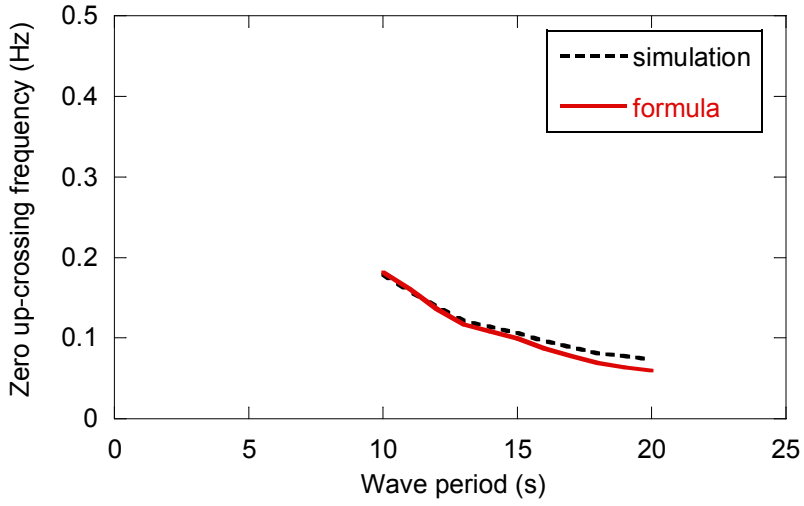

Figure 4.9 Zero up-crossing frequency of tower base shear force for tension leg system

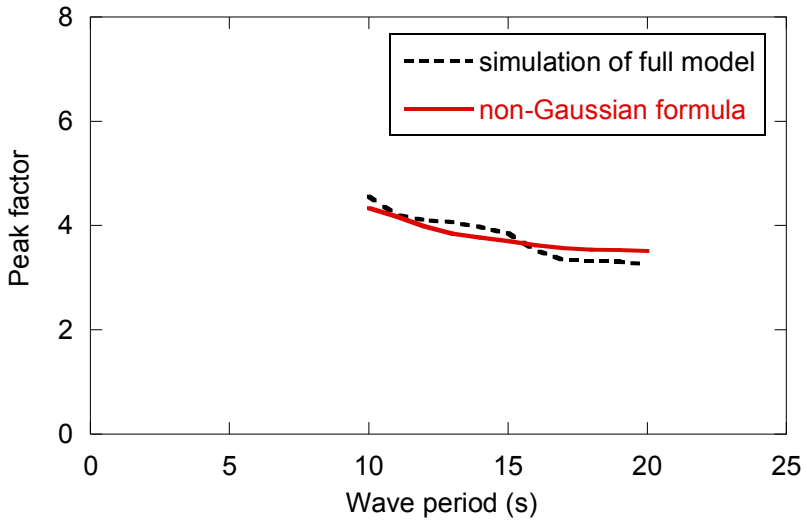

Figure 4.10 Peak factor of tower base shear force for tension leg system

Catenary System

Figure 4.11 gives the comparison of the power spectrum density of tower base shear force for catenary system. Like the tension leg system, the dynamic tower loading consists of three parts as well. Take the 10s case for example, the first part is the background motion part; The second part is due to the peak acceleration of the sway and rocking motion of the floater; The third part is the resonant part due to the tower vibration. It is indicated that the second and third peaks are negligibly small compared to the background motion part, since the floater sway and rocking modes are much more dominant, and the tower resonance is only slightly excited. In 15s case and 20s case, the two peaks will not exist, and only the background motion part is left. As a result a Gaussian process can be assumed for the tower base shear force of catenary system. This feature is just the reason why the skewness of tower base shear force in Figure 4.12 is close to zero for all wave periods. Therefore, a Gaussian peak factor could be used for the catenary system.

With $\alpha_3 = 0$, the non-Gaussian peak factor of Eq. (4.15) is reduced to the Gaussian form:

$$g_{CAT} = \sqrt{2\ln(\nu_0 T)} + \frac{0.5772}{\sqrt{2\ln(\nu_0 T)}} \qquad 4.19$$

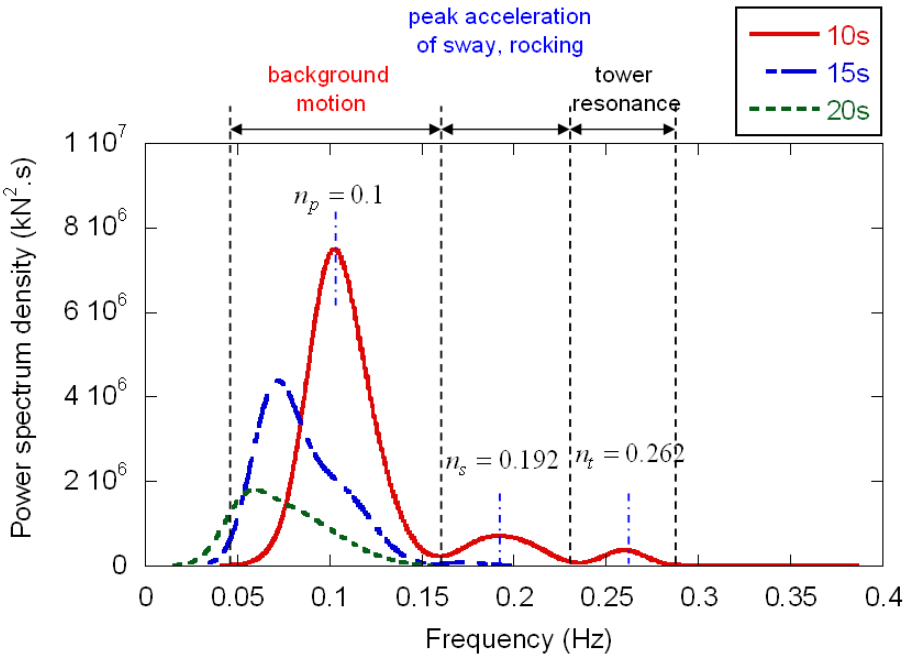

Figure 4.11 Comparison of power spectrum density of tower base shear force for catenary system

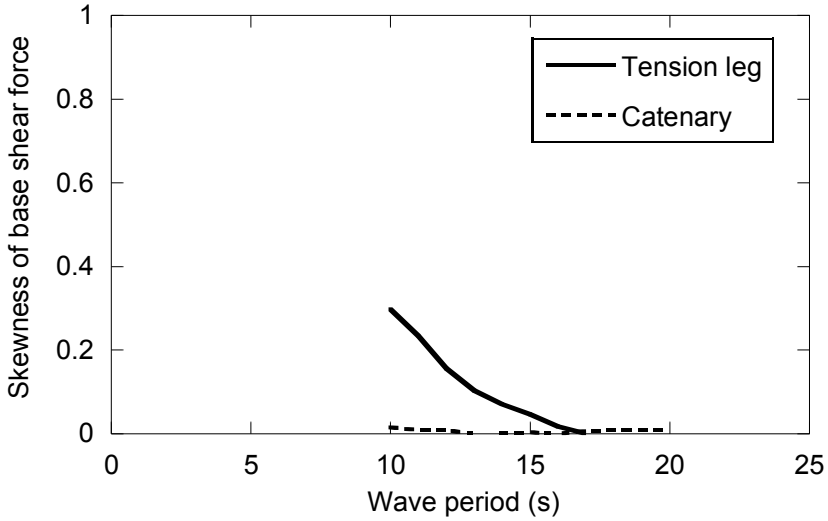

Figure 4.12 Comparison of skewness of tower base shear force between tension leg system and catenary system

Since the background motion part is dominant in the spectrum of tower base shear force for catenary system, the variance ratios R_s and R_t of standard deviation are negligibly small compared to those of tension leg system as shown in Figure 4.13. Hence, it can be assumed that $R_s \approx 0$, $R_t \approx 0$, then the zero up-crossing frequency in Eq. (4.18) will become:

$$\nu_0 = n_p \qquad 4.20$$

Eq. (4.19) can be used to calculate the peak factor approximately. Figure 4.14 indicates that the Gaussian peak factor is enough for catenary system and it doesn't change much with wave period. Compared to the non-Gaussian peak factor, the larger difference happens in the shorter wave periods 10s-15s.

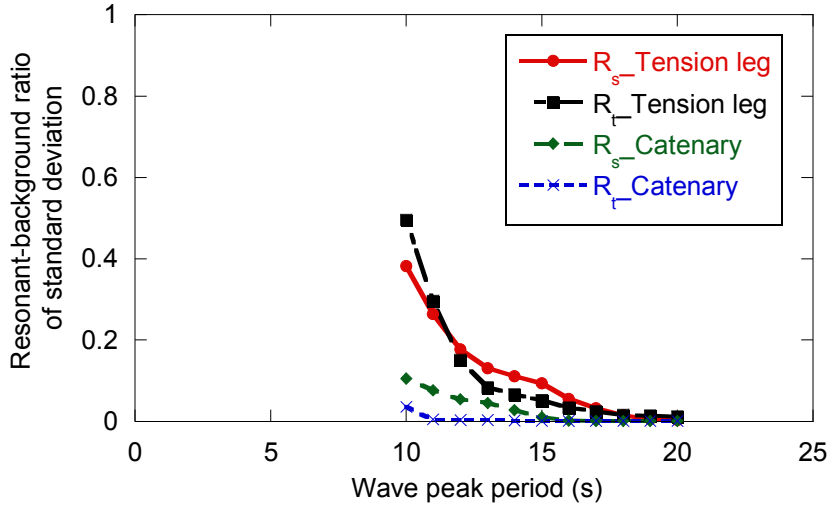

Figure 4.13 Comparison of variance ratios of standard deviation

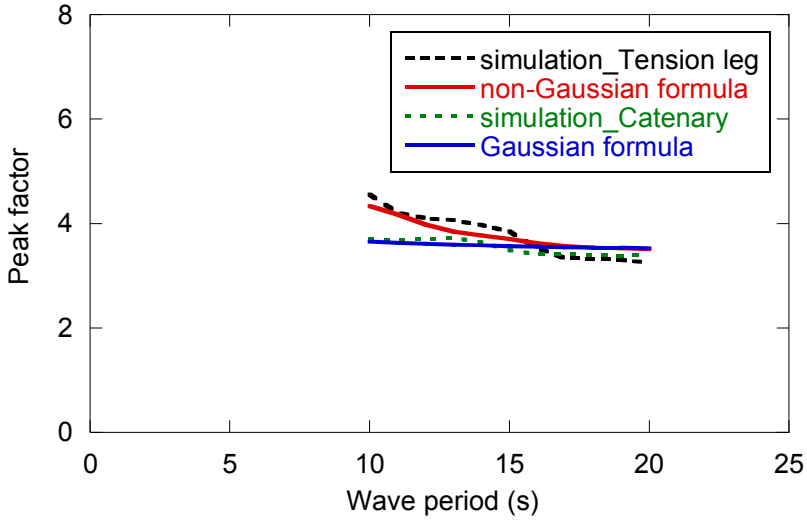

Figure 4.14 Comparison of peak factors between tension leg system and catenary system

4.4.3. Maximum Shear Force

With the standard deviation and peak factor, the maximum shear force for the two kinds of floating system can be calculated as:

$$Q_{\max,i} = g \cdot \sigma_i \qquad \left(g = g_{TLP} \ \ or \ \ g_{CAT}\right) \qquad 4.21$$

Figure 4.15 and Figure 4.16 show the maximum shear force for the two kinds of floating system. The proposed formulae can predict the tower loading very well.

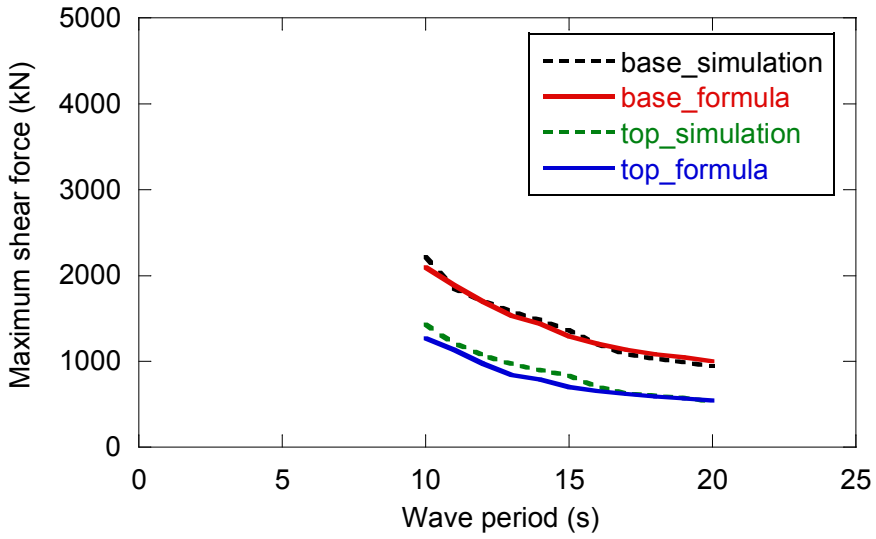

Figure 4.15 Comparison of maximum shear force for tension leg system

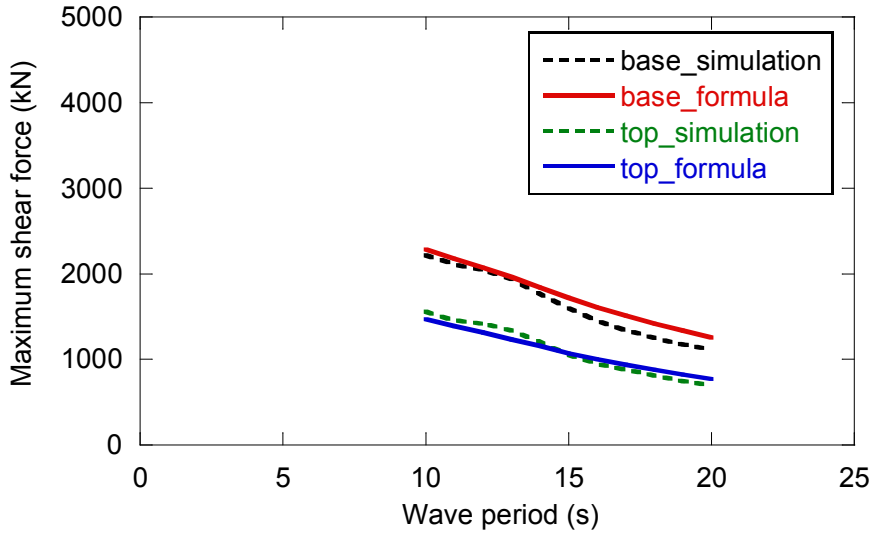

Figure 4.16 Comparison of maximum shear force for catenary system

4.5. Conclusions

The conclusions and findings of this chapter are summarized as follows:

- For the shear force amplitude under regular wave and the standard deviation of shear force under irregular wave, the combination of sway motion effect and rocking motion effect can be determined by complete quadratic combination (CQC) rule. The correlation between them only depends on the damping and natural frequency of the system.

- For tension leg system, a non-Gaussian peak factor is necessary. This non-Gaussian feature mainly results from the tower resonance. The non-Gaussianity will decrease with wave period, since the external exciting effect becomes weaker.
- For catenary system, the shear force history can be regarded as a Gaussian process. The effect from tower resonance is negligibly small compared to the background motion part, since the floater sway and rocking modes are much more dominant.

Reference

1. IEC-61400-3 (2008), Edition-1: Wind turbines – Part 3: Design requirements for offshore wind turbines.
2. Chaplin J. R, http://www.civil.soton.ac.uk/hydraulics/download/downloadtable.htm.
3. Chakrabarti S K, (1987), “Hydrodynamics of offshore structures”, Computational Mechanics Publications, Southampton.
4. Architectural Institute of Japan (AIJ), 2004. Recommendations for loads on buildings.
5. Kareem, A., Tognarelli, M.A., Gurley, K.R., 1998. Modeling and analysis of quadratic term in the wind effects on structures. Journal of Wind Engineering and Industrial Aerodynamics 74-76, 1101-1110.

Chapter 5. PREDICTION OF WIND-INDUCED LOAD

5.1. Introduction

This chapter gives details of the prediction of wind load. Equivalent static method is adopted to estimate the maximum wind load on wind turbine towers in this study. In both along-wind direction and across-wind direction, the theoretical formulae are proposed for mean wind load and gust loading factor which contains standard deviation and peak factor of fluctuating wind load. The critical parameters in the standard deviation such as mode correction factor, aerodynamic damping ratio and size reduction factor are investigated to identify the dominant influence factor and their characteristics. A consistent non-Gaussian peak factor which can be reduced to the standard Gaussian form for a Gaussian process is proposed. For floating wind turbine, SR model should be employed for the wind-induced load prediction, since the low natural frequency of floater increases the resonant standard deviation, while the large damping causes significant reduction. Considering the wind response correlation of along-wind direction and across-wind direction, a loads combination formula is proposed to calculate the final design wind load on towers.

5.2. Wind Load Evaluation Method

Wind load on wind turbine is usually evaluated either by FEM or by equivalent static method. While FEM simulation is commonly used in turbine design, equivalent static method is used widely in design of lower and other support structures. Equivalent static method is adopted in many design codes (AIJ [1]; DS472 [2]). This study will investigate the equivalent static method to estimate the wind load and use FEM simulation as validation.

5.2.1. Equivalent Static Method

Equivalent static method uses a coefficient called the peak factor proposed by Davenport [3] to account for fluctuating wind load. A study by Kareem and Zhou [4] proved

that the bending moment-based peak factor can yield more reliable results than displacement-based peak factor, because the mean value of displacement may be zero. Therefore, in this study, the bending moment-based peak factor is adopted. This means the term wind load should be interpreted as a bending moment. Then the maximum bending moment is estimated by Eq. (5.1).

$$M_f = G_f \overline{M}_f \tag{5.1}$$

$$G_f = 1 + \frac{g_f \cdot \sigma_{Mf}}{\overline{M}_f} \tag{5.2}$$

where $\overline{M}_f$ is the mean bending moment, G_f is the gust loading factor, g_f is the peak factor, σ_{Mf} is the standard deviation, the subscript *f=D* means along-wind and *f=L* means across-wind. The wind direction and wind load on wind turbine are defined as Figure 5.1.

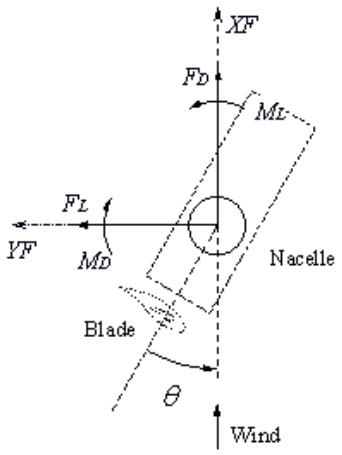

Figure 5.1 Wind direction and wind load

The assumptions used in this study are listed below:

1) The model of an elastic tower and a rigid rotor, shown in Figure 5.2 (b), is used to implement the theoretical formula of mean, standard deviation and the peak factor of wind load on a tower base. Since in wind load of wind turbine tower the effect of the first mode is dominant, only the first mode is considered. Referring to Ishihara [5], the first mode shape for rotor is assumed as $\mu_1(r) = 1$ and $\mu_1(r) = \mu_1(z) = (z / H_h)^{\beta_s}$ is used for tower, where $\beta_s = 2.0$;

2) The tower height is assumed to be equal to the hub height; The rotor part of this study includes blades, hub and nacelle;

3) Wind velocity and turbulence intensity at the hub of the wind turbine are used as representative for that of the whole rotor;

4) A uniform equivalent aerodynamic coefficient for the whole rotor is used instead of that varying with positions on the rotor;

5) The bending moment due to the rotor gravity can be neglected, since the deformation of tower is very small;

6) It is noted that this study is used for the commercial wind turbine with tubular tower.

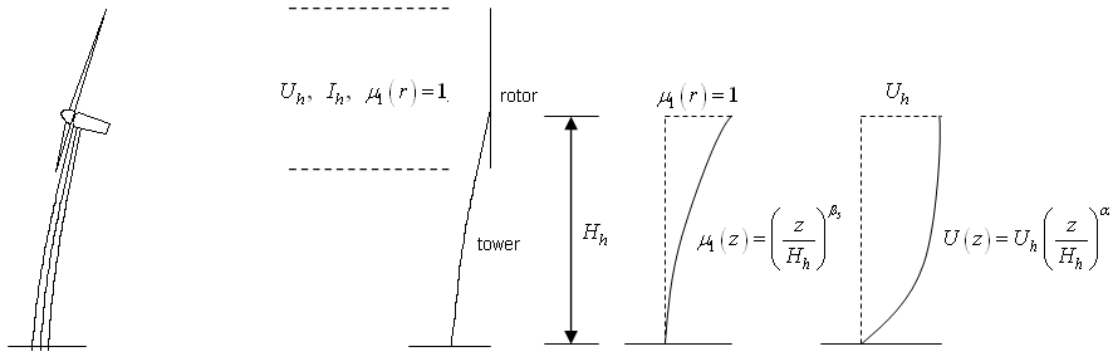

(a) Wind turbine (b) Simplified model with mode shape and wind profile

Figure 5.2 Wind turbine and simplified model

Considering a wind with longitudinal fluctuating component u and lateral fluctuating component v, the relation between wind velocity and a vibrated element in two-dimensional direction under wind direction θ is shown in Figure 5.3. Quasi-static method is used to calculate the wind force, in which after dropping the second order terms based on perturbation analysis and the terms caused by the across motion of the structure which cannot be obtained by the analytical method, and keeping the second order term $(1/2)\rho A C_f(\theta)u^2$, since the contribution of the non-linear part of wind pressure is large, especially for high wind turbulence (Binh et al. [6]) and the force $\rho A A_f(\theta)Uv$ due to the lateral wind fluctuation component v, the total wind force F_D can be expressed as Eqs. (5.3) and (5.4), referring the *Appendix A.2* for details.

$$F_D=\frac{1}{2}\rho c(r)C_D(\theta)U^2+\frac{1}{2}\rho c(r)C_D(\theta)u^2+\rho c(r)C_D(\theta)Uu+\rho c(r)A_D(\theta)Uv-\rho c(r)C_D(\theta)U\dot{x} \quad 5.3$$

$$F_L=\frac{1}{2}\rho c(r)C_L(\theta)U^2+\frac{1}{2}\rho c(r)C_L(\theta)u^2+\rho c(r)C_L(\theta)Uu+\rho c(r)A_L(\theta)Uv-\rho c(r)A_L(\theta)U\dot{y} \quad 5.4$$

where ρ is the air density, $c(r)$ is the characteristic length of the element at position r, U is the mean wind velocity, $C_D(\theta)$ and $C_L(\theta)$ are the drag and lift aerodynamic coefficients respectively, $A_D(\theta)=0.5\left(\partial C_D(\theta)/\partial\theta-C_L(\theta)\right)$ and $A_L(\theta)=0.5\left(C_D(\theta)+\partial C_L(\theta)/\partial\theta\right)$ are the aerodynamic coefficient gradients in along-wind and across-wind directions respectively, $\dot{x}$ and $\dot{y}$ are the structural vibration velocity in these two directions, respectively.

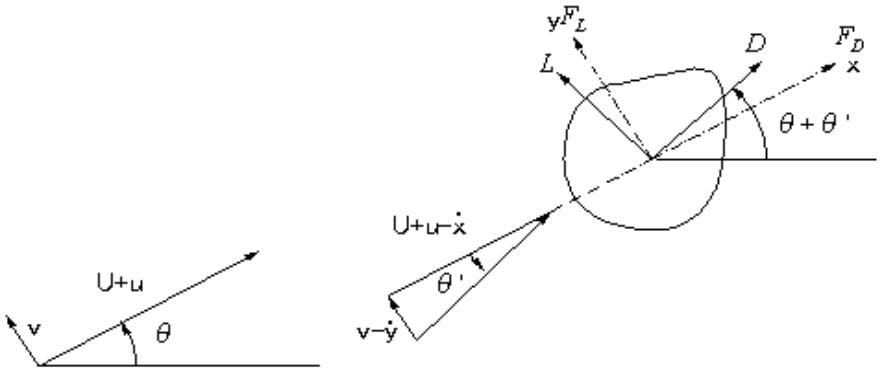

Figure 5.3 Relative wind speed under element vibrations

From Eqs. (5.3) and (5.4), the mean bending moment can be easily derived; The standard deviation of fluctuating wind load can be derived by means of modal analysis, which is illustrated in Eq. (5.5):

$$m_i\ddot{f}_i(t)+c_i\dot{f}_i(t)+m_i\omega_i^2 f_i(t)=\int \mu_i(r)q(r,t)dr \qquad 5.5$$

where m_i is the generalized mass, c_i is the generalized damping and ω_i is the modal natural frequency in radians per second, $f_i(t)$ is the tip displacement, $\mu_i(r)$ is the normalized mode shape of the *ith* mode, and *q*(*r,t*) is the fluctuating wind load per unit length; The peak factors are obtained based on Kareem's model [7]. All the derivation of integral forms is given in *Appendix*.

5.2.2. Wind Turbine Model

Seven stall-regulated wind turbine models of 100kW~2000kM are used in this study to investigate the tower wind load. The main information of each wind turbine is described in Table 5.1.

Table 5.1 Wind turbine description

Name	Description						
Rated power	100kW	400kW	500kW	600kW	1000kW	1500kW	2000kW
Rotor diameter	23.6m	31.0m	40.3m	51.6m	65.0m	76.5m	81.3m
Hub height	24.0m	36.0m	44.0m	50.0m	70.0m	69.0m	76.5m
The first frequency	2.03Hz	0.81Hz	0.50Hz	0.53Hz	0.41Hz	0.43Hz	0.49Hz

5.3. Mean Bending Moment

Since the integral forms of mean wind load, standard deviation and peak factor of fluctuating wind load derived from modal analysis are quite complex, it is necessary to propose formulae to make them easily applied for the estimation of wind load by engineers and get a clear understanding of the characteristics for each parameter as well.

From Eqs. (5.3) and (5.4), the mean wind force $\overline{F}_D$, $\overline{F}_L$ and mean bending moment $\overline{M}_D$, $\overline{M}_L$ can be obtained:

$$\overline{F}_D = \frac{1}{2}\rho C_D(\theta)c(r)\left(U^2+\sigma_u{}^2\right) = \frac{1}{2}\rho C_D(\theta)c(r)U^2\left(1+I_u{}^2\right) \quad 5.6$$

$$\overline{F}_L = \frac{1}{2}\rho C_L(\theta)c(r)\left(U^2+\sigma_u{}^2\right) = \frac{1}{2}\rho C_L(\theta)c(r)U^2\left(1+I_u{}^2\right) \quad 5.7$$

$$\overline{M}_D = \int \frac{1}{2}\rho C_D(r,\theta)c(r)U^2(r)\left[1+I_u{}^2(r)\right]rdr \approx \frac{1}{2}\rho U_h^2\left(1+I_{uh}^2\right)H_h\left[C_{D,r}(\theta)A_r + C_{D,t}(\theta)H_hD'\right] \quad 5.8$$

$$\overline{M}_L = \int \frac{1}{2}\rho C_L(r,\theta)c(r)U^2(r)\left[1+I_u{}^2(r)\right]rdr \approx \frac{1}{2}\rho U_h^2\left(1+I_{uh}^2\right)H_h\left[C_{L,r}(\theta)A_r + C_{L,t}(\theta)H_hD'\right] \quad 5.9$$

where

$$C_{D,r}(\theta) = \left(C_{D,n}(\theta)A_n + 3\int_0^R C_{D,b}(r,\theta)c(r)dr\right)/A_r ,$$

$$C_{L,r}(\theta) = \left(C_{L,n}(\theta)A_n + 3\int_0^R C_{L,b}(r,\theta)c(r)dr\right)/A_r ,$$

$$D' = \frac{1}{\left(1+I_{uh}^2\right)}\left[\frac{D_b+2(\alpha+1)D_t}{2(\alpha+1)(2\alpha+3)} + \frac{I_{uh}^2\left(D_b+1.9D_t\right)}{5.5}\right].$$

where U_h is the mean wind velocity at hub height; I_{uh} is the turbulence intensity at hub height in the along-wind direction; H_h is the hub height; A_r is the rotor area; A_n is wind-acting area of nacelle and hub; D_b and D_t are the diameter of the bottom and top of tower; $C_{D,t}(\theta)$ and $C_{L,t}(\theta)$ are the drag and lift aerodynamic coefficients of cylindrical tower, respectively, which are regarded to be constant. Referring to BSI code [8], $C_{D,t}(\theta)=0.6$ and $C_{L,t}(\theta)=0$ are used in this study (Figure 5.5); $C_{D,r}(\theta)$ and $C_{L,r}(\theta)$ are the equivalent drag and lift aerodynamic coefficients of rotor, calculated from those of nacelle $C_{D,n}$ and $C_{L,n}$ (Figure 5.4 (a)) and those of blade $C_{D,b}$ and $C_{L,b}$, which depend on the thickness ratio (thickness/chord) of the blade section. 2M wind turbine blade section (thickness ratio: 12%) by GH Bladed [9] and s809 (thickness ratio: 21%) by Somers [10], will be considered (Figure 5.4 (b)). Figure 5.5 illustrates the variation of equivalent drag

and lift aerodynamic coefficients of rotor as well, which strongly correlates with those of blade, where $C_{D,r}(\theta)$ shows minimum near ±90° and maximum near 0° and ±180°, while $C_{L,r}(\theta)$ becomes 0 near ±180°, 0° and ±90°.

From Eqs. (5.8) and (5.9), it is found that for along-wind direction, the mean bending moment is the summation of those from rotor and tower, while for across-wind direction, since $C_{L,t}(\theta)=0$, only rotor contributes to the mean bending moment, and becomes 0 at some yaw angles. Figure 5.6 shows how the proposed formulae strongly correlate with FEM.

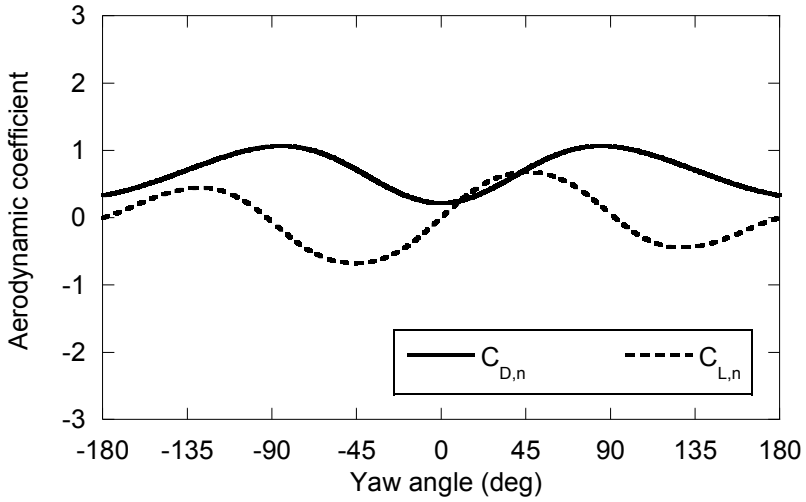

(a) Aerodynamic coefficients of nacelle

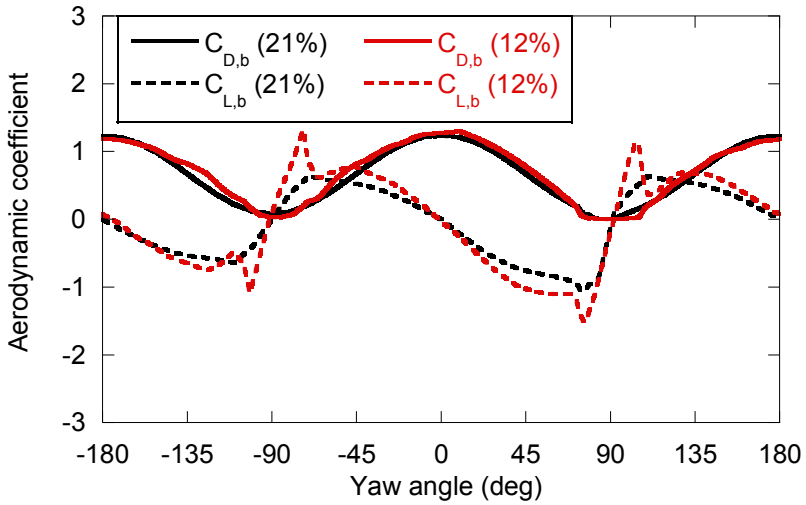

(b) Aerodynamic coefficients of blade

Figure 5.4 Aerodynamic coefficients for nacelle and blade

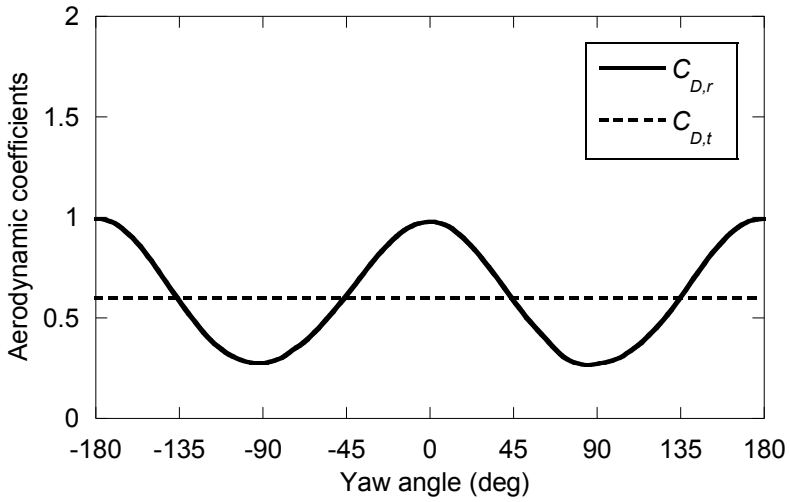

(a) Along-wind direction

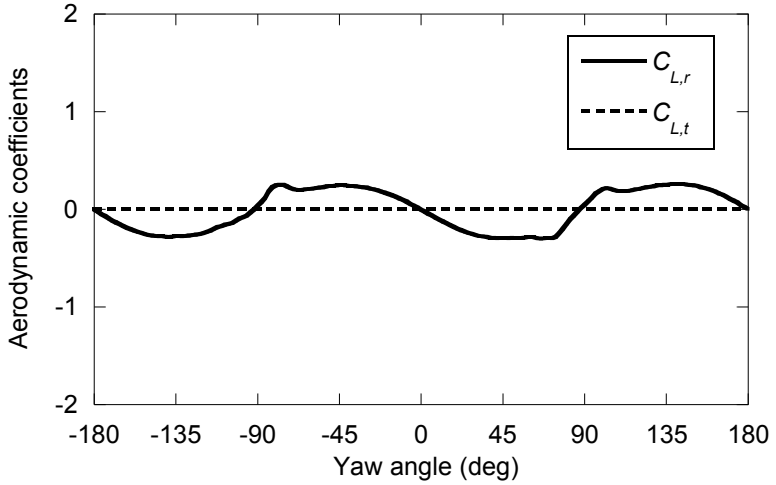

(b) Across-wind direction

Figure 5.5 Aerodynamic coefficients for rotor and tower (400kW)

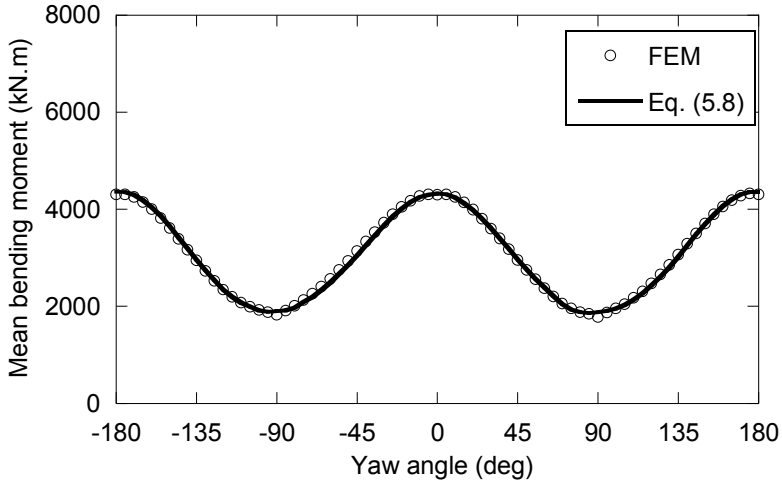

(a) Along-wind direction

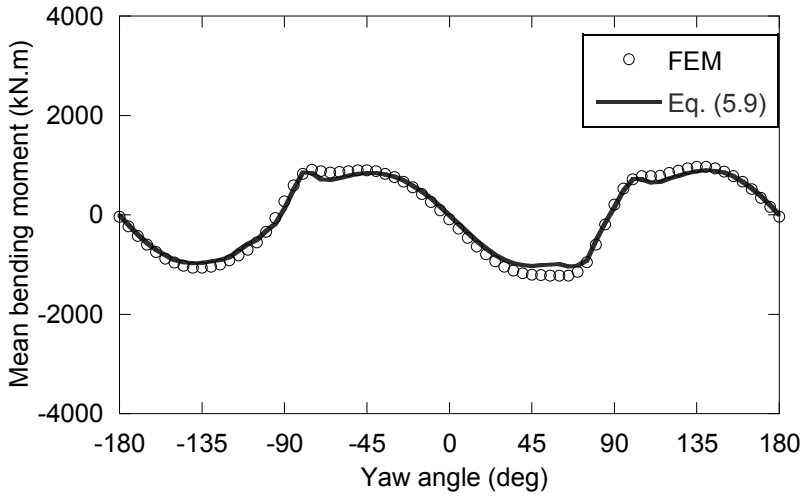

(b) Across-wind direction

Figure 5.6 Comparison of mean bending moment (400kW, $I_{uh} = 0.158$)

5.4. Gust Loading Factor

In Eq. (5.2), the gust loading factor is calculated from the mean bending moment, the standard deviation and peak factor of fluctuating bending moment. It is noted that this bending moment-based peak factor can be used for the calculation of shear force on the wind turbine tower.

5.4.1. Standard Deviation

Standard deviation of fluctuating wind load consists of a background part σ_{MBf} and a resonant part σ_{MRf} :

$$\sigma_{Mf} = \sqrt{\sigma_{MBf}^2 + \sigma_{MRf}^2} \tag{5.10}$$

For wind turbine, the across-wind mean bending moment becomes close to zero at some yaw angles. In this study the along-wind mean bending moment $\bar{M}_D$ is employed to calculate both along-wind and across-wind standard deviation of bending moment. The background standard deviation should include two components: σ_{MBfu} and σ_{MBfv} , which depend on the fluctuation component u and v , respectively, as well as resonant standard deviation which consists of σ_{MRfu} and σ_{MRfv} . By FEM simulation, it is found that for along-wind direction the standard deviation due to lateral wind fluctuation v can be neglected compared to that due to longitudinal wind fluctuation u , as shown in Figure 5.7 (a).

$$\sigma_{MBD} = \sqrt{\sigma_{MBDu}^2 + \sigma_{MBDv}^2} \tag{5.11}$$

$$\sigma_{MRD} = \sqrt{\sigma_{MRDu}^2 + \sigma_{MRDv}^2} \tag{5.12}$$

where

$$\sigma_{MBDu} = 2\frac{\overline{M}_D}{1+I_{uh}^2} I_{uh}\sqrt{K_{MBDu}\cdot\gamma_{MBDu}}\ , \qquad \sigma_{MBDv} = 2\frac{\overline{M}_D}{1+I_{uh}^2} I_{vh}\sqrt{K_{MBDv}\cdot\gamma_{MBDv}} \approx 0\ ,$$

$$\sigma_{MRDu} = 2\frac{\overline{M}_D}{1+I_{uh}^2} I_{uh}\frac{\pi\phi_D}{\sqrt{4\pi\xi_D}}\sqrt{R_{uh}(n_1)}\sqrt{K_{MRDu}(n_1)\cdot\gamma_{MRDu}}\ ,$$

$$\sigma_{MRDv} = 2\frac{\overline{M}_D}{1+I_{uh}^2} I_{vh}\frac{\pi\phi_D}{\sqrt{4\pi\xi_D}}\sqrt{R_{vh}(n_1)}\sqrt{K_{MRDv}(n_1)\cdot\gamma_{MRDv}} \approx 0\ .$$

While for across-wind direction in both background and resonant standard deviation σ_{MBL} and σ_{MRL}, neither part caused by the two wind fluctuation components can be neglected, since u contributes a lot to the standard deviation as well, although around the 0° and ±90° most of the standard deviation comes form v,as shown Figure 5.7 (b).

$$\sigma_{MBL}^2 = \sqrt{\sigma_{MBLu}^2 + \sigma_{MBLv}^2} \qquad 5.13$$

$$\sigma_{MRL} = \sqrt{\sigma_{MRLu}^2 + \sigma_{MRLv}^2} \qquad 5.14$$

where

$$\sigma_{MBLu} = 2\frac{\overline{M}_D}{1+I_{uh}^2} I_{uh}\sqrt{K_{MBLu}\cdot\gamma_{MBLu}}\ ,$$

$$\sigma_{MBLv} = 2\frac{\overline{M}_D}{1+I_{uh}^2} I_{vh}\sqrt{K_{MBLv}\cdot\gamma_{MBLv}}\ ,$$

$$\sigma_{MRLu} = \frac{2\overline{M}_D}{1+I_{uh}^2}\frac{I_{uh}\pi\phi_L}{\sqrt{4\pi\xi_L}}\sqrt{R_{uh}(n_1)}\sqrt{K_{MRLu}(n_1)\cdot\gamma_{MRLu}}\ ,$$

$$\sigma_{MRLv} = \frac{2\overline{M}_D}{1+I_{uh}^2}\frac{I_{vh}\pi\phi_L}{\sqrt{4\pi\xi_L}}\sqrt{R_{vh}(n_1)}\sqrt{K_{MRLv}(n_1)\cdot\gamma_{MRLv}}\ .$$

ϕ_D , ϕ_L are the mode correction factor, ξ_D and ξ_L are the damping ratio, K_{MBDu}, K_{MBDv} and $K_{MRDu}(n_1)$, $K_{MRDv}(n_1)$ are denoted the background and resonant size reduction factors of along-wind direction owing to the lack of correlation of longitudinal and lateral wind fluctuations, K_{MBLu}, K_{MBLv} and $K_{MRLu}(n_1)$, $K_{MRLv}(n_1)$ are the background and resonant size reduction factors of across-wind direction, n_1 is the first modal frequency of the tower, $I_{vh} = 0.8I_{uh}$ is the turbulence intensity at hub height in the across-wind direction, $R_{uh}(n_1)$ and $R_{vh}(n_1)$ are the normalized power spectral density of longitudinal and lateral wind fluctuation, γ_{MBDu} , γ_{MBDv} γ_{MRDu} , γ_{MRDv} , γ_{MBLu} γ_{MBLv} γ_{MRLu} γ_{MRLv} are the wind load ratios, which

can be considered as the correction factors to the size reduction factors, resulted from the employing of along-wind mean bending moment $\bar{M}_D$ to calculate the standard deviation of bending moment.

The formulae of wind load ratios are proposed as Table 5.2, employing a_B, a_R as rotor-tower ratios of area for background and resonant response, respectively and the average diameter of tower $D_a = (D_b + D_t)/2$. γ_{MBDv} and γ_{MRDv} are negligibly small, which is the reason why σ_{MBDv} and σ_{MRDv} can be ignored compared to σ_{MBDu} and σ_{MRDu}. Refers to *Appendix A.4.1* for the detailed derivation.

Table 5.2 Wind load ratios

Name	Along-wind	Across-wind
Background wind load ratio	$\gamma_{MBDu} = 1$	$\gamma_{MBLu} = \left(\frac{C_{L,r}(\theta) \cdot a_B}{1 + C_{D,r}(\theta) \cdot a_B} \right)^2$, $\gamma_{MBLv} = \left(\frac{A_{L,r}(\theta) \cdot a_B}{1 + C_{D,r}(\theta) \cdot a_B} \right)^2$, $a_B = \frac{A_r}{C_{D,t}(\theta) \cdot 0.47 D_a H_h}$
Resonant wind load ratio	$\gamma_{MRDu} = 1$	$\gamma_{MRLu} = \left(\frac{C_{L,r}(\theta) \cdot a_R}{1 + C_{D,r}(\theta) \cdot a_R} \right)^2$, $\gamma_{MRLv} = \left(\frac{A_{L,r}(\theta) \cdot a_R}{1 + C_{D,r}(\theta) \cdot a_R} \right)^2$, $a_R = \frac{A_r}{C_{D,t}(\theta) \cdot 0.3 D_a H_h}$

From Figure 5.7, it is noticed that in across-wind direction the standard deviation becomes maximum near ±90° resulted in the large gradient of aerodynamic coefficient $A_L(\theta)$ of rotor and show minimum value near 0° and ±180°, just opposite to the situation of along-wind direction. This is why the across-wind load should be considered when the inflow angle increases, and can be neglected compared to the along-wind load around 0° and ±180°. Analytical formulae will be proposed for the complex integral form of mode correction factor, aerodynamic damping ratio and size reduction factors in the following.

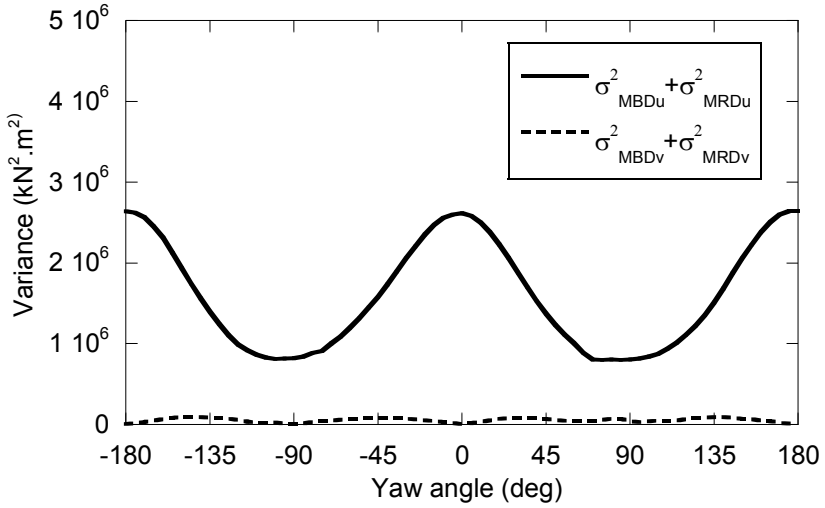

(a) Along-wind direction

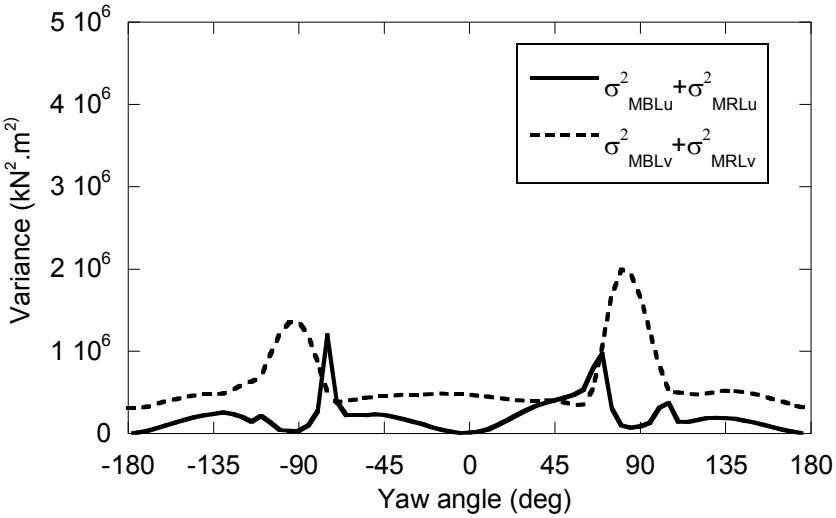

(b) Across-wind direction

Figure 5.7 Comparison of standard deviation from u and v (400kW, $I_{uh} = 0.158$)

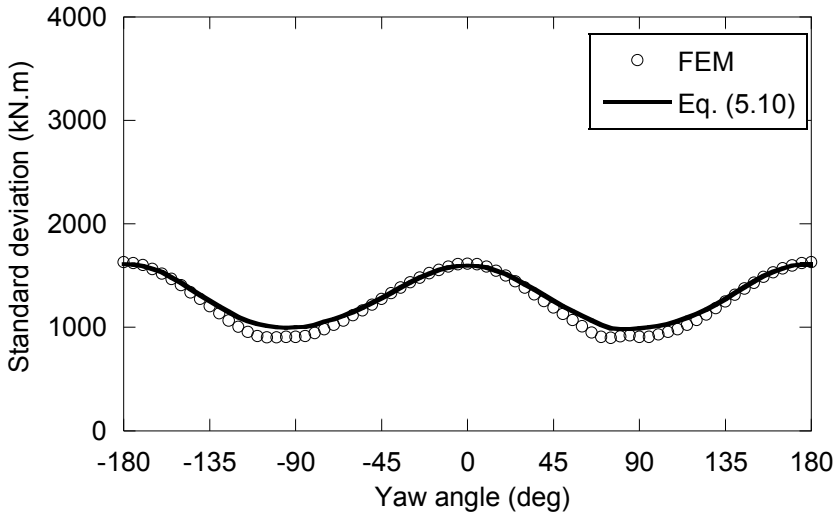

(a) Along-wind direction

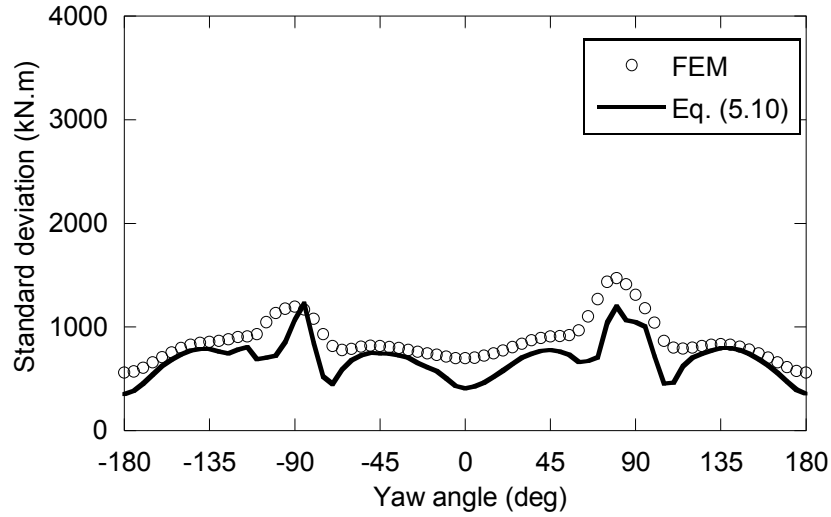

(b) Across-wind direction

Figure 5.8 Comparison of standard deviation (400kW, $I_{uh} = 0.158$)

Mode Correction Factor

Resulted from the employing of along-wind mean bending moment $\bar{M}_D$ to calculate the standard deviation of bending moment, the same mode correction factor can be used for along-wind and across-wind direction (Eq. 5.15). In the mode correction factor, the rotor part and tower part are first considered separately and then introduce the factors λ_a, λ_b to consider the rotor effect by the rotor-tower mass ratio γ_m and load ratio γ_F on the base of that for tower, i.e., a' and b'. Finally, the integral form of mode correction factor ϕ_D can be derived as the product of five non-dimensional parameters, as shown in Eq. (5.16):

$$\phi_D = \phi_L = \frac{\int C_D(r,\theta)\mu_1(r)c(r)dr}{\int C_D(r,\theta)c(r)rdr}\frac{\int m(r)\mu_1(r)rdr}{m_1} \quad 5.15$$

$$\phi_D = \phi_L \approx \frac{m_s}{m_1}\cdot\left(\frac{\gamma_m/a'+1}{\gamma_m+1}\cdot\frac{\int_0^{H_h} m(z)\mu_1(z)zdz}{m_t H_h}\right)\cdot\left(\frac{\gamma_F/b'+1}{\gamma_F+1}\cdot\frac{\int_0^{H_h} C_{D,t}(\theta)d(z)\mu_1(z)dz}{\int_0^{H_h} C_{D,t}(\theta)d(z)\frac{z}{H_h}dz}\right) = \gamma_M\cdot(\lambda_a a')\cdot(\lambda_b b') \quad 5.16$$

where $m(r)$ is the mass per length of the element at position r, m_s is the total mass of wind turbine, m_1 is the generalized mass of the whole wind turbine for the first mode, m_r and m_t are the mass of rotor and tower, respectively, $d(z) = D_b - (D_b - D_t)z/H_h$ is the diameter of tower. $\gamma_M = m_s/m_1$ changes very little for different wind turbines with an average of 1.96. $\lambda_a = (\gamma_m/a'+1)/(\gamma_m+1)$, where $\gamma_m = m_r/m_t$ is rotor-tower ratio of mass, also changing very little for different wind turbines with an average of 0.79. $a' = 1/(2+\beta_s)$ is derived theoretically, the same as that given by AIJ [1]. $\lambda_b = (\gamma_F/b'+1)/(\gamma_F+1) = 1.2 + 0.07\cos 2\theta$ is obtained by fitting the results of integral form, where $\gamma_F = C_{D,r}(\theta)A_r/(C_{D,t}(\theta)\cdot 0.42 D_a H_h)$ is rotor-tower ratio of load. $b' =$ 0.714 is derived theoretically and very close to $1-0.4\ln\beta_s$ which is given by AIJ [1]. *Appendix A.4.1* gives the details of mode correction factor.

A unified mode correction factor is obtained for different wind turbines. Figure 5.9 shows good agreement between the proposed formula and the integral form. Due to the existence of rotor, ϕ_D and ϕ_L varie with yaw angle in a range larger than that of tower. It is noticed that if the rotor is removed, like tower or high-rise building, i.e., $\gamma_m = \gamma_F = 0$, λ_a and λ_b will be 1.0, which will make the mode correction factor the same as that given in AIJ [1].

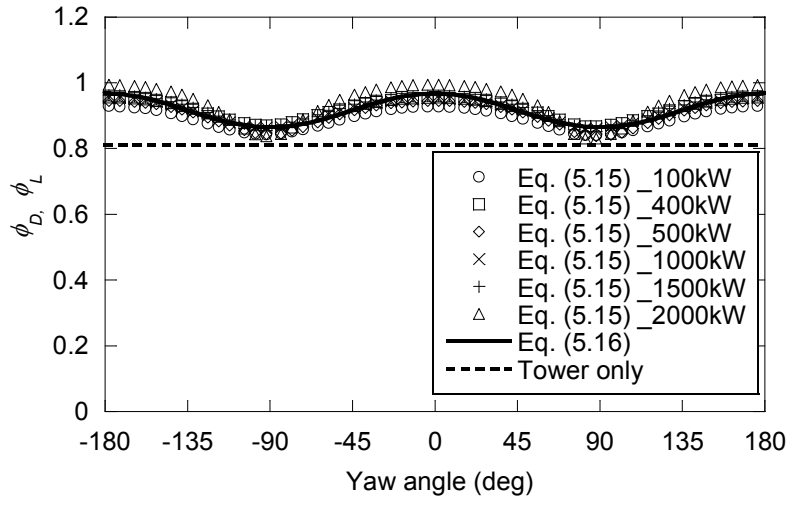

Figure 5.9 Comparison of mode correction factor

Damping Ratio

Due to the existence of rotor, the aerodynamic damping may become much larger than the structural one at some wind direction and cannot be neglected, which is different from the high-rise buildings and chimneys. Therefore, the total damping ratio should be the summation of structural damping ratio ξ_s (Ishihara et al. [11] indicates $\xi_s = 0.8\%$ for wind turbine with gear box) and aerodynamic damping ratio. It should be noted that for across-wind direction, since the aerodynamic damping ratio ξ_{aL} may become negative at some yaw angle, $\xi_L = \max\left(\xi_s + \xi_{aL}, \xi_s\right)$ is used to limit the total damping ratio ξ_L not less than the structural one in order to avert aero-elastic instability.

For along-wind direction, the aerodynamic damping ratio ξ_{aD} contains two parts: the aerodynamic damping ratio for the rotor and the tower, as expressed in Eq. (5.17). It is found that most of the aerodynamic damping of wind turbine comes from the rotor, which results in nearly 9 times of that from the tower at most. While for across-wind direction, since the aerodynamic coefficient gradient $A_{L,t}(\theta) = 0$ for tower, the aerodynamic damping ratio ξ_{aL} is totally caused by rotor, as expressed in Eq. (5.18). Refers to *Appendix A.4.1* for the detailed derivation of aerodynamic damping ratio.

$$\xi_{aD} = \frac{\int \rho C_D(r,\theta) U(r) c(r) \mu_1^2(r) dr}{4\pi m_1 n_1} = \frac{\rho U_h}{4\pi m_1 n_1}\left(C_{D,r}(\theta) A_r + C_{D,t}(\theta) H_h D''\right) \tag{5.17}$$

$$\xi_{aL} = \frac{\int \rho A_L(r,\theta) U(r) c(r) \mu^2(r) dr}{4\pi m_1 n_1} = \frac{\rho U_h A_r A_{L,r}(\theta)}{4\pi m_1 n_1} \tag{5.18}$$

where

$$D'' = \frac{D_b + (\alpha+5) D_t}{(\alpha+5)(\alpha+6)},$$

$$A_{L,r}(\theta) = 3\int_0^R \frac{1}{2}\left(C_{D,b}(r,\theta) + \frac{\partial C_{L,b}}{\partial \theta}(r,\theta)\right) c(r) dr / A_r .$$

$A_{L,r}(\theta)$ is the equivalent aerodynamic coefficient gradient of rotor, showing significant peaks near ±90° in Figure 5.10. From Eqs. (5.17) and (5.18), it is obvious that the variation of aerodynamic damping ratio with wind direction depends on the aerodynamic coefficients.

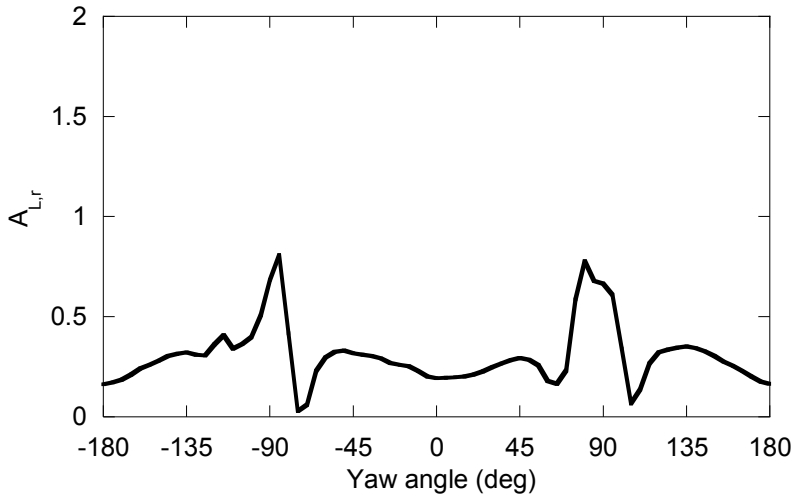

Figure 5.10 Equivalent aerodynamic coefficient gradient (400kW)

Size Reduction Factor

Appendix A.4.1 gives the integral form of each size reduction factor. From the integral calculation, it is found that the background and resonant size reduction factors are almost constant with different yaw angles. Hence, it can be assumed that they don't vary with yaw angle. In addition, it can be observed from the integral form that the background size reduction factor should be a function of the turbulence integral length scale L_u or L_v ($L_v = 0.33L_u$ is for the across-wind direction) and the rotor radius R which is taken as the characteristic size of the whole wind turbine in this study. Referring to AIJ [1], the formula format for lattice structures, $1/\left(1+\beta_B \cdot R/0.3L_u\right)$ or $1/\left(1+\beta_B \cdot R/0.3L_v\right)$ is adopted here. While the resonant size reduction factor should be a function of the non-dimensional decay factor C (Cramer [12] indicated values of C ranging from 7 to 50, so C = 8.0 is used here), the first modal natural frequency n_1, rotor radius R, and mean wind speed at hub height U_h , then the formula format becomes $1/\left(1+\beta_R \cdot Cn_1R/U_h\right)^2$. The unknown factors β_B and β_R can be identified by fitting the results from the integral form of seven different sizes of wind turbines. For each wind turbine, the mean value of different yaw angles is taken as the result of the integral form. Finally, the formulae of background and resonant size reduction factors for along-wind direction are proposed as

$$K_{MBDu} = \frac{1}{1+0.69\dfrac{R}{0.3L_u}} \tag{5.19}$$

$$K_{MRDu}\left(n_1\right) = \frac{1}{\left(1+0.26\dfrac{Cn_1R}{U_h}\right)^2} \tag{5.20}$$

And the formulae of background and resonant size reduction factors for across-wind direction are proposed as

$$K_{MBLu}=\frac{1}{1+0.5\dfrac{R}{0.3L_u}} \tag{5.21}$$

$$K_{MBLv}=\frac{1}{1+0.5\dfrac{R}{0.3L_v}} \tag{5.22}$$

$$K_{MRLu}(n_1)=K_{MRLv}(n_1)=\frac{1}{\left(1+0.21\dfrac{Cn_1R}{U_h}\right)^2} \tag{5.23}$$

Figure 5.11 shows good agreement between the proposed formula and the integral form for each size reduction factor. Both background and resonant size reduction factors vary in the range of 0 ~ 1.0, and the background one decreases when the wind turbine size increases. However, the resonant one doesn't have this feature, since it is also related to the natural frequency of wind turbine. It is noticed that the size reduction factors are close to those of tower and rotor, since the effect from rotor and tower cancel each other. The size reduction factors of across-wind direction totally come from the rotor, hence close to those of along-wind direction. Since L_v is smaller than L_u, K_{MBLv} is smaller than K_{MBLu}, which indicates that the smaller turbulence integral length scale results in the more lack of correlation of the fluctuating wind velocity and the size effect becomes more significant.

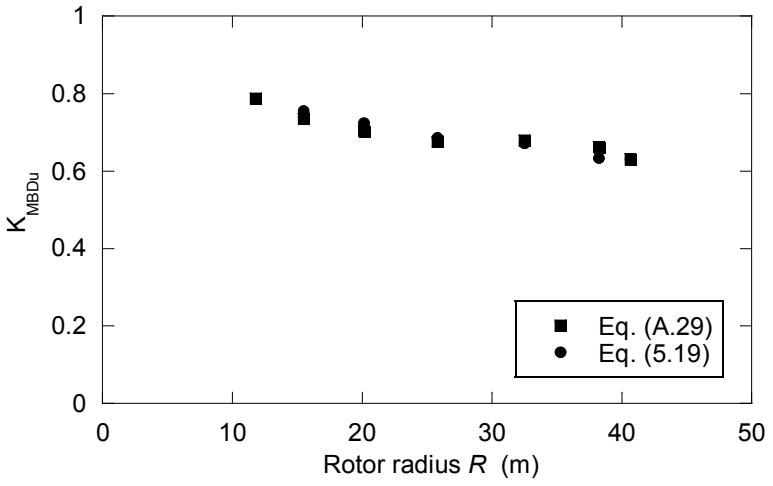

(a) Background one of along-wind direction

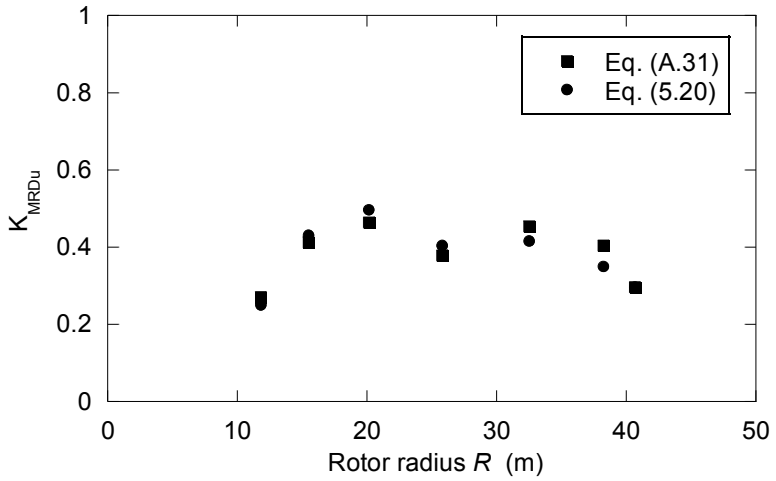

(b) Resonant one of along-wind direction

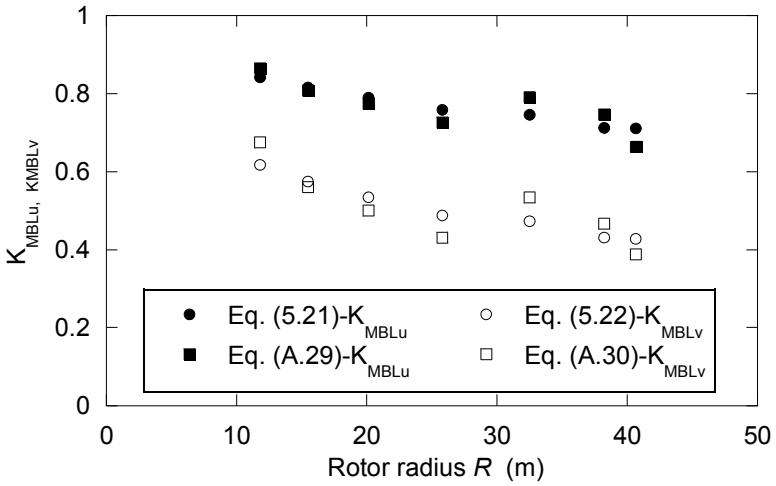

(c) Background one of across-wind direction

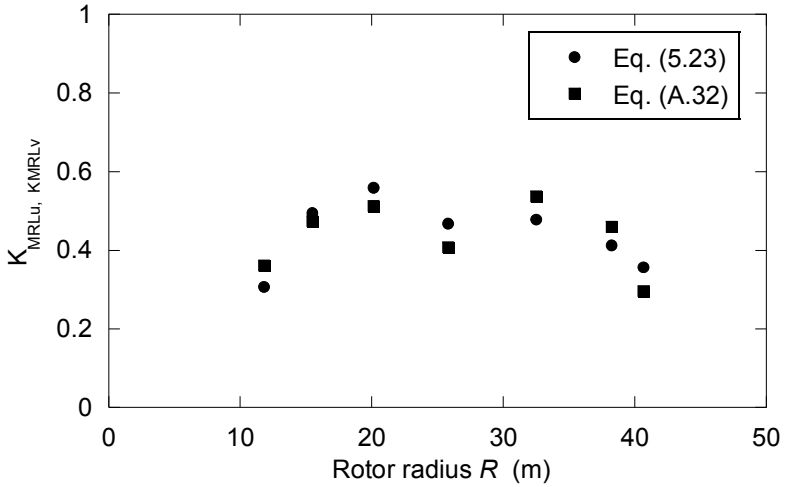

(d) Resonant one of across-wind direction

Figure 5.11 Comparison of size reduction factors

5.4.2. Peak Factor

In order to take the non-linear component of wind load into account, Kareem et al. [7] evaluated the peak factor for the non-Gaussian process by employing the moment-based Hermite transformation which has been shown to be accurate and robust in representing the tail regions of the PDF in a non-Gaussian process. It is a function of kurtosis α_4 and skewness α_3. Binh et al. [6] proved that the effect of kurtosis α_4 can be neglected since it is negligibly small compared to that of the second and third order from the order analysis of turbulence intensity I_u. α_4 is then assumed to be equal to the value of a Gaussian process (i.e., 3.0). Then the formula of the peak factor is simplified to a function of skewness α_3, as shown in Eq. (5.24). Refers to *Appendix A.4.2* for details.

$$g_D = \frac{1}{\sqrt{1+\frac{\alpha_3^2}{18}}}\left\{\left(\sqrt{2\ln\left(\nu_D' T\right)}+\frac{0.5772}{\sqrt{2\ln\left(\nu_D' T\right)}}\right)+\frac{\alpha_3}{6}\left(2\ln\left(\nu_D' T\right)-1\right)\right\} \tag{5.24}$$

where $\nu_D' = \nu_D / \sqrt{\left(1+\alpha_3^2/18\right)\left(1+\alpha_3^2/9\right)}$ is the zero up-crossing number in the estimated time interval *T* (normally 600s) of non-Gaussian process. Binh et al. [6] proposed a formula of skewness α_3 for wind turbines, considering both significant resonant response and spatial correlation of wind velocity using a correlation coefficient $\rho\left(r,r'\right)=\exp\left[-\left|r-r'\right|/0.3L_u\right]$.

$$\alpha_3 = \frac{1}{1.3R_D+1}\times\frac{3I_{uh}a_{r1D}}{(K_{MBDu})^{\frac{3}{2}}} \tag{5.25}$$

where

$$R_D = \left(\frac{\sigma_{MRD}}{\sigma_{MBD}}\right)^2,$$

$$a_{r1D} = \frac{\iiint \rho\left(r,r'\right)\rho\left(r',r''\right)C_D\left(r,\theta\right)C_D\left(r',\theta\right)C_D\left(r'',\theta\right)c\left(r\right)c\left(r'\right)c\left(r''\right)rr'r''drdr'dr''}{\left(\int C_D\left(r,\theta\right)c\left(r\right)rdr\right)^3} \approx \frac{1}{1+\beta_{1D}\frac{R}{0.3L_u}}.$$

where R_D is denoted the resonance-background ratio of along-wind standard deviation, and a_{r1D} is a size reduction factor, considering the lack of correlation of the fluctuating wind velocity. Since a_{r1D} is related to the background response, it can be formulated with the same analysis and approach as those of K_{MBDu} or K_{MBLu}, and the unknown factor $\beta_{1D}=1.67$ is proposed, which agrees well with its integral form, as shown in Figure 5.12.

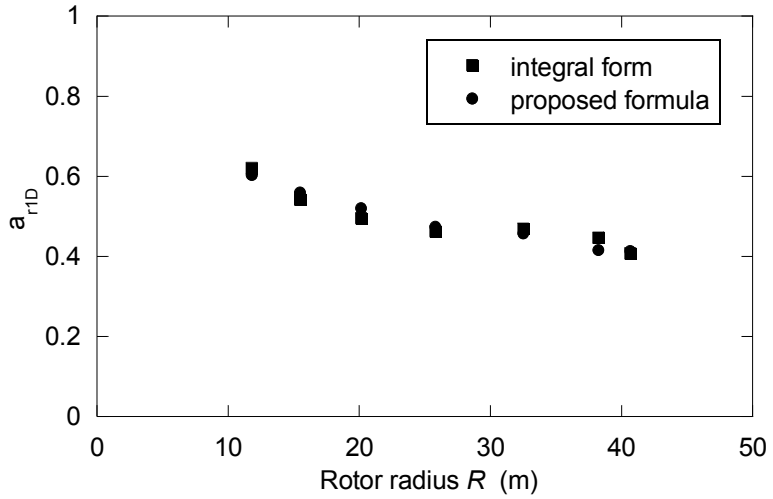

Figure 5.12 Size reduction factor a_{r1D}

It is noticed from the FEM simulation that for the across-wind response, since the skewness and kurtosis of fluctuating wind load are close to 0 and 3.0, respectively, the non-Gaussian peak factor of Eq. (5.26) can be reduced to the standard Gaussian form:

$$g_L = \sqrt{2\ln(\nu_L T)} + \frac{0.5772}{\sqrt{2\ln(\nu_L T)}} \qquad 5.26$$

where ν_L is the zero up-crossing number in the estimated time interval T (normally 600s) of Gaussian process of across-wind load. The peak factors change very little with the wind direction. Figure 5.13 shows the peak factor for $\theta = 0^\circ$, and it is noticed that the non-Gaussian peak factor increases when the turbulence intensity increases, while Gaussian peak factor keeps constant and lower value, which means an Gaussian peak factor will underestimate the wind load of along-wind direction, especially in the high turbulence intensity.

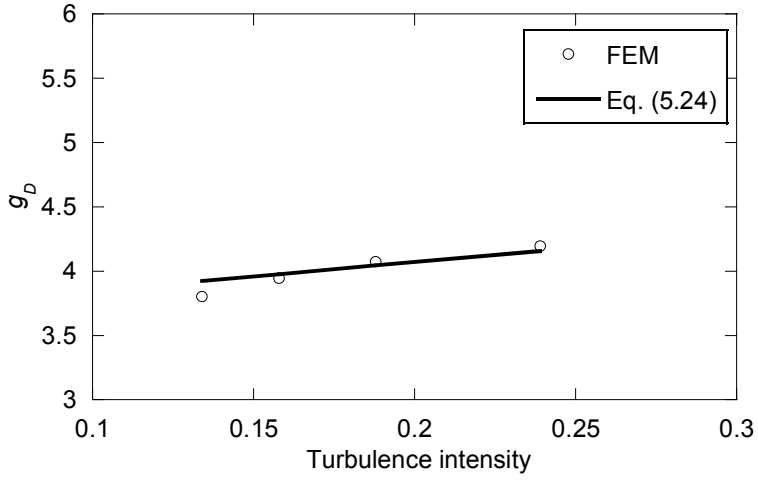

(a) Along-wind direction

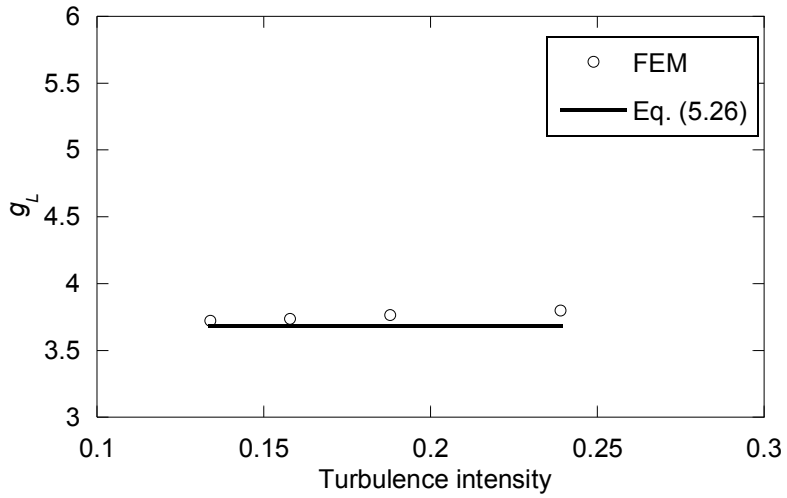

(b) Across-wind direction

Figure 5.13 Comparison of peak factor (400kW, $\theta = 0^\circ$)

5.5. Maximum Bending Moment

The maximum bending moments on tower base from proposed formulae have been verified by FEM simulation, as shown in Figure 5.14.

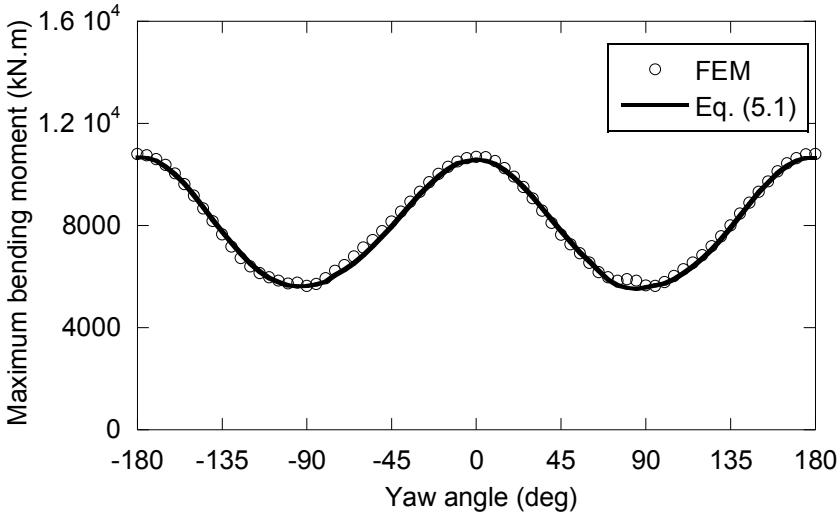

(a) Along-wind direction

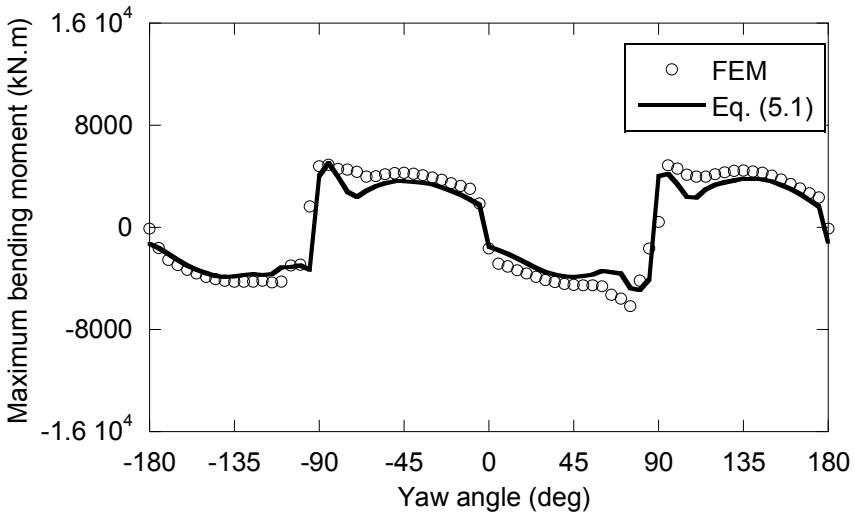

(b) Across-wind direction

Figure 5.14 Comparison of maximum bending moment (400kW, $I_{uh} = 0.158$)

5.6. Comparison between SR Model and Fixed-foundation Model

For floating wind turbine systems, it has to be judged whether the fixed-foundation model can be used to calculate the wind-induced load or not. The comparison between SR model and fixed-foundation model will be carried out in this section to explain why SR model should be employed for the wind-induced load prediction.

All the formulae proposed in the earlier sections are applicable to these two models. The differences between them are the values of the parameters in the formulae. Comparing the formulae of mean wind load, standard deviation and peak factor, it is easily found that the mean wind loads for these two models are the same; in the standard deviation, the background parts are the same, since it only depends on the wind itself, however, the resonant parts are different due to the difference of mode correction factor, damping ratio, wind spectrum and size reduction factor between these two models; the peak factor is the function of skewness and zero up-crossing frequency, which also change with models.

5.6.1. Standard Deviation

The resonant standard deviation is as follows:

$$\sigma_{FR} = 2\frac{\overline{F}}{1+I_{uh}^2} I_{uh} \frac{\pi\phi}{\sqrt{4\pi\xi}} \sqrt{R_{uh}(n_1)} \sqrt{K_{FR}(n_1)} \qquad 5.27$$

Since the wind spectrum $R_{uh}(n_1)$ and size reduction factor $K_{FR}(n_1)$ are the function of the first natural frequency, before comparison the first natural frequency of the two models should be determined. And their damping ratios are also in need.

Referring to AIJ [1], the equivalent single degree of freedom model (SDOF) of the MDOF model of a superstructure is often applied considering sway and rocking motions and is called condensed SR model (Figure 5.15). The mass, stiffness and damping ratio of the SDOF model are m_e, k_e and c_e, respectively. The force F acting on the SDOF model is

$$F = k_t x_t = k_e x_e = k_s x_s = k_r \theta / h_e \tag{5.28}$$

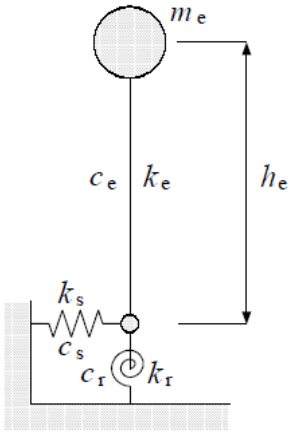

Figure 5.15 Condensed SR model

Hence, the total displacement is as follows.

$$x_t = x_e + x_s + x_r = x_e + x_s + \theta h_e \tag{5.29}$$

$$\frac{F}{k_t} = \frac{F}{k_e} + \frac{F}{k_s} + \frac{F h_e}{k_r} h_e \tag{5.30}$$

The total stiffness k_t is related to the stiffness of each element in Figure 5.15 as follows.

$$\frac{1}{k_t} = \frac{1}{k_e} + \frac{1}{k_s} + \frac{h_e^2}{k_r} \tag{5.31}$$

Multiplying $4\pi^2 m_e$ and using $T_t^2 = 4\pi^2 m_e / k_t$, $T_e^2 = 4\pi^2 m_e / k_e$, $T_s^2 = 4\pi^2 m_e / k_s$, $T_r^2 = 4\pi^2 m_e h_e^2 / k_r$, Eq. (5.31) is transformed as follows.

$$T_t^2 = T_e^2 + T_s^2 + T_r^2 \tag{5.32}$$

As T_t is the first natural period T_1 of the model in Figure 5.15, and T_e is equal to T_f which is the first natural period of fixed-foundation model, Eq. (5.33) in the text is obtained.

$$T_1 = \sqrt{T_f^2 + T_s^2 + T_r^2} \tag{5.33}$$

In order to obtain the damping ratio of the condensed SR model, let us consider the strain and absorbed energy E and ΔE during a cycle vibrating in the period T_1. The absorbed energy ΔE is expressed as:

$$\Delta E = \int c\dot{x}dx = \int c\dot{x}\cdot\dot{x}dt = \int c\left(\dot{x}\right)^2 dt \tag{5.34}$$

With $x = X\cos\omega_0 t$, Eq. (5.34) becomes

$$\begin{aligned}
\Delta E &= \int c\left(\dot{x}\right)^2 dt = \int c\left(-\omega_0 X\sin\omega_0 t\right)^2 dt = c\omega_0 X^2\int_{-\pi}^{\pi}\left(\sin\omega_0 t\right)^2 d\left(\omega_0 t\right) \\
&= c\omega_0 X^2\int_{-\pi}^{\pi}\left(\frac{1-\cos 2\omega_0 t}{2}\right)d\left(\omega_0 t\right) \\
&= c\omega_0 X^2\left(\pi - \int_{-2\pi}^{2\pi}\left(\frac{\cos\left(2\omega_0 t\right)}{4}\right)d\left(2\omega_0 t\right)\right) \\
&= c\omega_0 X^2\left(\pi - \frac{\sin\left(2\omega_0 t\right)}{4}\Big|_{-2\pi}^{2\pi}\right) \\
&= c\pi\omega_0 X^2
\end{aligned} \tag{5.35}$$

$$c = \frac{\Delta E}{\pi\omega_0 X^2} \tag{5.36}$$

The strain energy is $E = \frac{1}{2}kX^2$, so the damping ratio is expressed as follows.

$$\xi = \frac{c}{2m\omega_0} = \frac{c}{2\frac{k}{\omega_0^2}\omega_0} = \frac{c\omega_0}{2k} = \frac{\frac{\Delta E}{\pi\omega_0 X^2}\omega_0}{2\frac{2E}{X^2}} = \frac{1}{4\pi}\frac{\Delta E}{E} \tag{5.37}$$

The absorbed energy is as follows.

$$\Delta E = \pi\omega_1 c_t x_t^2 = \pi\omega_1\left(c_e x_e^2 + c_s x_s^2 + c_r\theta^2\right) \tag{5.38}$$

The strain energy is as follows.

$$E = \frac{1}{2}k_t x_t^2 = \frac{1}{2}\left(k_e x_e^2 + k_s x_s^2 + k_r\theta^2\right) \tag{5.39}$$

Substituting Eq. (5.38) and Eq. (5.39) into Eq. (5.37), the total damping ratio ξ_t becomes

$$\xi_t = \frac{1}{4\pi}\frac{\Delta E}{E} = \frac{1}{4\pi}\frac{\pi\omega_1\left(c_e x_e^2 + c_s x_s^2 + c_r\theta^2\right)}{\frac{1}{2}k_t x_t^2} = \frac{\pi\omega_1\left(c_e x_e^2 + c_s x_s^2 + c_r\theta^2\right)}{2\pi k_t x_t^2} \quad 5.40$$

From Eq. (5.28), the following relationship can be obtained

$$\frac{x_e}{x_t} = \frac{k_t}{k_e} \qquad \frac{x_s}{x_t} = \frac{k_t}{k_s} \qquad \frac{x_r}{x_t} = \frac{k_t h_e^2}{k_r} \quad 5.41$$

Using $T_t^2 = 4\pi^2 m_e / k_t$, $T_e^2 = 4\pi^2 m_e / k_e$, $T_s^2 = 4\pi^2 m_e / k_s$, $T_r^2 = 4\pi^2 m_e h_e^2 / k_r$, the following relationship can be obtained:

$$T_t^2 k_t = T_e^2 k_e = T_s^2 k_s = T_r^2 k_r / h_e^2 \quad 5.42$$

Hence,

$$\frac{x_e}{x_t} = \frac{k_t}{k_e} = \left(\frac{T_e}{T_1}\right)^2 \qquad \frac{x_s}{x_t} = \frac{k_t}{k_s} = \left(\frac{T_s}{T_1}\right)^2 \qquad \frac{x_r}{x_t} = \frac{k_t h_e^2}{k_r} = \left(\frac{T_r}{T_1}\right)^2 \quad 5.43$$

Using Eq. (5.43) and $\xi_e = c_e / 2\sqrt{m_e k_e}$, $\xi_s = c_s / 2\sqrt{m_e k_s}$, $\xi_r = c_r / 2\sqrt{m_e h_e^2 k_r}$ the damping ratio ξ_1 for the first mode in the SR model is calculated as Eq. (5.44) in the text as follows.

$$\begin{aligned}
\xi_1 &= \frac{\pi\omega_1\left(c_e x_e^2 + c_s x_s^2 + c_r\theta^2\right)}{2\pi k_t x_t^2} \\
&= \frac{\pi\omega_1\left(\xi_e 2\sqrt{m_e k_e}\, x_e^2 + \xi_s 2\sqrt{m_e k_s}\, x_s^2 + \xi_r 2\sqrt{m_e h_e^2 k_r}\,\theta^2\right)}{2\pi k_t x_t^2} \\
&= \frac{\omega_1\left(\xi_e\sqrt{m_e k_e}\, x_e^2 + \xi_s\sqrt{m_e k_s}\, x_s^2 + \xi_r\sqrt{m_e h_e^2 k_r}\,\frac{x_r^2}{h_e^2}\right)}{k_t x_t^2} \\
&= \frac{\omega_1\xi_e\sqrt{m_e k_e}}{k_t}\frac{x_e^2}{x_t^2} + \frac{\omega_1\xi_s\sqrt{m_e k_s}}{k_t}\frac{x_s^2}{x_t^2} + \frac{\omega_1\xi_r\sqrt{m_e k_r / h_e^2}}{k_t}\frac{x_r^2}{x_t^2} \\
&= \frac{\sqrt{\frac{k_t}{m_e}}\xi_e\sqrt{m_e k_e}}{k_t}\left(\frac{T_e}{T_1}\right)^4 + \frac{\sqrt{\frac{k_t}{m_e}}\xi_s\sqrt{m_e k_s}}{k_t}\left(\frac{T_s}{T_1}\right)^4 + \frac{\sqrt{\frac{k_t}{m_e}}\xi_r\sqrt{m_e k_r / h_e^2}}{k_t}\left(\frac{T_r}{T_1}\right)^4 \\
&= \xi_e\sqrt{\frac{k_e}{k_t}}\left(\frac{T_e}{T_1}\right)^4 + \xi_s\sqrt{\frac{k_s}{k_t}}\left(\frac{T_s}{T_1}\right)^4 + \xi_r\sqrt{\frac{k_r}{h_e^2 k_t}}\left(\frac{T_r}{T_1}\right)^4 \\
&= \xi_f\left(\frac{T_1}{T_e}\right)\left(\frac{T_e}{T_1}\right)^4 + \xi_s\left(\frac{T_1}{T_s}\right)\left(\frac{T_s}{T_1}\right)^4 + \xi_r\left(\frac{T_1}{T_r}\right)\left(\frac{T_r}{T_1}\right)^4 \\
&= \xi_f\left(\frac{T_f}{T_1}\right)^3 + \xi_s\left(\frac{T_s}{T_1}\right)^3 + \xi_r\left(\frac{T_r}{T_1}\right)^3
\end{aligned} \quad 5.44$$

Hence, the first natural period and damping ratio of SR model can be calculated by Eqs. (5.33) and (5.44), respectively. The necessary variables and T_1, ξ_1 are tabulated in Table 5.3.

With the first natural frequency n_1 calculated from T_1, the wind spectrum and size reduction factor can be obtained. Figure 5.16 and Figure 5.17 show the variation of wind spectrum $R_{uh}(n_1)$ and size reduction factor $K_{FR}(n_1)$ with the first natural frequency, respectively. It can be seen that the fixed-foundation shows much lower value than SR model due to its high frequency. That would reduce the resonant standard deviation in Eq. (5.27).

Table 5.3 The periods and damping ratios

	T_f (s)	T_s (s)	T_r (s)	T_1 (s)	ξ_f	ξ_s	ξ_r	ξ_1
fix-foundation	2.86	0	0	2.86	0.005	AV	AV	0.005
tension leg	2.86	31.30	0	31.43	0.005	0.20	AV	0.20
catenary	2.86	26.80	14.30	30.51	0.005	0.40	0.38	0.31

AV: Arbitrary value

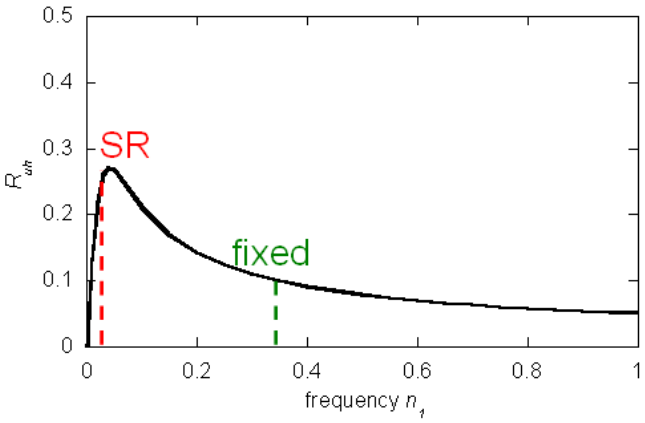

Figure 5.16 Comparison of wind spectrum

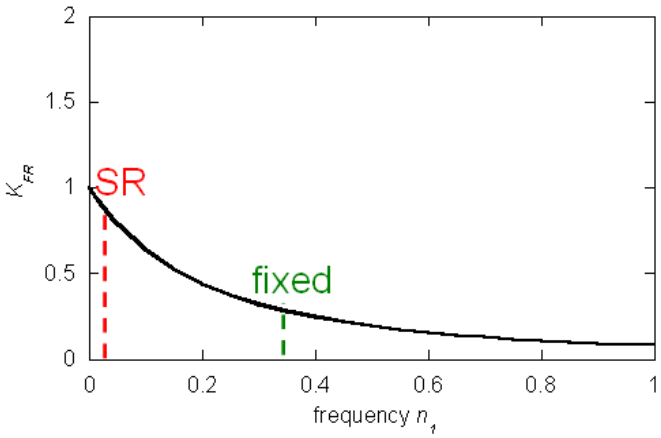

Figure 5.17 Comparison of size reduction factor

The large difference of the system damping ratio ξ_1 between fixed-foundation model and SR model results in the large difference of total damping ratio ξ, as shown in Figure 5.18. It can be seen that the fixed-foundation also shows much lower value than SR model. That would increase the resonant standard deviation in Eq. (5.27).

From Figure 5.19, the fixed-foundation shows a little lower mode correction factor ϕ than SR model but not so significant. Therefore, the dominant influence factor is the first natural frequency and systerm damping ratio. The fixed-foundation model and SR model have much different value in these two factors, so it can not be used to calculate the wind-induced load of floating wind turbine system, while SR model can give good result as shown in Figure 5.20. That is why the fixed-foundation model underestimates the standard deviation of tension leg system and overestimates that of catenary system. The standard deviation of catenary system is lower than that of tension leg system due to its larger damping ratio.

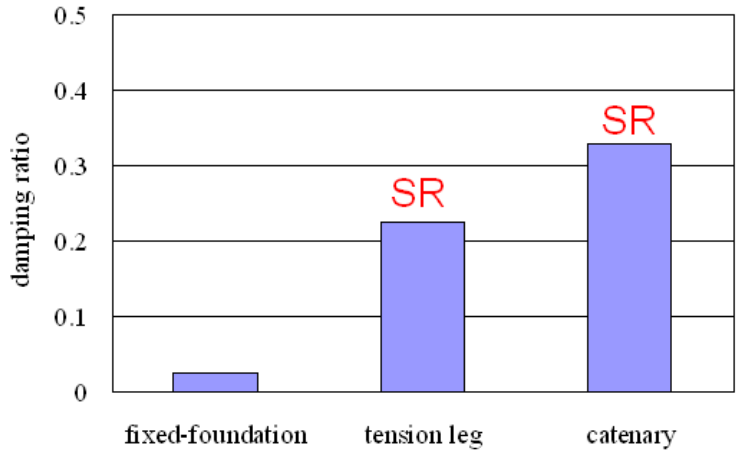

Figure 5.18 Comparison of total damping ratio ξ

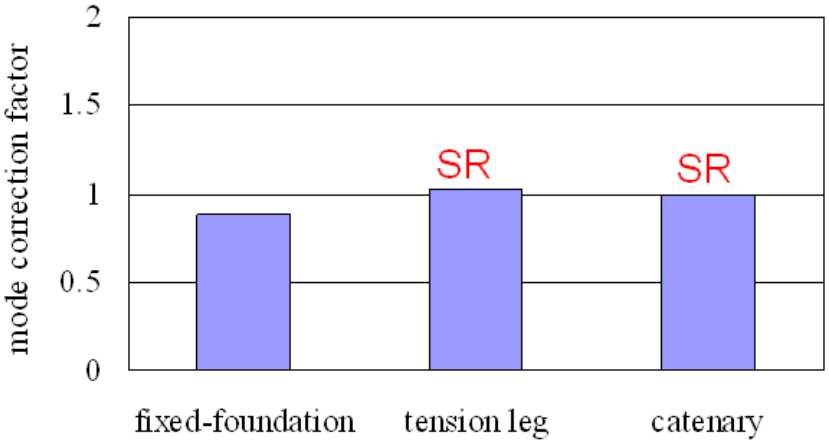

Figure 5.19 Comparison of mode correction factor ϕ

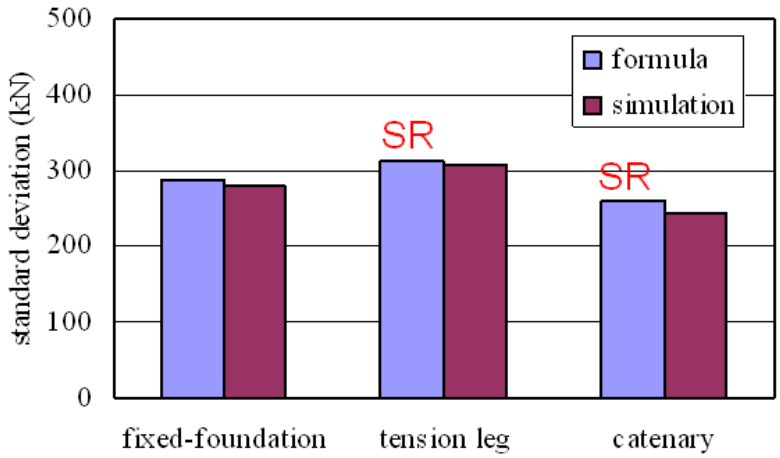

Figure 5.20 Comparison of standard deviation

5.6.2. Peak Factor

Due to the low turbulence intensity of offshore, the skewness becomes close to zero. Therefore, Gaussian peak factor can be assumed, which only depends on zero up-crossing frequency. Zero up-crossing frequency is much affected by the first natural frequency, so it changes a lot between fixed-foundation model and SR model. However, in Figure 5.21 which gives the variation of peak factor with zero up-crossing frequency, it is noticed that the peak factor is not sensitive to zero up-crossing frequency. Hence, the two models have close peak factor.

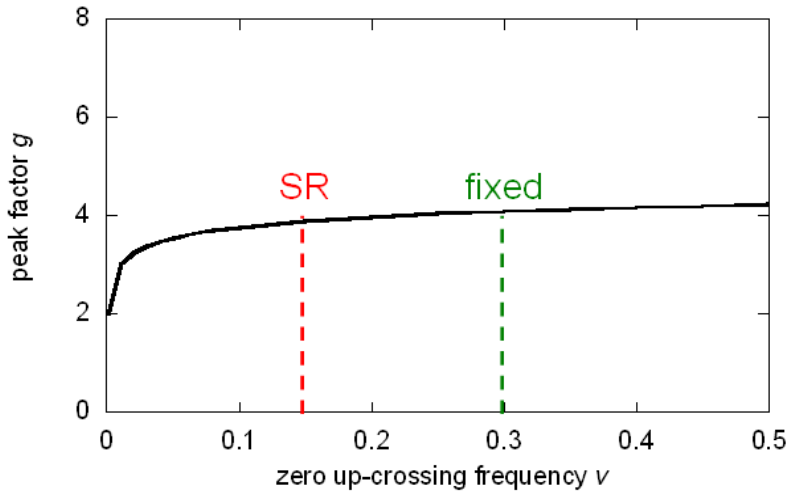

Figure 5.21 Comparison of peak factor

5.7. Combination of Wind Loads

Since the lift force on rotor becomes significant due to the increase of inflow angle, the combination of along-wind and across-wind loads is necessary for the estimation of

design wind load on wind turbine towers. Coupled vibration can result from the small anisotropy of the tower, as shown in Figure 5.22. It is noticed that the maximum values of along-wind and across-wind loads cannot appear simultaneously. Hence, the correlation coefficient of wind responses in the two directions should be considered.

Asami [13] proposed a formula of wind loads combination for high-rise buildings, in which the across-wind bending moment combined with the maximum along-wind bending moment can be express as $M_{LC} = \overline{M}_L + \left(\sqrt{2+2\rho_{DL}} - 1\right)\left(M_L - \overline{M}_L\right)$, where ρ_{DL} is the correlation coefficient between along wind and across wind responses. For the uncorrelated case ($\rho_{DL} = 0$), the coefficient multiplied to the maximum fluctuating component $\left(M_L - \overline{M}_L\right)$ is 0.4 approximately, while for the completely correlated case ($\rho_{DL} = 1$), this coefficient becomes 1. In the same way, the along-wind bending moment combined with the maximum across-wind bending moment can be express as $M_{DC} = \overline{M}_D + \left(\sqrt{2+2\rho_{DL}} - 1\right)\left(M_D - \overline{M}_D\right)$. Finally, therefore, the maximum wind bending moment acting on the tower can be estimated as

$$M_{DL} = \max\left(\sqrt{M_L^2 + \left(\bar{M}_D + \gamma_{DL}(M_D - \bar{M}_D)\right)^2}, \sqrt{M_D^2 + \left(\bar{M}_L + \gamma_{DL}(M_L - \bar{M}_L)\right)^2}\right) \qquad 5.45$$

where $\gamma_{DL} = \sqrt{2+2\rho_{DL}} - 1$. ρ_{DL} can be determined by fitting the results of FEM simulation. It varies with wind direction, as shown in Table 5.4. Figure 5.23 shows the comparison of combined maximum bending moment on the tower base. It is obvious that for arbitrary wind direction, the correlation coefficients shown in Table 5.4 give good agreement with FEM simulation. It is also noticed that the uncorrelated approximation ($\rho_{DL} = 0$) underestimates the maximum bending moment, while completely correlated approximation ($\rho_{DL} = 1$) gives a conservative result. Therefore, $M_{DL} = \sqrt{M_D^2 + M_L^2}$ is acceptable as a more simple alternative in the design.

Table 5.4 Correlation coefficients ρ_{DL} for stall-regulated wind turbines

	θ (deg)	ρ_{DL}
(1)	-180 ~ -110 -80 ~ 70 100 ~ 180	1.0
(2)	-90, 80	0.0
(3)	-110 ~ -90 -90 ~ -80 70 ~ 80 80 ~ 100	linear interpolation between (1) and (2)

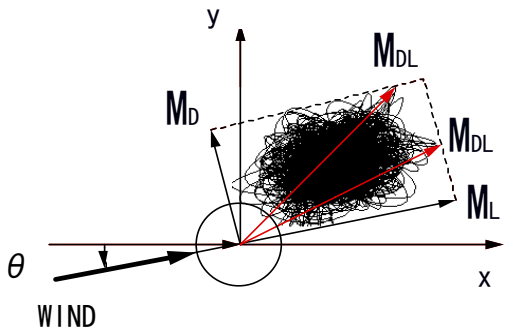

Figure 5.22 Tower bending moments plotted in X-Y plane

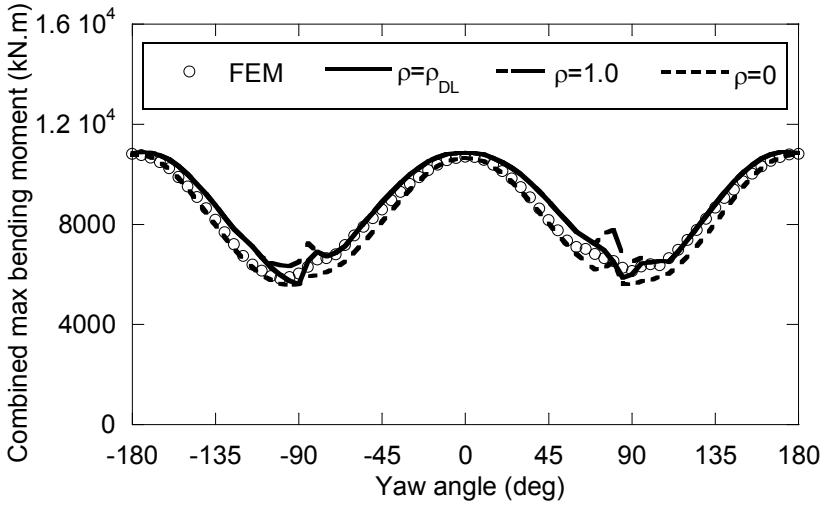

Figure 5.23 Comparison of combined maximum bending moment (400kW, $I_{uh} = 0.158$)

5.8. Conclusions

The conclusions and findings of this chapter are summarized as follows:

- A unified mode correction factor is proposed. Due to the existence of rotor, the mode correction factor varies with yaw angle in a range larger than that of tower.
- The background size reduction factor decreases when the wind turbine size increases, while the resonant one doesn't have this feature, since it is also related to the natural frequency of wind turbine. It is noticed that the size reduction factors are close to those of tower and rotor, since the effect from rotor and tower cancel each other. The size reduction factors of across-wind direction totally come from the rotor, hence close to those of along-wind direction.
- A non-Gaussian peak factor model is proposed for along-wind direction. When the skewness and kurtosis of fluctuating wind load are close to 0 and 3.0, respectively,

like across-wind direction, this peak factor can be reduced to the standard Gaussian form for a Gaussian process.

- SR model should be employed for the wind-induced load prediction, since the low natural frequency of floater increases the resonant standard deviation, while the large damping causes significant reduction.
- In the combination of along-wind and across-wind loads, the correlation coefficient of wind responses in the two directions is considered. It is noticed that the uncorrelated coefficient underestimates the maximum bending moment, while completely correlated one gives a conservative and acceptable result.

Reference

1. Architectural Institute of Japan (AIJ), 2004. Recommendations for loads on buildings.
2. The Danish Society of Engineers and the Federation of Engineers, 1992. Loads and safety of wind turbine construction Danish standard DS472.
3. Davenport, A.G., 1964. Note on the distribution of the largest value of a random function with application to gust loading. In: Proceedings of the Institute of Civil Engineering, pp. 187–196.
4. Kareem, A., Zhou, Y., 2003. Gust loading factor—past, present and future. Journal of Wind Engineering and Industrial Aerodynamics 91, 1301–1328.
5. Ishihara, T., 2010. Guidelines for design of wind turbine support structures and foundations. Japan Society of Civil Engineers, Tokyo. (in Japanese)
6. Binh, L.V., Ishihara, T., Phuc, P.V., Fujino, Y., 2008. A peak factor for non-Gaussian response analysis of wind turbine tower. Journal of Wind Engineering and Industrial Aerodynamics 96, 2217-2227.
7. Kareem, A., Tognarelli, M.A., Gurley, K.R., 1998. Modeling and analysis of quadratic term in the wind effects on structures. Journal of Wind Engineering and Industrial Aerodynamics 74-76, 1101-1110.
8. British Standards Institute: Code of basic data for the design of buildings, Chapter V, Loading.
9. GH Bladed, 2001. Generic 2MW Offshore Turbine, GH Bladed Version3.51, Garrad Hassan and Partners Limited.
10. Somers, D.M., 1997. Design and Experimental Results for the S809 Airfoil, NREL/SR-6918, Golden, Colorado, National Renewable Energy Lab.
11. Ishihara, T., Phuc, P.V., Takahara, K., Mekaru ,T., 2006. A study of wind response analysis on a wind turbine, Proceedings of 19th Symposium on Wind Engineering, 175-180. (in Japanese)
12. Cramer, H. E., 1958. Use of power spectra and scales of turbulence in estimating wind loads. Second National Conference on Applied Meteororlogy, Ann Arbor, Michigan, USA.
13. Asami, Y., 2000. Wind loads combination for high-rise building. 16th Symposium on Wind Engineering, 531-534. (in Japanese)

Chapter 6. COMBINATION OF WAVE-INDUCED LOAD AND WIND-INDUCED LOAD

6.1. Introduction

This chapter presents the combination of wave-induced load and wind-induced load. The reason why the assumption of perfect correlation between them causes overestimation has been clarified. It is shown that the combination without considering any correlation can predict the tower loading accurately.

Figure 6.1 compares the maximum tower loading of the case that wave and wind act simultaneously and the simple summation of the maximum wave load and maximum wind load. It is obvious that the simple summation overestimates the tower loading a lot. Therefore, the load reduction factor should be introduced into the combination. IEC 61400-3 [1] specifies a constant load reduction factor 0.7 to reduce the maximum wave load in the combination for bottom-mounted system. Whether this value is appropriate to floating wind turbine system or not should be investigated in this chapter.

Considering the correlation between wind and wave conditions, the load reduction factor for floating wind turbine system is proposed. It is found that the load reduction factor is almost constant to the mean wind speed at hub height. For tension leg system, the load reduction factor is lower than that given in IEC 61400-3 [1] used for bottom-mounted system, while for catenary system it is a little higher than that of IEC.

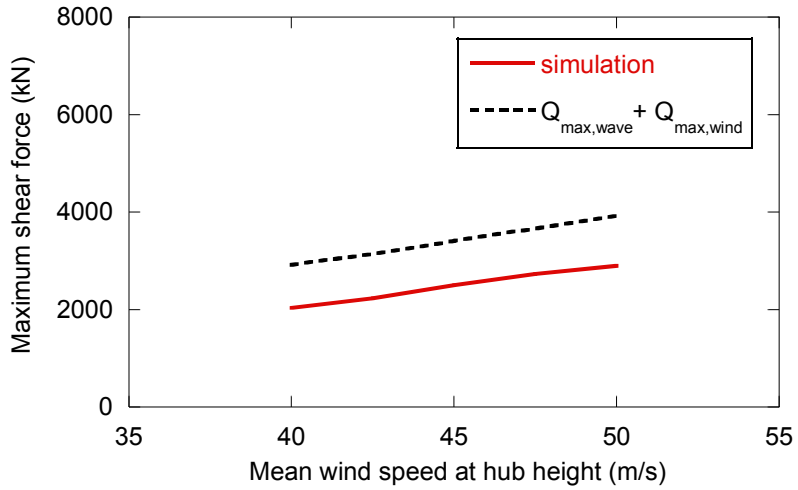

(a) Tension leg system

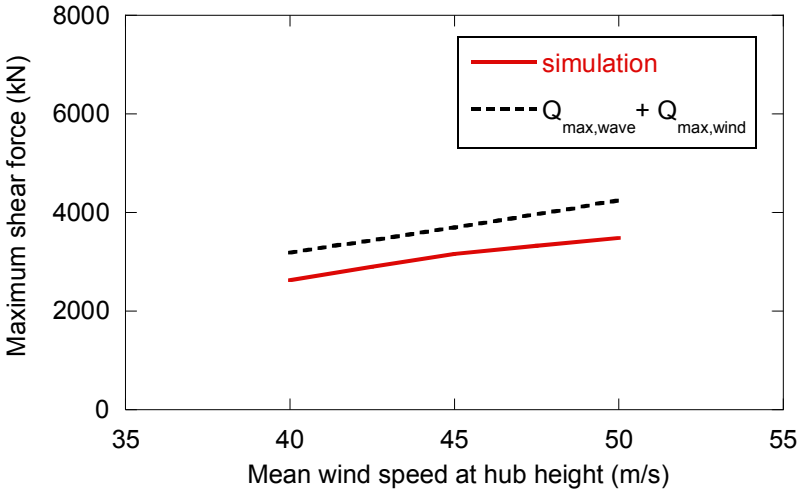

(b) Catenary system

Figure 6.1 Comparison of 'wave+wind' simulation and simple summation of the maximum wave and wind loads

6.2. Correlated Wind and Wave Conditions

Accurate and realistic modeling of the wind conditions is extremely essential for proper prediction of aerodynamic characteristics of the wind turbine and the power generation. Wind velocity and turbulence, are the most important characteristics used to define the wind conditions at a particular site.

For DLC 6.1a [1], the turbulent extreme wind model shall be taken together with the extreme sea state (ESS) conditions. The response shall be estimated using full dynamic simulation based on at least six 1-hour realizations for each combination of extreme wind speed and extreme sea state. In this case, the hub height mean wind speed, turbulence standard deviation and significant wave height shall be taken as 50-year recurrence

values each referenced to a 1-hour simulation period. The hub height mean wind speed of 10 min value with a 50-year recurrence is considered as 40~50 m/s.

$$U(z) = U_{10\min,hub}\left(\frac{z}{z_{hub}}\right)^{0.11} \tag{6.1}$$

Further, for representation of turbulent wind speeds, the turbulent extreme wind model makes use of a characteristic turbulence intensity $I_{10\min,hub} = 0.11$[2], [3]. The turbulence models [4] may be calculated as:

$$I(z) = I_{10\min,hub}\left(\frac{z}{z_{hub}}\right)^{-0.11-0.05} \tag{6.2}$$

In this study the method developed in [5] has been used for the generation of wind time history. The method [5] uses the von-Karman model to generate the frequency content of the wind history. The method can develop three dimensional wind time histories at several points considering auto spectral and cross-spectral functions. The details about the model are out of scope of the current discussion and reader is requested to refer to [5] for further details. Using this method, the wind histories are generated at each node of the tower, nacelle, and blades.

In this study, the SMB method [6], [7], [8] is used to consider the correlation between the mean wind speed U_{10} at 10m height from the sea level and the significant wave height H_s and wave peak period T_p :

$$H_s = \alpha H_{0,SMB} + (1-\alpha) H_{0,swell}$$

$$\begin{cases} \alpha = \max\left(0.4\tan^{-1}\left(0.34U_{10} - 1.88\right) + 0.39, 0\right) \\ H_{0,SMB} = \dfrac{0.3U_{10}^2}{g}\left[1 - \left\{1 + 0.004\left(\dfrac{Fg}{U_{10}^2}\right)^{1/2}\right\}^{-2}\right] \\ H_{0,swell} = 1.31 + \dfrac{(2.46 - 1.31)U_{10}}{12} \end{cases} \tag{6.3}$$

$$T_p = \alpha T_{0,SMB} + (1-\alpha) T_{0,swell}$$

$$\begin{cases} \alpha = \max\left(0.4\tan^{-1}\left(0.34U_{10} - 1.88\right) + 0.39, 0\right) \\ T_{0,SMB} = \dfrac{1.37 \cdot 2\pi U_{10}}{g}\left[1 - \left\{1 + 0.008\left(\dfrac{Fg}{U_{10}^2}\right)^{1/3}\right\}^{-5}\right] \\ T_{0,swell} = 8 \end{cases} \qquad 6.4$$

where $F = 235000$ m. Figure 6.2 shows the variation of significant wave height H_s and wave peak period T_p with the mean wind speed at hub height.

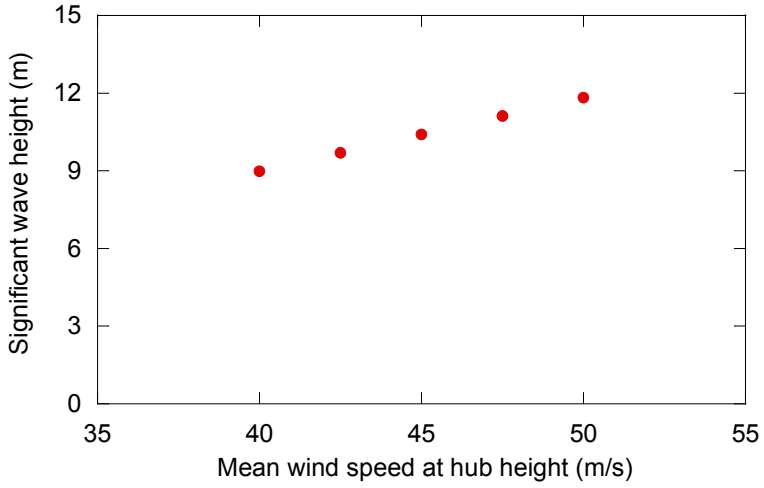

(a) Significant wave height

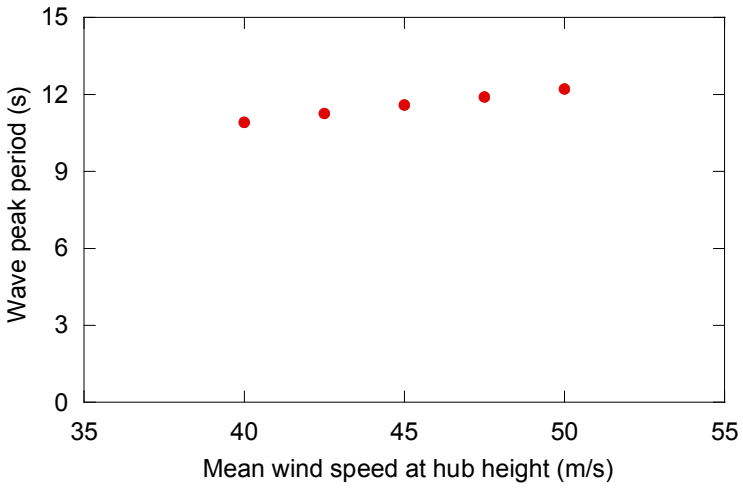

(b) Wave peak period

Figure 6.2 Significant wave height H_s and wave peak period T_p

6.3. Combination of Wave and Wind Loads

6.3.1. Contributions of Wave and Wind

The environmental loads (wind and wave) are considered independently to understand their respective contributions. Using the wind and wave conditions discussed in Section 6.2, simulations with full model are carried out in two sets considering 'wave only' and 'wind only'. The wind is set to act in the same direction as wave, as shown in Figure 2.9, which will cause the most unfavourable load effect. The mean value, standard deviation and maximum value of the shear force at tower base are compared for the two sets of environmental conditions, as shown in Figure 6.3 for tension leg system and in Figure 6.4 for catenary system, respectively.

From the comparison of mean value, it is indicated that the mean shear force depends on the wind, and the wave doesn't cause any mean loading. It is also noticed that the two kinds of mooring systems have the same mean wind shear force, and the reason can be known from Section 5.6.

From the comparison of standard deviation and maximum value, it is found that wave contributes more than wind to the dynamic loading for the two kinds of mooring systems. That is why the wave-induced load has to be taken into account for floating wind turbine system, and the combination of wind and wave loads are needed. The catenary system has the larger value than the tension leg system due to the influence of rocking (pitch) motion.

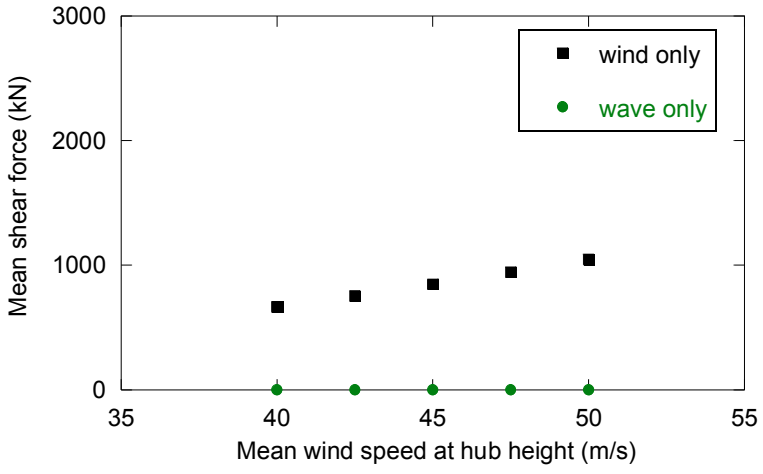

(a) Mean

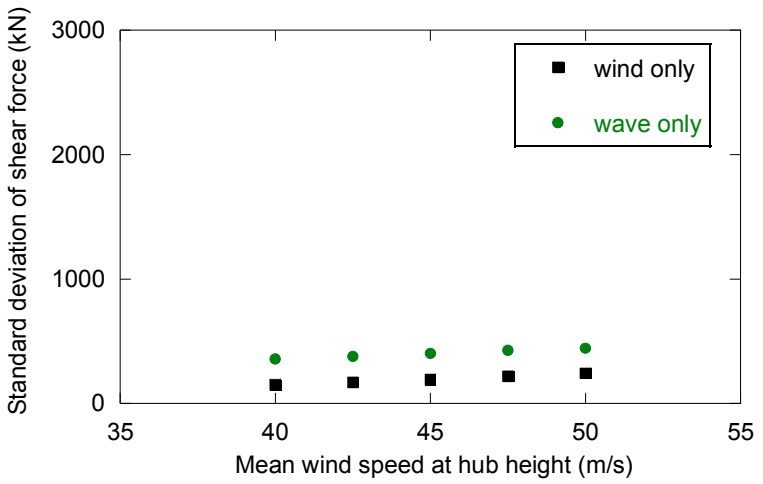

(b) Standard deviation

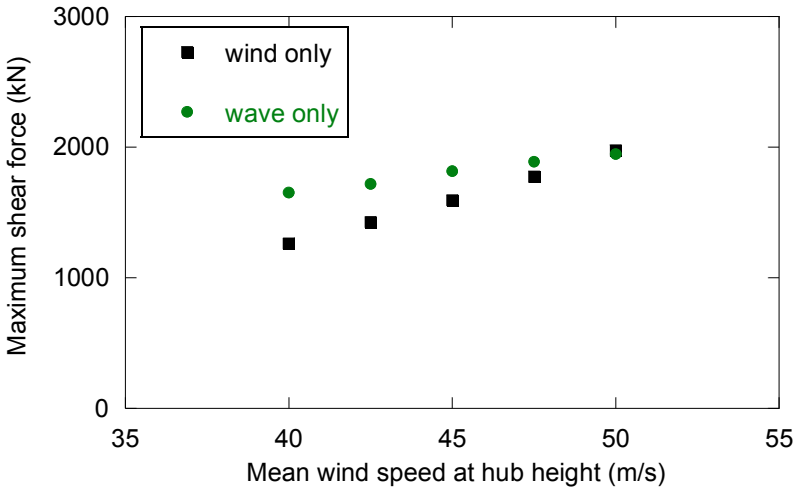

(c) Maximum

Figure 6.3 Shear force on tower base for tension leg system

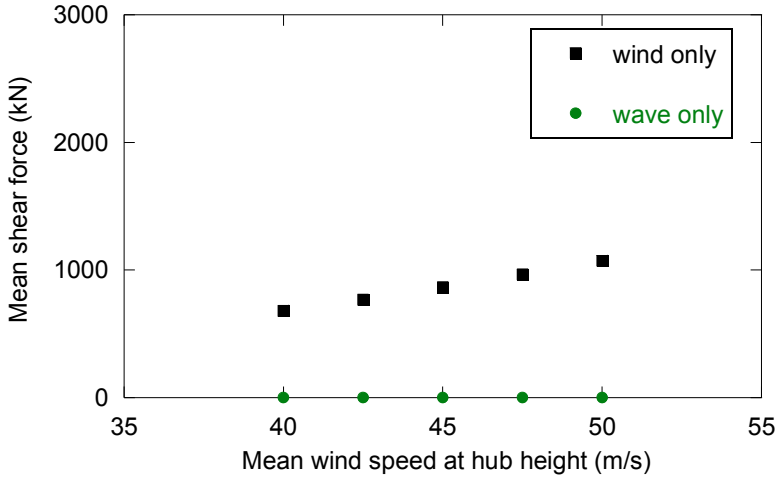

(a) Mean

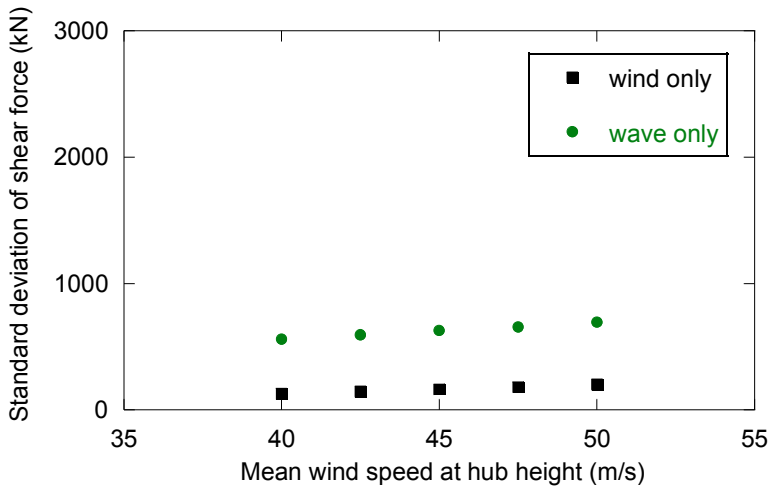

(b) Standard deviation

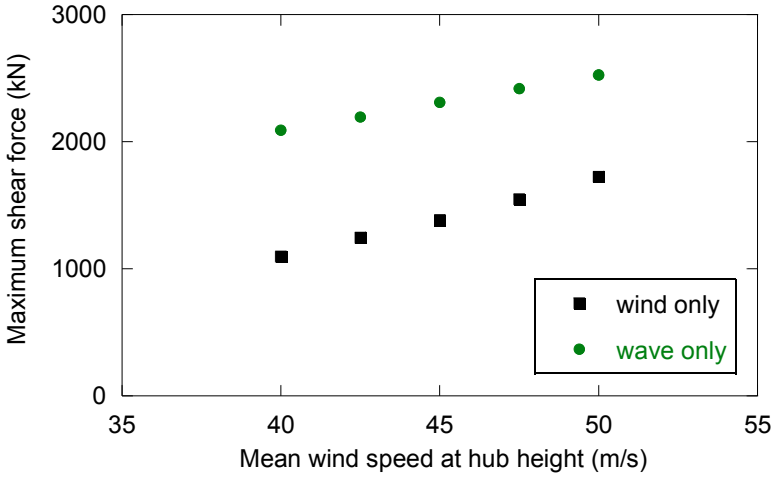

(c) Maximum

Figure 6.4 Shear force on tower base for catenary system

6.3.2. Correlation between Wave Load and Wind Load

Since the mean shear force in the 'wave+wind' case depends on the wind, and the wave doesn't cause any mean loading, the combination of wave-induced load and wind-induced load can also be performed by equivalent static method using mean wind load $\bar{Q}_{wind}$, combined standard deviation σ_{cb} and combined peak factor g_{cb}:

$$Q_{cb} = \bar{Q}_{wind} + g_{cb} \cdot \sigma_{cb} \qquad 6.5$$

In the 'wave+wind' case, the general equation of motion can be expressed as:

$$M\ddot{x}+C\dot{x}+Kx=F_{wave}+\frac{1}{2}C_d\rho A\left[U+u-\left(\dot{s}+\dot{x}'\right)\right]^2$$
$$=F_{wave}+\frac{1}{2}C_d\rho A\left(U^2+u^2+\dot{x}'^2+2Uu-2U\dot{x}'-2u\dot{x}'\right) \quad 6.6$$
$$+\frac{1}{2}C_d\rho A\left(\dot{s}^2-2U\dot{s}-2u\dot{s}+2\dot{s}\dot{x}'\right)$$

where F_{wave} is the wave force, C_d is the drag aerodynamic coefficient, ρ is the air density, A is the wind acting area, $x=s+x'$ is the total displacement, s is the displacement due to wave and x' is the displacement due to wind, U is the mean wind speed, u is the fluctuating wind speed. In the right hand side of Eq. (6.6), the second term is the wind force which is totally same as discussed in Chapter 5; the third term is the coupling aerodynamic force which causes the correlation between wave-induced load and wind-induced load. Since the wave-induced vibration velocity $\dot{s}$ is negligibly small compared to the mean wind speed in the extreme condition, the second order terms with $\dot{s}^2$, $u\dot{s}$ and $\dot{s}\dot{x}'$ can be neglected in the third term. Therefore, Eq. (6.6) can be decomposed into two equations of motion under wave and wind, respectively:

$$M\ddot{s}+C\dot{s}+Ks=F_{wave}-C_d\rho AU\dot{s} \quad 6.7$$

$$M\ddot{x}'+C\dot{x}'+Kx'=F_{wind} \quad 6.8$$

The aerodynamic damping force $-C_d\rho AU\dot{s}$ in Eq. (6.7) will reduce the wave-induced response in Chapter 4. This reduction can be considered by aerodynamic damping. However, the aerodynamic damping ratio is just 1/10~1/20 of the system damping ratio in SR model for floating wind turbine, hence can be neglected. Thus, all the coupling aerodynamic forces in the third term of Eq. (6.6) are ignored, which means the correlation between wave-induced load and wind-induced load is neglected as a matter of course. Therefore, the combined standard deviation σ_{cb} is calculated as:

$$\sigma_{cb}=\sqrt{\sigma_{wave}^2+\sigma_{wind}^2} \quad 6.9$$

where σ_{wave} and σ_{wind} are the standard deviations due to wave and wind that are calculated independently in Chapter 4 and Chapter 5, respectively.

It is shown in Figure 6.5 that the combination without considering any correlation between wave-induced load and wind-induced load can predict the standard deviation of 'wave+wind' case accurately.

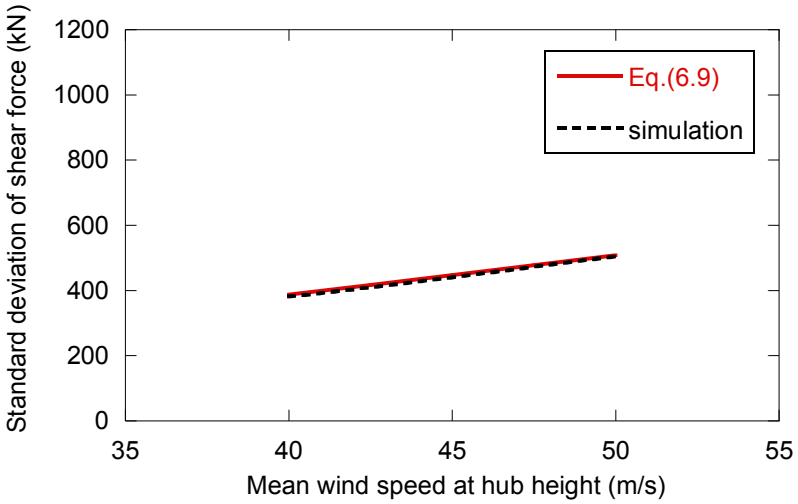

(a) Tension leg system

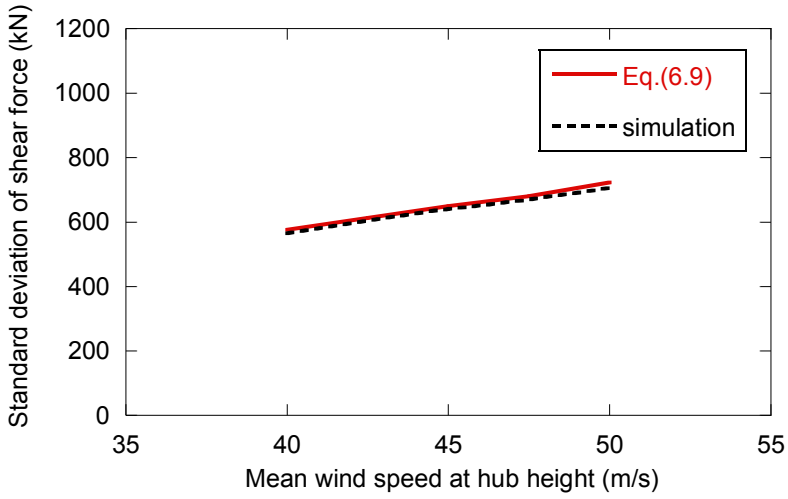

(b) Catenary system

Figure 6.5 Comparison of combined standard deviation

The combined peak factor g_{cb} is able to be calculated using Eqs. (4.15) ~ (4.17) of the non-Gaussian peak factor model in the same method as 'wave only' case in Section 4.4.2. The difference is the calculation of zero up-crossing frequency of base shear force. As shown in Figure 6.6, the wind part is added to the power spectrum:

$$\nu_0 = \sqrt{\frac{n_{wind}^2\sigma_{wind}^2 + n_p^2\sigma_b^2 + n_s^2\sigma_s^2 + n_t^2\sigma_t^2}{\sigma_{wind}^2 + \sigma_b^2 + \sigma_s^2 + \sigma_t^2}} \qquad 6.10$$

where

$$n_{wind}^2\sigma_{wind}^2 = n_{wind,b}^2\sigma_{wind,b}^2 + n_1^2\sigma_{wind,r}^2$$

$$\sigma_{wind}^2 = \sigma_{wind,b}^2 + \sigma_{wind,r}^2 \ , \qquad n_{wind,b} = 0.3\frac{U_h}{\sqrt{L_u\sqrt{A_{wt}}}}$$

σ_{wind}^2, σ_b^2, σ_s^2 and σ_t^2 are the variance of fluctuating wind load, background motion part due to wave, peak sway or rocking acceleration part and tower resonant part, respectively; $\sigma_{wind,b}$ and $\sigma_{wind,r}$ are the background part and resonant part of wind load standard deviation, respectively; n_p, n_s, n_t and n_1 are the wave peak frequency, the peak frequency of sway or rocking acceleration, tower natural frequency and the first natural frequency of the floating system, respectively; U_h is the mean wind velocity at hub height; L_u is the turbulence integral length scale; A_{wt} is the wind acting area of the whole wind turbine. Figure 6.7 shows the comparison of combined peak factor. It can be seen that the non-Gaussian peak factor model can predict the peak factor well.

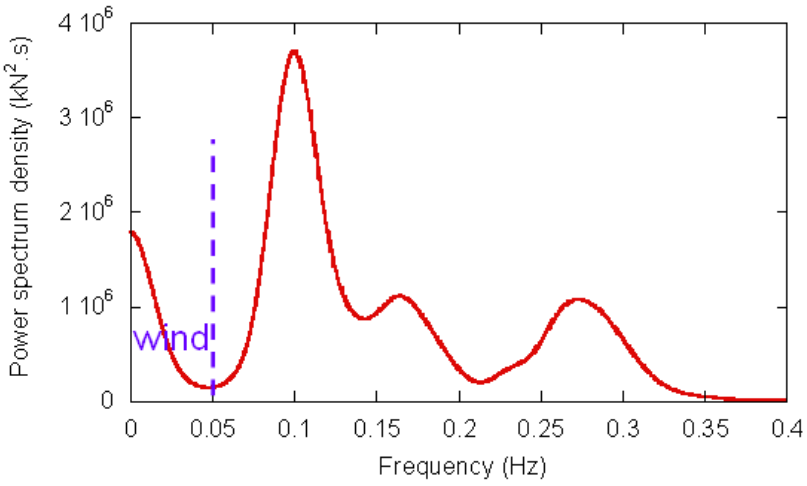

(a) Tension leg system

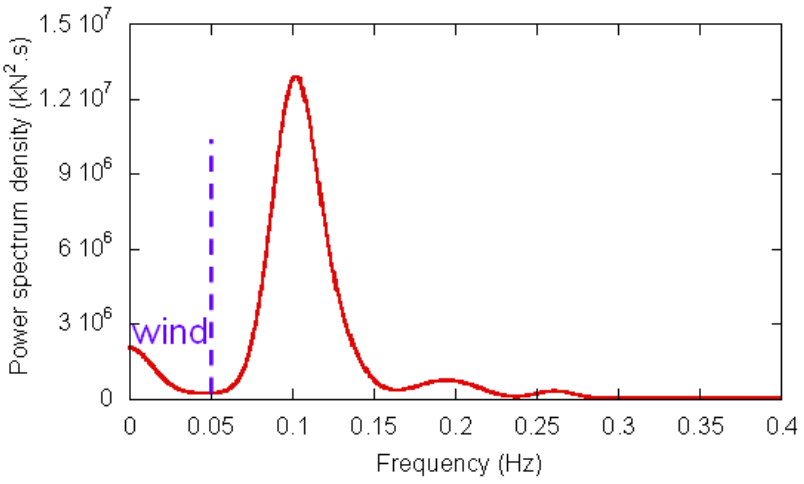

(b) Catenary system

Figure 6.6 Power spectrum density of tower base shear force in 'wave+wind' case

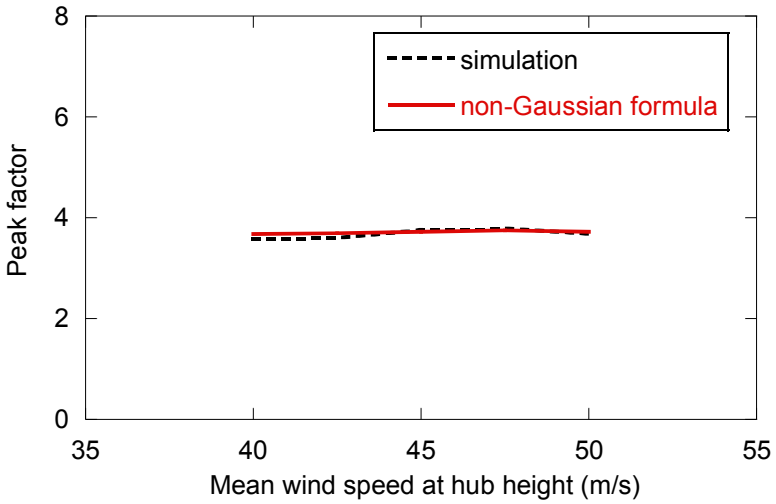

(a) Tension leg system

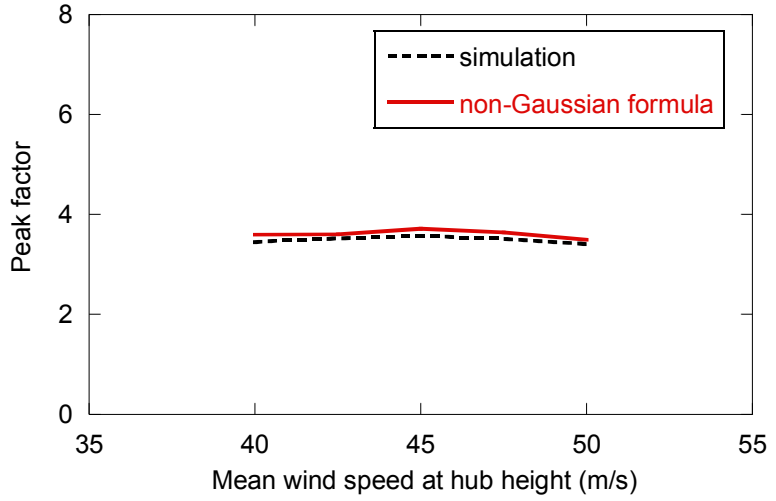

(b) Catenary system

Figure 6.7 Comparison of combined peak factor

6.3.3. Load Reduction Factor

In IEC 61400-3 [1], the occurrences of the extreme wind speed averaged over three seconds and the extreme wave height are assumed to be uncorrelated and their combination is conservative. The following reduced wave height shall therefore be used in combination with the extreme wind speed:

$$H_{red50} = 1.3H_{s50} \qquad 6.11$$

Since the extreme wave height $H_{50} = 1.86H_{s50}$, where H_{s50} is the significant wave height with a recurrence period of 50 years. It indicates that IEC reduces the extreme wave height by $1.3/1.86 = 0.7$. From Figure 6.8, it is found that the maximum shear force

increases with the extreme wave height linearly approximately, so it can be considered that the load reduction factor of wave-induced load is 0.7. It should be noted that this value is used for bottom-mounted system.

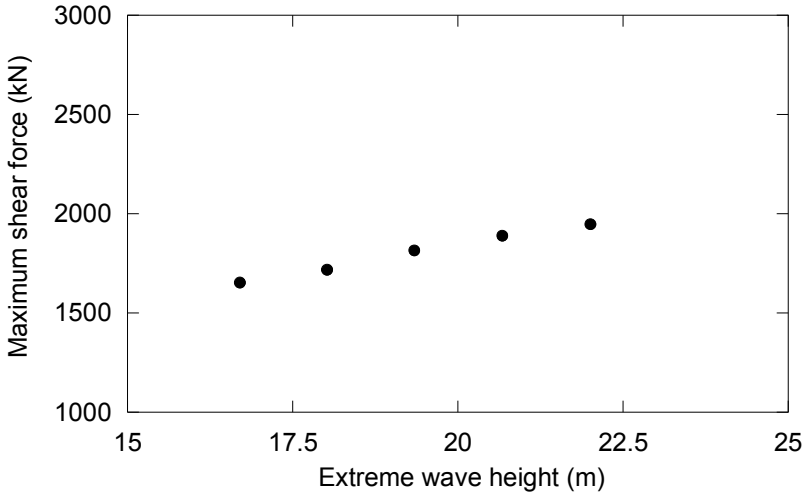

(a) Tension leg system

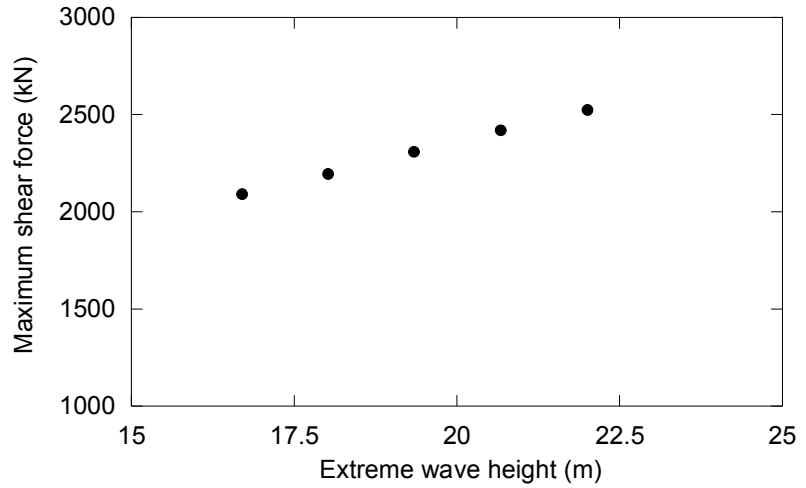

(b) Catenary system

Figure 6.8 Linear relation between extreme wave height and maximum shear force

In order to use the same way as IEC 61400-3, the load reduction factor is introduced into the combination for floating wind turbine systems. The wind-induced load is not reduced, only the maximum value of wave-induced load is reduced:

$$Q_{cb} = Q_{\max,wind} + \gamma_{wave} \cdot Q_{\max,wave} \tag{6.12}$$

where $Q_{\max,wind}$ and $Q_{\max,wave}$ are the maximum values of wind-induced shear force and wave-induced shear force, respectively; γ_{wave} is the load reduction factor.

The load reduction factors can be obtained by fitting the simulation results of the case that wave and wind act simultaneously, and the values are found to be almost constant to the mean wind speed at hub height, as shown in Figure 6.9 (a) for tension leg system and Figure 6.9 (b) for catenary system. For tension leg system, the load reduction factor is around 0.49, lower than 0.7 specified for bottom-mounted wind turbine in IEC 61400-3 [1], while for catenary system it is around 0.73, a little higher than that of IEC. Hence, 0.7 used for bottom-mounted system will overestimate the combined load of tension leg system significantly, however, it will give a little underestimation for catenary system.

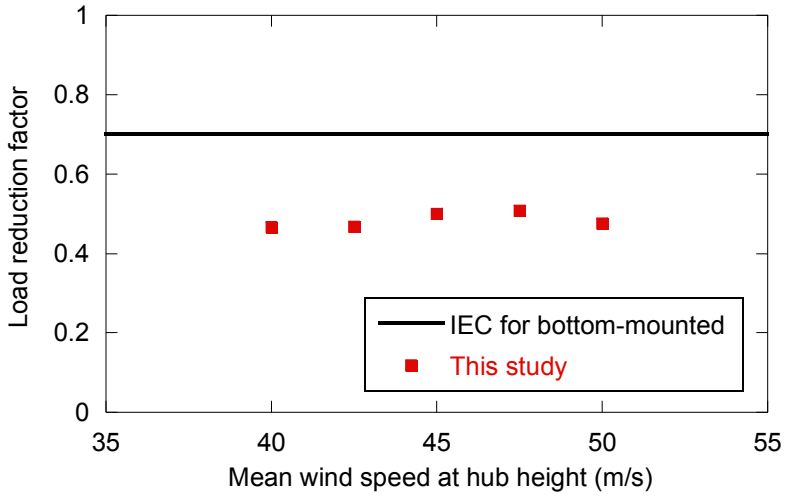

(a) Tension leg system

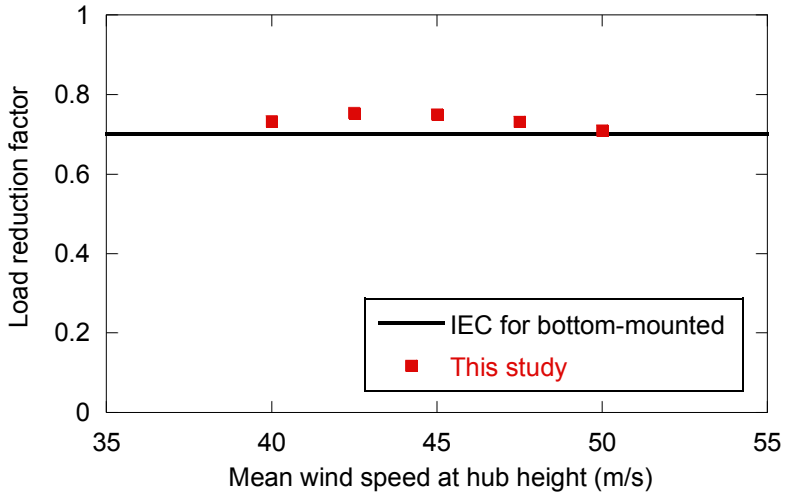

(b) Catenary system

Figure 6.9 Load reduction factors

6.4. Conclusions

The conclusions and findings of this chapter are summarized as follows:

- The mean tower loading depends on the wind and the wave doesn't cause any mean loading. Wave contributes more than wind to the dynamic loading for the two kinds of mooring systems.
- The assumption of perfect correlation between wave-induced load and wind-induced load causes overestimation. It is shown that the combination without considering any correlation can predict the tower loading accurately.
- Considering the correlation between wind and wave conditions, the load reduction factor for floating wind turbine system is proposed. It is found that the load reduction factor is almost constant to the mean wind speed at hub height. For tension leg system, the load reduction factor is lower than that given in IEC 61400-3 used for bottom-mounted system, while for catenary system it is a little higher than that of IEC.

Reference

1. IEC-61400-3 (2008), Edition-1: Wind turbines – Part 3: Design requirements for offshore wind turbines.
2. International Electrotechnical Commission, 2005. International Standard: Wind turbines – Part 1: Design requirements, IEC 61400-1, Edition 3.0, Geneva.
3. Offshore Standard DNV-OS-J101, Design of offshore wind turbine structures, 2011.
4. Ishihara, T., 2010. Guidelines for design of wind turbine support structures and foundations. Japan Society of Civil Engineers, Tokyo. (in Japanese)
5. Pham Van Phuc (2005), Numerical and Theoretical Study on the Wind Response of Wind Turbine in the Strong Wind Condition, M.Sc Thesis, Department of Civil Engineering, The University of Tokyo, Japan.
6. Sverdrup, H.U. and W.H. Munk (1947): Wind, sea, and swell; theory of relations for forecasting, U.S. Navy Hydro-graphic Office, H.O. Pub. 601, pp. 1-44.
7. Bretschneider, C.L. (1952): Revised wave forecasting relationships, Proc. 2nd Conf. Coastal Engg., ASCE, pp. 1-5.
8. Bretschneider, C.L. (1958): Revisions in wave forecasting: Deep and shallow water, Proc. 6th Conf. Coastal Engg., ASCE, pp. 30-67.

Chapter 7. CONCLUSIONS AND FUTURE WORK

7.1. Summary

The urgent concern about global warming from the emission of greenhouse gases has provided a strong impetus for engineers and scientists worldwide to research alternative renewable and clean energy. Wind power is one of the fastest growing renewable energy technologies. Onshore wind farms are, however, unsightly and they swallow up valuable land for agriculture and urban development. Already some countries, are considering constructing huge wind farms offshore to take advantage of the generally steadier and stronger winds found in the sea. Moreover, the wind turbines can be larger than those on land because they can be transported to the site by sea. In Japan, the offshore consist of a vast wind resource in deep water where use of conventional bottom-mounted wind turbines is not possible, and floating wind turbines are the most attractive. Thus, it is necessary to consider the effect of floater motion on the tower loading to check the serviceability of the wind turbines which are designed for the bottom-mounted systems.

In the current study, the theoretical formulae to predict the tower loading of floating offshore wind turbine systems in the extreme wind and wave conditions are proposed. Since the floating offshore wind turbine is affected significantly by floater motion, the conventional fixed-foundation model which is applicable to the onshore wind turbine can not be used theoretically to predict the tower loading of floating offshore wind turbine systems. In this study, SR model is proposed to consider the floater surge and pitch motions which have large influence on the tower loading of floating wind turbine, so that the tower loading can be estimated by the equivalent static method. Meanwhile, the problems of using conventional fixed-foundation model have been clarified. In SR model for wave-induced load, the influence of each floater motion is investigated separately by locking the other mode, and their combination is carried out. Both regular wave and irregular wave are considered for two kinds of floating systems: tension leg mooring and

catenary mooring. In addition, the fluctuating wave load and fluctuating wind load become non-Gaussian processes with multiple peaks corresponding to different frequencies in their spectra, hence, a non-Gaussian peak factor model is proposed in order to predict wave-induced load and wind-induced load on the floating offshore wind turbine tower by equivalent static method analytically. Furthermore, in the combination of wave-induced load and wind-induced load, the load reduction factor is proposed since the correlation between their maximum values can be neglected. All the results have been verified by the dynamic response analysis of a fully coupled finite element model.

7.2. Conclusions

The conclusions and findings of this study are summarized as follows:

(1) In the equivalent SR model for floating wind turbine system, the following conclusions are obtained:

- An equivalent SR model is proposed to consider the influence of floater surge and pitch motions on the tower loading of floating wind turbine. The stiffness and damping of sway and rocking modes are recognized by eigenvalue analysis or free vibration simulation using FEM; the equivalent wave force and moment are obtained with the tower base displacements.
- The evaluation formulae of tower loading due to sway as well as rocking motion of floater are investigated separately by locking the other mode with modal analysis.
- Through the theoretical comparison between SR model and fixed-foundation model, it is found that in short wave period, the fixed-foundation model may give significant overestimation, which can be larger than 15%; while in long wave period, it underestimates the tower loading.

(2) In the prediction of wave-induced load, the following conclusions are obtained:

- For the shear force amplitude under regular wave and the standard deviation of shear force under irregular wave, the combination of sway motion effect and rocking motion effect can be determined by complete quadratic combination (CQC) rule. The correlation between them only depends on the damping and natural frequency of the system.
- For tension leg system, a non-Gaussian peak factor is necessary. This non-Gaussian feature mainly results from the tower resonance. The non-Gaussianity will decrease with wave period, since the external exciting effect becomes weaker.
- For catenary system, the shear force history can be regarded as a Gaussian process. The effect from tower resonance is negligibly small compared to the

background motion part, since the floater sway and rocking modes are much more dominant.

(3) The evaluation formulae of both along-wind load and across-wind load are proposed for arbitrary wind direction, and the following conclusions are obtained:

- A unified mode correction factor is proposed. Due to the existence of rotor, the mode correction factor varies with yaw angle in a range larger than that of tower.
- The background size reduction factor decreases when the wind turbine size increases, while the resonant one doesn't have this feature, since it is also related to the natural frequency of wind turbine. It is noticed that the size reduction factors are close to those of tower and rotor, since the effect from rotor and tower cancel each other. The size reduction factors of across-wind direction totally come from the rotor, hence close to those of along-wind direction.
- A non-Gaussian peak factor model is proposed for along-wind direction. When the skewness and kurtosis of fluctuating wind load are close to 0 and 3.0, respectively, like across-wind direction, this peak factor can be reduced to the standard Gaussian form for a Gaussian process.
- SR model should be employed for the wind-induced load prediction, since the low natural frequency of floater increases the resonant standard deviation, while the large damping causes significant reduction.
- In the combination of along-wind and across-wind loads, the correlation coefficient of wind responses in the two directions is considered. It is noticed that the uncorrelated coefficient underestimates the maximum bending moment, while completely correlated one gives a conservative and acceptable result.

(4) In the combination of wave-induced load and wind-induced load, the following conclusions are obtained:

- The mean tower loading depends on the wind and the wave doesn't cause any mean loading. Wave contributes more than wind to the dynamic loading for the two kinds of mooring systems.
- The assumption of perfect correlation between wave-induced load and wind-induced load causes overestimation. It is shown that the combination without considering any correlation can predict the tower loading accurately.
- Considering the correlation between wind and wave conditions, the load reduction factor for floating wind turbine system is proposed. It is found that the load reduction factor is almost constant to the mean wind speed at hub height. For tension leg system, the load reduction factor is lower than that given in IEC 61400-

3 used for bottom-mounted system, while for catenary system it is a little higher than that of IEC.

7.3. Future Work

In the combination of wave-induced load and wind-induced load of this study, the wind and wave are assumed to be aligned (co-directional) and acting from a single, worst case direction (uni-directional), since it is the most unfavorable load case. In real situation, the wind and wave may be misaligned and act from multi-direction. Then the combination of wave-induced load and wind-induced load will be different from this study. The correlation between them should be investigated and the load reduction factor should be proposed accordingly in the future.

Appendix A. DYNAMIC RESPONSE IN TURBULENT WIND

A.1. Introduction

This appendix describes how the aerodynamic force acting on the wind turbine is analyzed in both along-wind and across-wind directions. Then for each direction, the derivation of integral forms and analytical formulae of mean, standard deviation and peak factor of bending moments is presented. In the standard deviation, the details how the estimation formulae of mode correction factor, aerodynamic damping ratio and size reduction factor are proposed from their integral forms are given as well.

A.2. Aerodynamic Force

From Figure 5.3, the total relative wind velocity can be written as follows:

$$V\left(\theta+\theta'\right)=\frac{U+u-\dot{x}}{\cos\theta'} \tag{A.1}$$

Quasi-static method is employed to calculate the aerodynamic force acting on the element. The drag force *D* and the lift force *L* per unit length can be calculated as

$$D=\frac{1}{2}\rho c\left(r\right)V^2\left(\theta+\theta'\right)C_D\left(\theta+\theta'\right),\ L=\frac{1}{2}\rho c\left(r\right)V^2\left(\theta+\theta'\right)C_L\left(\theta+\theta'\right) \tag{A.2}$$

Based on Eqs (A.1) and (A.2) the wind force in along-wind direction is obtained as the following equation:

$$F_D\left(\theta+\theta'\right)=D\cos\theta'-L\sin\theta'=\frac{1}{2}\rho c\left(r\right)\left(U+u-\dot{x}\right)^2\left(C_D\left(\theta+\theta'\right)\sec\theta'-C_L\left(\theta+\theta'\right)\sec\theta'\tan\theta'\right) \tag{A.3}$$

By using Taylor expansion around $\theta' = 0$, and noting $\theta' \approx \tan\theta' = (v - \dot{y})/(U + u - \dot{x})$ since θ' is very small, Eq. (A.3) can be written as

$$\begin{aligned} F_D(\theta) &= \frac{1}{2}\rho c(r)(U+u-\dot{x})^2\left(C_D(\theta) + \left(\frac{\partial C_D}{\partial\theta}(\theta) - C_L(\theta)\right)\cdot\theta'\right) \\ &= \frac{1}{2}\rho c(r)C_D(\theta)U^2 + \frac{1}{2}\rho c(r)C_D(\theta)u^2 + \rho c(r)C_D(\theta)Uu + \rho c(r)A_D(\theta)Uv - \rho c(r)C_D(\theta)U\dot{x} \\ &+ \frac{1}{2}\rho c(r)C_D(\theta)\dot{x}^2 - \rho c(r)C_D(\theta)u\dot{x} + \rho c(r)A_D(\theta)uv - \rho c(r)A_D(\theta)u\dot{y} - \rho c(r)A_D(\theta)v\dot{x} + \rho c(r)A_D(\theta)\dot{x}\dot{y} \\ &- \rho c(r)A_D(\theta)U\dot{y} \end{aligned}$$

A.4

In Eq. (A.4), the second order terms from the 6th term to 11th term, can be dropped based on perturbation analysis. The last term $-\rho A A_D(\theta)U\dot{y}$ caused by the across motion $\dot{y}$ of the structure which cannot be obtained by the analytical method is removed as well. Binh et al. [1] considered the second order term $(1/2)\rho A C_D(\theta)u^2$, since the contribution of the non-linear part of wind pressure is large, especially for high wind turbulence. In this study, the force $\rho A A_D(\theta)Uv$ due to the lateral wind fluctuation component v is also picked up. Finally, the first five terms are taken as the total wind force F_D as shown in Eq. (A.5). Mean wind force $\overline{F}_D$ and fluctuating wind force q_D in along-wind direction becomes Eqs. (A.6) and (A.7).

$$F_D = \frac{1}{2}\rho c(r)C_D(\theta)U^2 + \frac{1}{2}\rho c(r)C_D(\theta)u^2 + \rho c(r)C_D(\theta)Uu + \rho c(r)A_D(\theta)Uv - \rho c(r)C_D(\theta)U\dot{x} \quad \text{A.5}$$

$$\overline{F}_D = \frac{1}{2}\rho C_D(\theta)c(r)\left(U^2 + \sigma_u{}^2\right) = \frac{1}{2}\rho C_D(\theta)c(r)U^2\left(1 + I_u{}^2\right) \quad \text{A.6}$$

$$q_D = \rho c(r)C_D(\theta)Uu + \rho c(r)A_D(\theta)Uv - \rho c(r)C_D(\theta)U\dot{x} + \frac{1}{2}\rho c(r)C_D(\theta)u^2 - \frac{1}{2}\rho c(r)C_D(\theta)U^2 I_u{}^2$$

A.7

The wind force in across-wind direction can be derived as

$$F_L(\theta) = D\sin\theta' + L\cos\theta' = \frac{1}{2}\rho c(r)(U+u-\dot{x})^2\left(C_D(\theta+\theta')\sec\theta'\tan\theta' + C_L(\theta+\theta')\sec\theta'\right) \quad \text{A.8}$$

By using Taylor expansion around $\theta' = 0$, and noting $\theta' \approx \tan\theta' = (v - \dot{y})/(U + u - \dot{x})$ since θ' is very small, Eq. (A.8) can be written as

$$F_L(\theta)=\frac{1}{2}\rho c(r)(U+u-\dot{x})^2\left[C_L(\theta)+\left(C_D(\theta)+\frac{\partial C_L}{\partial\theta}(\theta)\right)\cdot\theta'\right]$$
$$=\frac{1}{2}\rho c(r)C_L(\theta)U^2+\frac{1}{2}\rho c(r)C_L(\theta)u^2+\rho c(r)C_L(\theta)Uu+\rho c(r)A_L(\theta)Uv-\rho c(r)A_L(\theta)U\dot{y}$$
$$+\frac{1}{2}\rho c(r)C_L(\theta)\dot{x}^2-\rho c(r)C_L(\theta)u\dot{x}+\rho c(r)A_L(\theta)uv-\rho c(r)A_L(\theta)u\dot{y}-\rho c(r)A_L(\theta)v\dot{x}+\rho c(r)A_L(\theta)\dot{x}\dot{y}$$
$$-\rho c(r)C_L(\theta)U\dot{x}$$

A.9

Based on the same analysis as along-wind direction, the total, mean and fluctuating wind force in across-wind direction can be written as

$$F_L=\frac{1}{2}\rho c(r)C_L(\theta)U^2+\frac{1}{2}\rho c(r)C_L(\theta)u^2+\rho c(r)C_L(\theta)Uu+\rho c(r)A_L(\theta)Uv-\rho c(r)A_L(\theta)U\dot{y} \quad \text{A.10}$$

$$\overline{F}_L=\frac{1}{2}\rho C_L(\theta)c(r)\left(U^2+\sigma_u{}^2\right)=\frac{1}{2}\rho C_L(\theta)c(r)U^2\left(1+I_u{}^2\right) \quad \text{A.11}$$

$$q_L=\rho c(r)C_L(\theta)Uu+\rho c(r)A_L(\theta)Uv-\rho c(r)A_L(\theta)U\dot{y}+\frac{1}{2}\rho c(r)C_L(\theta)u^2-\frac{1}{2}\rho c(r)C_L(\theta)U^2I_u{}^2 \quad \text{A.12}$$

A.3. Mean Bending Moment

From Eqs. (A.6) and (A.11), the mean bending moment at the tower base can be expressed as Eq. (A.13) in general, taking the mean wind velocity and turbulence intensity at the hub as representative for that of the whole wind turbine.

$$\overline{M}_f=\int\frac{1}{2}\rho C_f(r,\theta)c(r)U^2(r)\left[1+I_u{}^2(r)\right]rdr$$
$$\approx\frac{1}{2}\rho\left(C_{f,r}(\theta)U_h^2\left(1+I_{uh}^2\right)A_rH_h+C_{f,t}(\theta)\int_0^{H_h}U_h^2\left(\frac{z}{H_h}\right)^{2\alpha}\left(1+I_{uh}^2\left(\frac{z}{H_h}\right)^{-2\alpha-0.1}\right)d(z)zdr\right) \quad \text{A.13}$$
$$=\frac{1}{2}\rho U_h^2\left(1+I_{uh}^2\right)H_h\left(C_{f,r}(\theta)A_r+C_{f,t}(\theta)H_hD'\right)$$

where

$$D'=\frac{1}{\left(1+I_{uh}^2\right)}\left[\frac{D_b+2(\alpha+1)D_t}{2(\alpha+1)(2\alpha+3)}+\frac{I_{uh}^2\left(D_b+1.9D_t\right)}{5.5}\right].$$

The subscript *f=D* means along-wind and *f=L* means across-wind. The wind-acting area of nacelle and hub $A_n=L_NH_N+(\pi/4)R_NH_N$ is illustrated in Figure A.1.

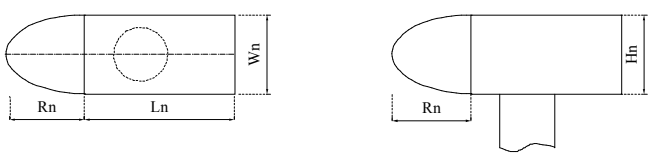

Figure A.1 Configuration of nacelle and hub

A.4. Gust Loading Factor

A.4.1. Standard Deviation

Since the non-linear parts in Eqs. (A.7) and (A.12) contribute very little to the standard deviation of tower base bending moment compared to linear parts, in this paper only linear parts are used in the following derivation. Therefore, the fluctuating loading per unit length on wind turbine in along-wind and across-wind directions is finally determined as:

$$q_D(r,t) = \left[\rho c(r) C_D(\theta) U u + \rho c(r) A_D(\theta) U v\right] - \rho c(r) C_D(\theta) U \dot{x},$$

$$q_L(r,t) = \left[\rho c(r) C_L(\theta) U u + \rho c(r) A_L(\theta) U v\right] - \rho c(r) A_L(\theta) U \dot{y} \qquad \text{A.14}$$

- **Background Response of Base Bending Moment**

From Eq. (A.14), the background response of base bending moment can be expressed as Eq. (A.15) in general.

$$M_{Bf}(t) = \int q_f(r,t) r dr = \int \rho c(r) C_f(r,\theta) U(r) u(r,t) r dr + \int \rho c(r) A_f(r,\theta) U(r) v(r,t) r dr \qquad \text{A.15}$$

Assuming that the cross correlation function of *u, v* components is zero, the standard deviation of background base bending moment can be derived as the summation of two independent parts due to longitudinal and lateral wind component (*u* and *v*) as well. Here, the mean wind velocity and turbulence intensity at the hub are also taken as representative for that of the whole wind turbine.

$$\begin{aligned}
\sigma_{MBf}^2 &= \rho^2 \iint \rho_u(r,r') \sigma_u(r) \sigma_u(r') C_f(r) C_f(r') U(r) U(r') c(r) c(r') r r' dr dr' \\
&\quad + \rho^2 \iint \rho_v(r,r') \sigma_v(r) \sigma_v(r') A_f(r) A_f(r') U(r) U(r') c(r) c(r') r r' dr dr' \\
&= \rho^2 I_{uh}^2 U_h^4 \iint \rho_u(r,r') C_f(r) C_f(r') c(r) c(r') r r' dr dr' \\
&\quad + \rho^2 I_{vh}^2 U_h^4 \iint \rho_v(r,r') A_f(r) A_f(r') c(r) c(r') r r' dr dr' \\
&= \sigma_{MBfu}^2 + \sigma_{MBfv}^2
\end{aligned} \qquad \text{A.16}$$

where $\rho_u(r,r')$, $\rho_v(r,r')$ are the normalized cross correlation function between simultaneous wind fluctuation at *r, r'*, and measurements indicate that the normalized cross correlation function decays exponentially, so it can be expressed as $\rho_u(r,r') = \exp\left[-|r-r'|/0.3L_u\right]$ and $\rho_v(r,r') = \exp\left[-|r-r'|/0.3L_v\right]$. For design purpose, the background standard deviation can be expressed with mean bending moment, size reduction factor and wind load ratio. For wind turbine, the across-wind mean bending moment becomes close to zero at some yaw angles. And it is well known that the lateral turbulence intensity is defined as the ratio of standard deviation of lateral fluctuation component to the longitudinal mean wind speed. Based on the same idea, therefore, in this study the along-wind mean bending moment is employed to calculate both along-wind and across-wind standard deviation of bending moment. Therefore, the background standard deviation can be expressed as:

$$\sigma_{MBfu} = 2\frac{\bar{M}_D}{1+I_{uh}^2} I_{uh}\sqrt{K_{MBfu}\cdot\gamma_{MBfu}}\ , \qquad \sigma_{MBfv} = 2\frac{\bar{M}_D}{1+I_{uh}^2} I_{vh}\sqrt{K_{MBfv}\cdot\gamma_{MBfv}} \tag{A.17}$$

where K_{MBfu} and K_{MBfv} are the background size reduction factors for the base bending moment due to longitudinal and lateral wind fluctuations, respectively, and γ_{MBfu} and γ_{MBfv} are wind load ratios.

- **Resonant Response of Base Bending Moment**

Substituting Eq. (A.14) to Eq. (5.5), the modal equations of motion for the two directions become

$$m_i\ddot{f}_i(t) + \left(c_i + \int \rho C_D U c(r)\mu_i^2(r)dr\right)\dot{f}_i(t) + m_i\omega_i^2 f_i(t) = \int\left[\rho C_D c(r)Uu + \rho A_D c(r)Uv\right]\mu_i(r)dr\ ,$$

$$m_i\ddot{f}_i(t) + \left(c_i + \int \rho A_L U c(r)\mu_i^2(r)dr\right)\dot{f}_i(t) + m_i\omega_i^2 f_i(t) = \int\left[\rho C_L c(r)Uu + \rho A_L c(r)Uv\right]\mu_i(r)dr \tag{A.18}$$

The generalized loading of the right hand side of Eq. (A.18) can be expressed as Eq. (A.19) in general with respect to the first mode.

$$Q_1(t) = \int \rho U(r) C_f(r,\theta) u(r,t) c(r)\mu_1(r)dr + \int \rho U(r) A_f(r,\theta) v(r,t) c(r)\mu_1(r)dr \tag{A.19}$$

Assuming that the cross correlation function of *u,v* components is zero, the standard deviation σ_{Q1} of $Q_1(t)$ is given by

$$\sigma_{Q1}^2 = \frac{1}{T}\int_0^T Q_1^2(t)\,dt$$

$$= \rho^2 \iint \left[\frac{1}{T}\int_0^T u(r,t)u(r',t)dt\right] U(r)U(r')C_f(r,\theta)C_f(r',\theta)c(r)c(r')\mu_1(r)\mu_1(r')\,drdr'$$

$$+\rho^2 \iint \left[\frac{1}{T}\int_0^T v(r,t)v(r',t)dt\right] U(r)U(r')A_f(r,\theta)A_f(r',\theta)c(r)c(r')\mu_1(r)\mu_1(r')\,drdr'$$

$$+2\rho^2 \iint \left[\frac{1}{T}\int_0^T u(r,t)v(r',t)dt\right] U(r)U(r')C_f(r,\theta)A_f(r',\theta)c(r)c(r')\mu_1(r)\mu_1(r')\,drdr'$$

$$= \rho^2 \iint \left[\int_0^\infty S_{uu}(r,r',n)\,dn\right] U(r)U(r')C_f(r,\theta)C_f(r',\theta)c(r)c(r')\mu_1(r)\mu_1(r')\,drdr'$$

$$+\rho^2 \iint \left[\int_0^\infty S_{vv}(r,r',n)\,dn\right] U(r)U(r')A_f(r,\theta)A_f(r',\theta)c(r)c(r')\mu_1(r)\mu_1(r')\,drdr' \qquad \text{A.20}$$

where S_{uu}, S_{vv} is the cross spectrum of wind fluctuating component *u,v* respectively, which is defined by normalized co-spectrum $\psi_{uu}^N(r,r',n)$, $\psi_{vv}^N(r,r',n)$ and power spectrum density of its wind fluctuations $S_u(n)$, $S_v(n)$.

$$S_{uu}(r,r',n) = \psi_{uu}^N(r,r',n)S_u(n), \quad S_{vv}(r,r',n) = \psi_{vv}^N(r,r',n)S_v(n)$$

Therefore, the power spectrum of generalized load with respect to the first mode is

$$S_{Q1}(n) = \rho^2 \iint \psi_{uu}^N(r,r',n)S_u(n)U(r)U(r')C_f(r,\theta)C_f(r',\theta)c(r)c(r')\mu_1(r)\mu_1(r')\,drdr'$$

$$+\rho^2 \iint \psi_{vv}^N(r,r',n)S_v(n)U(r)U(r')A_f(r,\theta)A_f(r',\theta)c(r)c(r')\mu_1(r)\mu_1(r')\,drdr' \qquad \text{A.21}$$

As derived by Wind Energy Handbook [2], in the case of the dominant first mode, the power spectrum of the tip deflection is $S_{x1}(n) = S_{Q_1}(n)\left|H_1(n)\right|^2$, where $S_{Q_1}(n)$ is assumed constant over the narrow band of frequencies straddling the resonant frequency, $\left|H_1(n)\right|$ is the modulus of the complex frequency response function, and can be used to transform the power spectrum of the wind incident into the power spectrum of the displacement. It has been shown by Newland [3] that $\int_0^\infty \left|H_1(n)\right|^2 dn = \left(\pi^2/2\delta_f\right)\left(n_1/k_1^2\right)$. Then the standard deviation of resonant response becomes which can be written in two independence parts of longitude and lateral wind component (*u* and *v*).

$$\sigma_{x1}^2 = \int_0^\infty S_{x1}(n)\,dn = \int_0^\infty S_{Q1}(n)\left|H_1(n)\right|^2 dn \approx S_{Q1}(n_1)\int_0^\infty \left|H_1(n)\right|^2 dn = S_{Q1}(n_1)\frac{\pi^2}{2\delta_f}\frac{n_1}{k_1^2}$$

$$= \left[\frac{\pi^2}{2\delta_f}\frac{\rho^2}{k_1^2}\right] R_{uh}(n_1) I_{uh}^2 U_h^2 \iint \psi_{uu}(r,r',n_1) U(r) U(r') C_f(r,\theta) C_f(r',\theta) c(r) c(r') \mu_1(r) \mu_1(r')\,dr dr'$$

$$+ \left[\frac{\pi^2}{2\delta_f}\frac{\rho^2}{k_1^2}\right] R_{vh}(n_1) I_{vh}^2 U_h^2 \iint \psi_{vv}(r,r',n_1) U(r) U(r') A_f(r,\theta) A_f(r',\theta) c(r) c(r') \mu_1(r) \mu_1(r')\,dr dr'$$

$$= \sigma_{x1u}^2 + \sigma_{x1v}^2 \qquad \text{A.22}$$

where δ_f is the logarithmic decrement of damping, which is 2π times the damping ratio ξ_f, $R_{uh}(n_1) = n_1 S_u(n_1)/\sigma_{uh}^2$ and $R_{vh}(n_1) = n_1 S_v(n_1)/\sigma_{vh}^2$ are the normalized power spectral density of longitudinal and lateral wind fluctuation.

The standard deviation of the first mode resonant base bending moment is derived below. Defining $M_{Rf}(t)$ as the fluctuating base bending moment due to wind excitation of the first mode

$$M_{Rf}(t) = \int m(r)\ddot{x}_1(t,r)\,r dr = \int m(r)\omega_1^2 x_1(t,r)\,r dr = \omega_1^2 f_1(t)\int m(r)\mu_1(r)\,r dr \qquad \text{A.23}$$

Hence, based on Eqs. (A.22) and (A.23) the standard deviation of resonant base bending moment fluctuation can be derived as the summation of two independent parts resulted from longitudinal and lateral wind component (u and v) as well. Here, the mean wind velocity $U(r)$ and $U(r')$ in the integrals are assumed constant as U_h at the hub.

$$\sigma_{MRf}^2 = \omega_1^4\left(\sigma_{x1u}^2 + \sigma_{x1v}^2\right)\left(\int m(r)\mu_1(r)\,r dr\right)^2 = \sigma_{MRfu}^2 + \sigma_{MRfv}^2,$$

$$\sigma_{MRfu}^2 = \omega_1^4 \sigma_{x1u}^2 \left(\int m(r)\mu_1(r)\,r dr\right)^2$$

$$= \frac{k_1^2}{m_1^2}\left[\frac{\pi^2}{2\delta_f}\frac{\rho^2}{k_1^2}\right] R_{uh}(n_1) I_{uh}^2 U_h^4 \iint \psi_{uu}(r,r',n_1) C_f(r,\theta) C_f(r',\theta) c(r) c(r') \mu_1(r)\,\mu_1(r')\,dr dr' \cdot \left(\int m(r)\mu_1(r)\,r dr\right)^2,$$

$$\sigma_{MRfv}^2 = \omega_1^4 \sigma_{x1v}^2 \left(\int m(r)\mu_1(r)\,r dr\right)^2$$

$$= \frac{k_1^2}{m_1^2}\left[\frac{\pi^2}{2\delta_f}\frac{\rho^2}{k_1^2}\right] R_{vh}(n_1) I_{vh}^2 U_h^4 \iint \psi_{vv}(r,r',n_1) A_f(r,\theta) A_f(r',\theta) c(r) c(r') \mu_1(r)\,\mu_1(r')\,dr dr' \cdot \left(\int m(r)\mu_1(r)\,r dr\right)^2 \qquad \text{A.24}$$

On an empirical basis, Davenport [4] has proposed an exponential expression for the normalized co-spectrum as $\psi_{uu}^{N}(r,r',n)=\psi_{vv}^{N}(r,r',n)\approx\exp\left[-C\left|r-r'\right|n/U_h\right]$. Based on the same analysis, the resonant standard deviation can be expressed with along-wind mean bending moment, mode correction factor, size reduction factor and wind load ratio:

$$\sigma_{MRfu}=2\frac{\bar{M}_D}{1+I_{uh}^2}I_{uh}\frac{\pi\phi_f}{\sqrt{4\pi\xi_f}}\sqrt{R_{uh}(n_1)}\sqrt{K_{MRfu}(n_1)\cdot\gamma_{MRfu}}\ ,$$

$$\sigma_{MRfv}=2\frac{\bar{M}_D}{1+I_{uh}^2}I_{vh}\frac{\pi\phi_f}{\sqrt{4\pi\xi_f}}\sqrt{R_{vh}(n_1)}\sqrt{K_{MRfv}(n_1)\cdot\gamma_{MRfv}} \qquad \text{A.25}$$

where ϕ_f is the mode correction factor, ξ_f is the damping ratio, $K_{MRfu}(n_1)$ and $K_{MRfv}(n_1)$ are denoted the resonant size reduction factors for the base bending moment due to longitudinal and lateral wind fluctuations, respectively, which result from the lack of correlation of the fluctuating wind velocity, and γ_{MRfu} and γ_{MRfv} are wind load ratios. All these parameters will be discussed in follows.

Mode Correction Factor

The five non-dimensional parameters in the mode correction factor are determined as follows. During the derivation of a', mass distribution is assumed to be uniform of *m* per unit length along the tower. Although λ_b can be determined from γ_F, a more simple formula $1.2+0.07\cos 2\theta$ obtained by fitting the results of integral form is used instead here.

$$\begin{aligned}\phi_f&=\frac{\int C_D(r,\theta)\mu_1(r)c(r)dr}{\int C_D(r,\theta)c(r)rdr}\frac{\int m(r)\mu_1(r)rdr}{m_1}\\&=\frac{m_s}{m_1}\cdot\frac{\int_0^{H_h}m(z)\mu_1(z)zdz+m_rH_h}{m_tH_h+m_rH_h}\cdot\frac{C_{D,r}(\theta)A_r+\int_0^{H_h}C_{D,t}(\theta)d(z)\mu_1(z)dz}{C_{D,r}(\theta)A_r+\int_0^{H_h}C_{D,t}(\theta)d(z)\frac{z}{H_h}dz}\\&=\frac{m_s}{m_1}\cdot\left(\frac{\gamma_m/a'+1}{\gamma_m+1}\cdot\frac{\int_0^{H_h}m(z)\mu_1(z)zdz}{m_tH_h}\right)\cdot\left(\frac{\gamma_F/b'+1}{\gamma_F+1}\cdot\frac{\int_0^{H_h}C_{D,t}(\theta)d(z)\mu_1(z)dz}{\int_0^{H_h}C_{D,t}(\theta)d(z)\frac{z}{H_h}dz}\right)\\&=\gamma_M\cdot(\lambda_a a')\cdot(\lambda_b b')\end{aligned} \qquad \text{A.26}$$

where

$$\gamma_M=\frac{m_s}{m_1},\qquad \lambda_a=\frac{\gamma_m/a'+1}{\gamma_m+1},\qquad a'=\frac{\int_0^{H_h}m(z)\mu_1(z)zdz}{m_tH_h}=\frac{\int_0^{H_h}m\left(\frac{z}{H_h}\right)^{\beta_s}zdz}{mH_h\cdot H_h}=\frac{1}{2+\beta_s}=0.25\ ,$$

$$\lambda_b = \frac{\gamma_F / b' + 1}{\gamma_F + 1} = 1.2 + 0.07\cos 2\theta$$

$$(\gamma_F = C_{D,r}(\theta) A_r / \int_0^{H_h} C_{D,t}(\theta) d(z) \frac{z}{H_h} dz = C_{D,r}(\theta) A_r / \left(C_{D,t}(\theta) \cdot 0.42 D_a H_h\right)),$$

$$b' = \int_0^{H_h} C_{D,t}(\theta) d(z) \mu_1(z) dz / \int_0^{H_h} C_{D,t}(\theta) d(z) \frac{z}{H_h} dz \approx \frac{C_{D,t}(\theta) \cdot 0.3 D_a H_h}{C_{D,t}(\theta) \cdot 0.42 D_a H_h} = 0.714 .$$

Damping Ratio

From Eq. (A.18), in the case of the dominant first mode, damping ratio in along-wind and across-wind should consist of two components, structural $\xi_s = c_1 / 4\pi m_1 n_1$ and aerodynamic ξ_{aD} and ξ_{aL} as shown in Eqs. (A.27) and (A.28).

$$\xi_{aD} = \frac{\int \rho C_D(r,\theta) U(r) c(r) \mu_1^2(r) dr}{4\pi m_1 n_1} = \frac{\rho U_h A_r C_{D,r}(\theta) + \rho C_{D,t}(\theta) \int U(z) d(z) \mu_1^2(z) dz}{4\pi m_1 n_1}$$
$$= \frac{\rho U_h}{4\pi m_1 n_1} \left(C_{D,r}(\theta) A_r + C_{D,t}(\theta) H_h D''\right) \quad \text{A.27}$$

$$\xi_{aL} = \frac{\int \rho A_L(r,\theta) U(r) c(r) \mu_1^2(r) dr}{4\pi m_1 n_1} = \frac{\rho U_h A_r A_{L,r}(\theta)}{4\pi m_1 n_1} \quad \text{A.28}$$

where $D'' = \frac{D_b + (\alpha+5) D_t}{(\alpha+5)(\alpha+6)}$.

Size Reduction Factor

The integral forms of background and resonant size reduction factors are as Eqs. (A.29) ~ (A.32):

$$K_{MBfu} = \frac{\iint \exp\left[-|r-r'|/0.3L_u\right] C_f(r,\theta) C_f(r',\theta) c(r) c(r') rr' dr dr'}{\left(\int C_f(r,\theta) c(r) r dr\right)^2} \quad \text{A.29}$$

$$K_{MBfv} = \frac{\iint \exp\left[-|r-r'|/0.3L_v\right] A_f(r,\theta) A_f(r',\theta) c(r) c(r') rr' dr dr'}{\left(\int A_f(r,\theta) c(r) r dr\right)^2} \quad \text{A.30}$$

$$K_{MRfu}(n_1) = \frac{\iint \exp\left[-C|r-r'|n_1/U_h\right] C_f(r,\theta) C_f(r',\theta) c(r) c(r') \mu_1(r) \mu_1(r') dr dr'}{\left(\int C_f(r,\theta) c(r) \mu_1(r) dr\right)^2} \quad \text{A.31}$$

$$K_{MRfv}(n_1)=\frac{\iint \exp\left[-C\left|r-r'\right|n_1/U_h\right]A_f(r,\theta)A_f(r',\theta)c(r)c(r')\mu_1(r)\mu_1(r')drdr'}{\left(\int A_f(r,\theta)c(r)\mu_1(r)dr\right)^2} \quad \text{A.32}$$

The formulae of background and resonant wind load ratios are derived as Eqs. (A.33) ~ (A.36) from their integral forms:

$$\gamma_{MBfu}=\frac{\left(\int C_f(r,\theta)c(r)rdr\right)^2}{\left(\int C_D(r,\theta)c(r)rdr\right)^2}=\left(\frac{C_{f,r}(\theta)A_rH_h+\int_0^{H_h}C_{f,t}(\theta)d(z)zdz}{C_{D,r}(\theta)A_rH_h+\int_0^{H_h}C_{D,t}(\theta)d(z)zdz}\right)^2 \quad \text{A.33}$$
$$=\left(\frac{C_{f,r}(\theta)A_rH_h+C_{f,t}(\theta)\cdot 0.47D_aH_h^2}{C_{D,r}(\theta)A_rH_h+C_{D,t}(\theta)\cdot 0.47D_aH_h^2}\right)^2=\left(\frac{C_{f,t}(\theta)/C_{D,t}(\theta)+C_{f,r}(\theta)\cdot a_B}{1+C_{D,r}(\theta)\cdot a_B}\right)^2$$

$$\gamma_{MBfv}=\frac{\left(\int A_f(r,\theta)c(r)rdr\right)^2}{\left(\int C_D(r,\theta)c(r)rdr\right)^2}=\left(\frac{A_{f,r}(\theta)A_rH_h+\int_0^{H_h}A_{f,t}(\theta)d(z)zdz}{C_{D,r}(\theta)A_rH_h+\int_0^{H_h}C_{D,t}(\theta)d(z)zdz}\right)^2 \quad \text{A.34}$$
$$=\left(\frac{A_{f,r}(\theta)A_rH_h+A_{f,t}(\theta)\cdot 0.47D_aH_h^2}{C_{D,r}(\theta)A_rH_h+C_{D,t}(\theta)\cdot 0.47D_aH_h^2}\right)^2=\left(\frac{A_{f,t}(\theta)/C_{D,t}(\theta)+A_{f,r}(\theta)\cdot a_B}{1+C_{D,r}(\theta)\cdot a_B}\right)^2$$

$$\gamma_{MRfu}=\frac{\left(\int C_f(r,\theta)c(r)\mu_1(r)dr\right)^2}{\left(\int C_D(r,\theta)c(r)\mu_1(r)dr\right)^2}=\left(\frac{C_{f,r}(\theta)A_r+\int_0^{H_h}C_{f,t}(\theta)d(z)\mu_1(z)dz}{C_{D,r}(\theta)A_r+\int_0^{H_h}C_{D,t}(\theta)d(z)\mu_1(z)dz}\right)^2 \quad \text{A.35}$$
$$=\left(\frac{C_{f,r}(\theta)A_r+C_{f,t}(\theta)\cdot 0.3D_aH_h}{C_{D,r}(\theta)A_r+C_{D,t}(\theta)\cdot 0.3D_aH_h}\right)^2=\left(\frac{C_{f,t}(\theta)/C_{D,t}(\theta)+C_{f,r}(\theta)\cdot a_R}{1+C_{D,r}(\theta)\cdot a_R}\right)^2$$

$$\gamma_{MRfv}=\frac{\left(\int A_f(r,\theta)c(r)\mu_1(r)dr\right)^2}{\left(\int C_D(r,\theta)c(r)\mu_1(r)dr\right)^2}=\left(\frac{A_{f,r}(\theta)A_r+\int_0^{H_h}A_{f,t}(\theta)d(z)\mu_1(z)dz}{C_{D,r}(\theta)A_r+\int_0^{H_h}C_{D,t}(\theta)d(z)\mu_1(z)dz}\right)^2 \quad \text{A.36}$$
$$=\left(\frac{A_{f,r}(\theta)A_r+A_{f,t}(\theta)\cdot 0.3D_aH_h}{C_{D,r}(\theta)A_r+C_{D,t}(\theta)\cdot 0.3D_aH_h}\right)^2=\left(\frac{A_{f,t}(\theta)/C_{D,t}(\theta)+A_{f,r}(\theta)\cdot a_R}{1+C_{D,r}(\theta)\cdot a_R}\right)^2$$

A.4.2. Peak Factor

Kareem et al. [5] evaluated the peak factor for the non-Gaussian process as Eq. (A.37).

$$g_D=\kappa\left\{\left(\beta+\frac{\gamma}{\beta}\right)+h_3\left(\beta^2+2\lambda-1\right)+h_4\left[\beta^3+3\beta(\gamma-1)+\frac{3}{\beta}\left(\frac{\pi^2}{12}-\gamma+\frac{\gamma^2}{2}\right)\right]\right\} \quad \text{A.37}$$

where $\gamma = 0.5772$ (Euler's constant), $\beta = \sqrt{2\ln(\nu'_D T)}$, $\nu'_D = \frac{1}{\kappa\sqrt{1+4h_3^2+18h_4^2}}\nu_D$,

$\nu_D = n_1\sqrt{\frac{(n_{0D}/n_1)^2 + R_D}{1+R_D}}$, $n_{0D} = 0.3\frac{U_h}{\sqrt{L_u\sqrt{A_{wt}}}}$, $\kappa = \frac{1}{\sqrt{1+2h_3^2+6h_4^2}}$, $h_3 = \frac{\alpha_3}{4+2\sqrt{1+1.5(\alpha_4-3)}}$,

$h_4 = \frac{\sqrt{1+1.5(\alpha_4-3)}-1}{18}$.

ν'_D and ν_D are the zero up-crossing number in the estimated time interval *T* (normally 600s) of non-Gaussian process and Gaussian process of along-wind load, respectively, A_{wt} is the wind acting area of the whole wind turbine, and κ , h_3 , h_4 are functions of skewness α_3 and kurtosis α_4 of fluctuating wind load. Binh et al. [1] proved that the effect of kurtosis α_4 can be neglected since it is negligibly small compared to that of the second and third order from the order analysis of turbulence intensity I_u . α_4 is then assumed to be equal to the value of a Gaussian process (i.e., 3.0). Then the formula of the peak factor is simplified to a function of skewness, as shown in Eq. (A.38).

$$g_D = \frac{1}{\sqrt{1+\frac{\alpha_3^2}{18}}}\left\{\left(\sqrt{2\ln(\nu'_D T)} + \frac{0.5772}{\sqrt{2\ln(\nu'_D T)}}\right) + \frac{\alpha_3}{6}\left(2\ln(\nu'_D T) - 1\right)\right\} \qquad \text{A.38}$$

For the across-wind response, since the skewness and kurtosis of fluctuating wind load are close to 0 and 3.0, respectively, the non-Gaussian peak factor of Eq. (A.38) can be reduced to the standard Gaussian form:

$$g_L = \sqrt{2\ln(\nu_L T)} + \frac{0.5772}{\sqrt{2\ln(\nu_L T)}} \qquad \text{A.39}$$

where $\nu_L = n_1\sqrt{\frac{(n_{0L}/n_1)^2 + R_L}{1+R_L}}$, $n_{0L} = 0.3\frac{U_h}{\sqrt{L_v\sqrt{A_{wt}}}}$, $R_L = \left(\frac{\sigma_{MRL}}{\sigma_{MBL}}\right)^2$.

Reference

1. Binh, L.V., Ishihara, T., Phuc, P.V., Fujino, Y., 2008. A peak factor for non-Gaussian response analysis of wind turbine tower. Journal of Wind Engineering and Industrial Aerodynamics 96, 2217-2227.
2. Burton, T., Sharpe, D., Jenkins, N., Bossanyi, E., 2001. Wind energy handbook. WILEY, England.
3. Newland, D. E., 1984. Random vibrations and spectral analysis. Longman, UK.
4. Davenport, A. G., 1962. The response of slender, line-like structures to a gusty wind. Proc. Inst. Civ. Eng., 23, 389–408.
5. Kareem, A., Tognarelli, M.A., Gurley, K.R., 1998. Modeling and analysis of quadratic term in the wind effects on structures. Journal of Wind Engineering and Industrial Aerodynamics 74-76, 1101-1110.